EXPERIMENTAL SPRAY INVESTIGATION OF METHYL ESTER AND ETHYL ESTER TYPE BIODIESEL FUELS IN A CONSTANT VOLUME COMBUSTION CHAMBER

A Thesis Submitted to
the the Graduate School of
İzmir Institute of Technology
in Partial Fulfillment of the Requirements for the Degree of

MASTER OF SCIENCE

in Mechanical Engineering

by
Anılcan ULU

July 2020
İZMİR

ACKNOWLEDGMENTS

ABSTRACT

EXPERIMENTAL SPRAY INVESTIGATION OF METHYL ESTER AND ETHYL
ESTER TYPE BIODIESEL FUELS IN A CONSTANT VOLUME COMBUSTION
CHAMBER

Biodiesel fuels are promising fuels that can reduce pollutant emissions from diesel engines. Therefore, they are still being investigated in every aspect. In this study, it was aimed at comparing the spray characteristics of methyl ester and ethyl ester type biodiesel fuels with those of fossil diesel fuel. Besides, this study aimed to investigate the spray characteristics of ethyl esters on which few studies have been done, and to help eliminate this gap in the literature.

For these purposes, 4 different methyl esters from corn, sunflower, canola and cotton oils, and 2 different ethyl esters from corn and sunflower oils were produced. Commercial diesel fuel was used to compare the characteristics of these fuels. Firstly, physical properties of the fuels produced were investigated to better understand the spray investigation, and it was observed that biodiesel fuels had bigger density and viscosity values than fossil diesel fuel. Additionally, it was found that methyl esters had larger density and smaller viscosity values than ethyl esters. After that, spray characteristics of all fuels were investigated in a constant volume combustion chamber under ambient pressures of 0, 5 and 10 bar, and injection pressures of 600 and 800 bar. Then, these fuels were compared to each other.

After the experiments, biodiesel fuels were found to have longer spray penetration lengths and narrower spray angles than diesel fuel, although there were no significant differences between them. This may be due to higher density and viscosity values of biodiesel fuels. Furthermore, no significant distinctions were found between the spray characteristics of ethyl esters and methyl esters. In addition, it was observed that ambient and injection pressures were important parameters affecting the spray pattern.

As a result, it was obtained that biodiesel-air mixing was slightly worse than diesel-air mixing. However, their potential to reduce pollutant emissions may cause this difference to be ignored. Moreover, it was found that ethyl esters had similar spray characteristics as methyl esters. Hence, ethyl esters are promising to replace methyl esters.

Keywords: Biodiesel, Methyl Ester, Ethyl Ester, Spray Investigation.

ÖZET

METİL ESTER VE ETİL ESTER TÜRÜ BİYODİZEL YAKITLARIN PÜSKÜRMELERİNİN SABİT HACİMLİ YANMA ODASINDA DENEYSEL İNCELENMESİ

Biyodizel yakıtlar dizel motorların zararlı gaz salınımını azaltabilecek umut verici yakıtlardır. Bu nedenle, çeşitli yönlerden biyodizel araştırması devam etmektedir. Bu çalışmada metil ester ve etil ester türlerinde biyodizellerin püskürme özelliklerinin fosil dizel yakıtın püskürme özellikleriyle karşılaştırılması amaçlanmıştır. Ayrıca bu çalışma, üzerinde az sayıda çalışma yapılmış olan etil esterlerin püskürme özelliklerini araştırmayı ve literatürdeki bu boşluğu gidermeye yardımcı olmayı amaçlamıştır.

Bu hedefler doğrultusunda mısır, ayçiçeği, kanola ve pamuk yağlarından 4 farklı metil ester ve mısır ve ayçiçeği yağlarından 2 farklı etil ester üretilmiştir. Bu yakıtların özelliklerini karşılaştırmak için dizel yakıtı kullanılmıştır. Öncelikle, püskürme araştırmasının daha iyi anlaşılabilmesi için üretilen yakıtların fiziksel özellikleri incelenmiştir ve biyodizellerin dizele göre daha fazla özkütleye ve viskoziteye sahip olduğu görülmüştür. Ayrıca, metil esterlerin etil esterlere göre daha yüksek özkütle ve daha düşük viskozite değerlerine sahip oldukları bulunmuştur. Sonrasında bütün yakıtların püskürme özellikleri 0, 5 ve 10 barlık ortam basınçlarında ve 600 ve 800 barlık enjeksiyon basınçlarında sabit hacimli yanma odasında incelenmiştir ve yakıtlar birbirleriyle karşılaştırılmıştır.

Yapılan deneyler sonrasında arada ciddi farklar olmamasına rağmen biyodizel yakıtların dizel yakıta göre daha fazla püskürme uzunluğuna ve daha dar püskürme açılarına sahip olduğu bulunmuştur. Bu sonuç biyodizellerin daha yüksek viskozite ve özkütle değerlerine sahip olmalarına bağlanmıştır. Ayrıca etil esterler ve metil esterler karşılaştırıldığında iki tür yakıtın birbirlerine püskürme özellikleri bakımından önemli üstünlükleri olmadığı gözlemlenmiştir. Ek olarak, ortam ve enjeksiyon basınçlarının püskürme özellikleri üzerinde önemli etkenler olduğu görülmüştür.

Sonuç olarak, biyodizel yakıtların hava ile karışımı dizel ile hava karışımına göre biraz daha kötü olduğu görülmüştür. Ancak, zararlı gaz salınımını düşürme potansiyeline sahip olmaları aradaki bu farkın göz ardı edilmesini sağlayabilir. Bunun ötesinde, etil esterlerin metil esterler ile benzer püskürme özelliklerine sahip olduğu bulunmuştur. Bu nedenle etil esterler metil esterlerin yerine geçebilme konusunda umut verici olabilirler.

Anahtar Sözcükler: Biyodizel, Metil Ester, Etil Ester, Püskürme Araştırması.

TABLE OF CONTENTS

LIST OF FIGURES

LIST OF TABLES

LIST OF SYMBOLS

NO_x . . . . nitric oxides

HC . . . . hydrocarbon

KOH . . . . potassium hydroxide

NaOH . . . . sodium hydroxide

CO_2 . . . . carbon dioxide

$\dot{m}$ . . . . mass flow rate

γ . . . . specific heat ratio

NO . . . . nitric oxide

NO_2 . . . . nitric dioxide

CO . . . . carbon monoxide

F . . . . force

Re . . . . Reynolds number

Z . . . . Ohnesorge number

μ . . . . viscosity

ρ . . . . density

u . . . . velocity

σ . . . . surface tension at the liquid-gas interface

We . . . . Weber number

S . . . . spray penetration length

ϕ . . . . spray cone angle

BXX . . . . XX% biodiesel content of blended fuels

e . . . . error

$G_c(s)$ . . . . transfer function of the controller in s-domain

K_P . . . . coefficient for proportional

K_I . . . . coefficient for integral

K_D . . . . coefficient for derivative

$y(t)$ . . . . equation for the output in time domain

$e(t)$ . . . . error function in time domain

LIST OF ABBREVIATIONS

EPA . . . . Environmental Protection Agency

PM . . . . particulate matter

CVCC . . . . constant volume combustion chamber

CI . . . . compression-ignition

CARB . . . . California Air Resources Board

LEV . . . . low emission vehicle

SI . . . . spark-ignition

IEA . . . . International Energy Outlook

WVO . . . . waste vegetable oil

PBR . . . . photobioreactor

FT . . . . Fischer-Tropsch

SOI . . . . start-of-injection

EOI . . . . end-of-injection

IVC . . . . intake valve closing

EVO . . . . exhaust valve opening

SOC . . . . start-of-combustion

EOC . . . . end-of-combustion

HRR . . . . heat release rate

CA . . . . crank angle

ORE . . . . optical research engine

RCEM . . . . rapid compression and expansion machine

CPFR . . . . constant pressure flow rig

FAME . . . . fatty acid nethyl ester

WC . . . . water cooled

AC . . . . air cooled

NA . . . . naturally aspirated

TC . . . . turbocharged

EGR . . . . exhaust gas recirculation

CR . . . . compression ratio

RP . . . . rated power

RS . . . . rated speed

CV . . . . calorific value

CHAPTER 1

INTRODUCTION

1.1. Basic Concepts

Diesel engines have been very important devices for power generation so far. Firstly, diesel engines were widely utilized in industrial applications. However, higher thermal efficiency over gasoline engines led engineers and researchers to focus on these engines. Then, they became one of the prominent power generation devices in different areas such as the automotive industry [1]. Also, advances in fuel economy and drivability increased their demands [2]. Thus, diesel engines are nowadays very important devices for producing power in automobiles, trucks, marine vehicles, lightweight aircrafts, etc.

For a long time, diesel engines have been subject of criticism in the automotive industry due to the use of fossil fuels which have several drawbacks. Firstly, the need for energy is increasing day by day in the world, and fossil fuel resources are not sustainable [3]. Secondly, prices of fossil fuels are getting increased [4, 5]. Thirdly, pollutant emission levels from diesel engines are critical. Important organizations like European Union (EU) and Environmental Protection Agency (EPA) in the United States of America (USA) brought strict regulations to pollutant levels from automobiles (see Table 2.1). These regulations have been obligating researchers to find ways of decreasing emissions since 1990s [2]. Therefore, investigation of pollutant emissions in every aspect has had an important place in engine research up to now.

Diesel emissions are one of the most affecting sources of air pollution. Thus, comprehension of pollutant formation mechanisms is very critical to solve the pollution problem of diesel engines. The pollutants that need attention are nitric oxides (NO_x), particulate emissions (PM) and unburned hydrocarbons (HC). NO_x forms at high temperatures at which nitrogen and excess oxygen react. Particulate matter originates in the core of spray which contains unburned fuel [6]. Formation of hydrocarbons is related with the fuel which is remained without burning on the chamber walls.

Pollutants from diesel engines as a result of using fossil fuels have a greenhouse effect in the atmosphere leading climate change. Hence, alternative energy sources need

to be developed to decrease the share of fossil fuels. One of the promising energy sources is biodiesel fuel which is derived from biological resources. Biodiesel fuels can be ideal sources of power generation for diesel engines owing to following advantages: being renewable and biodegradable, having higher flash points resulting in ease of storage, and reduced pollutant emissions [4, 5, 7]. Also, some biodiesel fuels can show comparable spray pattern and combustion properties with those of conventional diesel fuels [8]. Besides, biodiesel fuels can be directly utilized in diesel engines with no or little modifications [9]. Hence, biodiesel fuels deserve more attention to be investigated in depth.

Biodiesel fuels are liquid biofuels that can be obtained from various feed stocks. Mostly used feed stocks are animal fats [10] and vegetable oils such as corn oil, canola oil [1], soybean oil [4], etc. Several processes are available for biodiesel production, which are gasification followed by Fischer-Tropsch synthesis, transesterification of vegetable oils or animal fats, fast pyrolysis and micro-emulsions [8, 11]. However, technology to be preferred to produce biodiesel depends on desired quality of biodiesel, type of resources, economic situation and scope of the project. Among these techniques Fischer-Tropsch synthesis following gasification is the most developed technique but it is the least commercialized method due to its complexity and cost [8]. The most commercial technique for biodiesel production is transesterification of animal fats or vegetable oils [5, 11, 12] with alcohols in the presence of catalysts such as KOH, NaOH, etc. [13].

In transesterification technique, the most widespread used alcohol is methanol owing to its wide availability and low cost [4]. Biodiesel derived as a result of transesterification of any animal fat or vegetable oil with methanol is called as methyl ester. Besides, ethanol can also be utilized for biodiesel production. Biodiesel produced through transesterification of the resources with ethanol is named as ethyl ester. The utilization of ethanol in transesterification process has some advantages over the usage of methanol. First of all, methanol is obtained from fossil sources such as natural gas and coal while ethanol can be obtained from vegetable sources like potatoes, sugar cane, corn, sugar beet through fermentation which is a biochemical process [5, 14]. Secondly, ethyl esters have better oxidation stability and lubrication properties than biodiesels produced with methanol [4, 15]. Thirdly, ethyl esters have lower cloud and pour points than methyl esters [4, 5]. Namely, cold flow properties of ethyl esters are better than those of methyl esters thus ethyl esters can have better performances in cold weathers. Additionally, some studies [16, 17] showed that higher alcohols like propanol and butanol can also be utilized to produce biodiesel fuel.

To reduce the pollutant emissions, the combustion process must be improved in addition to fuel replacement. In this context, mixture formation has a critical role in combustion process. The injection quantity, fuel atomization and spray pattern specify the development of combustion process thus the output performance, fuel consumption and emission levels. Control of the fuel injection system is very crucial to obtain a good combustion leading to good performance and low emission levels. Behaviour of the injection system must be adjusted by considering in-cylinder flow field, the design of combustion chamber and piston bowl. Hence, it is critical to investigate the spray pattern of the fuels to understand how these fuels behave in the cylinder.

Spray analysis is generally performed in order to investigate the spray characteristics of fuels. Key parameters for a spray analysis are spray break-up length or time, spray tip penetration length, spray cone angle and droplet size. These parameters can help researchers predict how fuel mixes with surrounding air. Several techniques can be employed for spray measurement. Among available techniques, constant volume combustion chambers (CVCC) which are covered with transparent windows are globally used owing to wide range of gas pressures and temperatures [18]. Transparent windows allow the light to pass the chamber for spray visualization. A high-speed camera is utilized to record the spray images which are then processed by image processing algorithms to obtain the desired key parameters.

1.2. Purpose of the Study

In this study, it was aimed at investigating the spray characteristics of various biodiesel fuels developed by transesterification of vegetable oils in comparison with mineral diesel fuel. Besides, studies investigating the characteristics of ethyl esters are very limited compared to methyl esters, and these studies have mostly focused on the combustion, performance and emission characteristics. Therefore, the main purpose of this study was to fill this gap in the literature by investigating the spray characteristics of ethyl esters.

The primary objectives of this study were:

- Optimizing the existing constant volume combustion chamber for spray analysis,

- Developing the optical system for spray visualization,

- Producing the biodiesel fuels,

- Measuring the spray characteristics of fuels in terms of spray cone angle and spray penetration length,

- Comparing the results of biodiesel fuels with those of the fossil diesel fuel,

- Comparing the spray behaviours of methyl esters and ethyl esters.

1.3. Outline of the Thesis

After a short introduction is given in Chapter 1, Chapter 2 gives a detailed explanation from the literature. Firstly, a brief review on diesel engines including the fuel types is given. Secondly, biofuels are reviewed in terms of types, classification and production methods. Then, basics of diesel engines including features of combustion process, pollutant formation mechanisms and spray formation are explained. After that, spray measurement techniques and optical diagnostics related with spray analysis are presented. Finally, studies on biodiesel fuels from the literature are expressed.

Chapter 3 introduces the experimental system in every aspect. It explains the production method of biodiesel fuels employed in this study and the experimental setup for spray analysis. Also, spray visualization system is described as well as the image processing algorithm. Furthermore, fuel properties and test conditions are given.

Chapter 4 presents the experimental investigation of spray characteristics of methyl esters and ethyl esters employed in this study under variable chamber and injection pressures. The data obtained from spray visualization is presented and discussed. The effects of biodiesel properties are expressed.

Chapter 5 gives a brief conclusion about the present work then makes suggestions for possible future works which can advance the research.

CHAPTER 2

LITERATURE SURVEY

2.1. An Overview of Diesel Engines

Diesel engines are compression-ignition type of internal combustion engines that utilize the chemical energy contained in a fuel to obtain mechanical energy. They were invented by Rudolph Diesel in 1892 [6]. When diesel engines first developed, they were used in industrial applications. Then, they were evolved to be utilized in automobiles owing to their high thermal efficiency, fuel economy and high torque generation. Also, advances in noise problem and drivability were achieved. These improvements strengthened the position of diesel engines in automotive industry. In 2017, around 16.7 million cars were produced in European Union and 44.8% of these cars were installed with diesel engines [19, 20].

In the 1940s, air pollution problem of automobiles was begun to be discussed in Los Angeles [6]. Since then, pollutant emissions from automobiles have been considered so much. One of the sources of air pollution is diesel engines emitting hydrocarbons, nitric oxides and particulate matters. Because of environmental concerns, some foundations around the world brought regulations to emission levels from vehicles. For instance, the California Air Resources Board (CARB) introduced the Low Emission Vehicle (LEV) legislation. In EU, Euro 6 legislations were implemented in 2014. Before that, Euro 1 regulations was first introduced in 1993 followed by Euro 2, 3, 4 and 5. For the future, Euro 7 legislations are expected to come into force in 2020 [21]. Regulations based on EU are shown in Table 2.1.

Table 2.1. EU regulations on emission levels of cars having spark-ignition (SI) or compression-ignition (CI) engine [2, 21].

Euro Standart	Year	Engine Type	CO (mg/km)	THC (mg/km)	NO$_x$ (mg/km)	THC+NO$_x$ (mg/km)	PM (mg/km)
Euro 4	2004	CI	500	-	250	300	25
		SI	1000	100	80	-	-
Euro 5	2009	CI	500	-	180	230	5
		SI	1000	100	60	-	5
Euro 6	2014	CI	500	-	80	170	5
		SI	1000	100	60	-	5

These constraints force researchers to discover new ways and produce alternative fuels to overcome the pollution problem of diesel engines. In the followings, fuel types utilized in diesel engines will be explained briefly.

2.1.1. Fuel Types for Diesel Engines

The most widely used fuel in diesel engines is mineral diesel fuel which is obtained from petroleum. Diesel fuel is a mixture of hydrocarbons which contain three major classes as paraffinic, naphthenic and aromatic hydrocarbons. Normally, conventional diesel fuels contain large amount of energy. Therefore, they are still in use. However, limited resources for fossil fuels, and pollutant emission levels due to the use of mineral diesel fuel have been obligating researchers to develop alternative fuels such as water-in-diesel emulsion and biodiesel fuel.

Water-in-diesel emulsion is a fuel-based solution. The existence of water in diesel engines reduces the maximum in-cylinder temperature because water vaporizes by taking some amount of heat available inside the cylinder. Thus, NO_x decreases owing to decrease in cylinder temperature. Moreover, the presence of water inside the cylinder increases the oxidation of soot particles which results in a decrease in particulate emissions. Many researchers [22, 23, 24, 25, 26, 27] discussed the effects of water-in-diesel emulsions on engine performance and emissions.

Another alternative fuel for diesel engines is biodiesel fuel which can be derived from vegetable oils, some seed crops, algae, etc. Biodiesel fuels have potential to decrease the demand for fossil fuels. In the following section, detailed information about biodiesel fuels will be given by starting from the general knowledge about biofuels.

2.2. Biofuels

Exhaust gases such as nitric oxides, carbon monoxide, etc. from fossil fuels have a greenhouse effect in the atmosphere leading climate change. Hence, it is necessary to develop renewable energy sources such as hydro-power, solar power, wind power and biofuels [28, 29]. Biofuels can be suitable choice to replace traditional fuels owing to following advantages: being renewable and biodegradable, reducing dependence on fos-

sil resources and decreasing pollutant emissions [7, 30, 31]. Moreover, biofuels can be solid, liquid or gaseous. Liquid biofuels can be alternative fuels to be used in internal combustion engines. Some liquid biofuels such as ethanol and biodiesel show analogous combustion characteristics like conventional fuels [8]. In addition, liquid biofuels can easily take place of fossil fuels in internal combustion engines with little or no changes. Therefore, biofuels have an important issue for both development of new kind of energy resources and engine research.

Liquid fuels are widely used around the world despite being somehow harmful to environment, and they may still be one of the important energy sources in the near future. In 2019, International Energy Outlook (IEA) estimated that liquid fuel consumption would rise from 2018 to 2050 with an average rate of 0.6% annually [32]. Figure 2.1 presents the increase in demand for energy with time by indicating the values in the recent history and the predictions in the near future. Among the solid, liquid and gaseous fuel types, liquid fuels are predicted as primary source of energy up to 2050. For this reason, the use of liquid biofuels needs to be increased in order to reduce the usage of fossil liquid fuels.
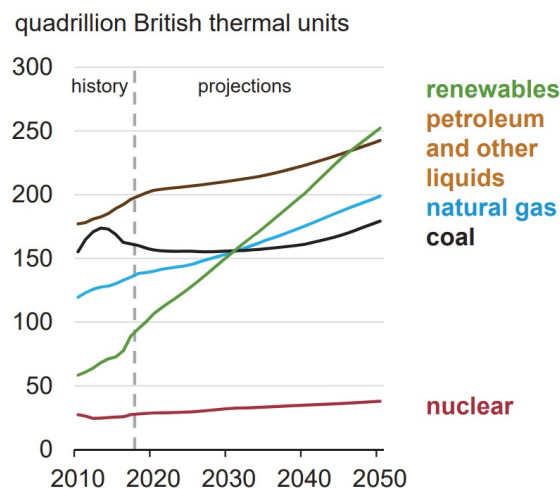
Figure 2.1. Energy consumption around the World from 2010 to now, and projections for 2050 [32].

Considering all types of renewable energy sources, biofuels possess the highest market potential [8]. Therefore, significant number of developing and developed countries have underlined the biofuel production in order to supply energy. In 2018, European

Union aimed at obtaining 32% of their total energy consumption from renewable energy sources up to 2030, and 14% of this 32% of renewable energy will be supplied by biofuels [33, 34]. Alongside, European Union have made several attempts to accomplish the target: investing in infrastructure for biofuel generation, lowering taxes, allowing increase in the percentage of biofuel to be mixed with traditional fuel, etc. [8, 35].

After a brief introduction to biofuels, types and classification of liquid biofuels will be introduced in the followings. After that, the production methods including both conventional and advanced technologies will be briefly stated. After liquid biofuels will be explained in details, a summary on biodiesel fuels which are one of the liquid biofuels will be given.

2.2.1. Types and Classification of Liquid Biofuels

The most important liquid biofuels are primarily biodiesel fuel, bio-jet fuel and bio-alcohols such as ethanol, propanol and butanol [8, 36]. Ethanol, biodiesel, and bio-jet fuels are alternative fuels for gasoline, diesel and jet engines, respectively. Liquid biofuels can be divided into three different generations in which there are different fuels. The difference between these generations is the feedstock used for the production of a specific type of fuel. In the followings, different kinds of liquid biofuels will be explained regarding to their generations as well as feedstocks for these fuels.

2.2.1.1. First Generation Biofuels

The first generation biofuels are produced from food crops like animal fats, vegetable oils, starch, etc. [37]. Wheat, corn, soybeans and sugarcane are the most common resources for the production of first generation biofuels [8]. But, these feed stocks are not sustainable and green due to the competition with food and land uses for food crops.

The most widely used feed stock for producing first generation biofuels, especially ethanol, is corn [38]. There are some advantages of corn as a feed stock for generating biofuel [8]. It is a simple process to obtain ethanol from corn crops. Besides, all parts of the corn can be utilized for the production of ethanol. Also, land use costs are cheap. Furthermore, corn can decrease the demand for gasoline. Conversely, there are some

serious drawbacks of using corn as a source for biofuel production [8]. Corn farming needs fertilizer and pesticides which are expensive and pollutant for the soil and water. Also, corn production rate and the energy generated from the cultivated corn is at very low levels. In addition, the use of corn in biofuel production disturbs the food chain thus increases the food prices around the world. Due to these limitations, corn is not a stable source for the biofuel generation.

Sugar cane is the second important feed stock for generating first generation biofuels especially ethanol [8, 39]. Sugar cane has several advantages as well as drawbacks like corn [8]. Firstly, more ethanol can be obtained by using sugar cane instead of corn. Also, carbon dioxide (CO_2) emission level reduces up to 90% when the biofuel derived from sugar cane is used as fuel instead of gasoline in case land use is not changed [8, 40]. In contrast, cultivation region of sugar cane is very limited, and it is a very important food source for people living in Central and South America [8, 41]. Because of these disadvantages, sugar cane is not a stable source for biofuel production as the situation in corn.

Soybean is the third largest source for first generation biofuel production [8, 42]. Unlike ethanol production from sugar cane and corn, soybean is utilized to produce biodiesel. Although soybean is available in many regions around the world, having severe drawbacks makes soybean the worst feed stock for first generation biofuel production [8, 40, 43]. These drawbacks are: having higher prices and lower energy densities in comparison to corn and sugar cane.

Vegetable oil which can be used for cooking is another resource for first generation biofuel production especially biodiesel [8]. Edible oils have some benefits for production of first generation biofuels as follows: they are widely available all over the world [44], obtaining biofuel from vegetable oils is easy, and these kinds of fuels can be used in compression-ignition engines with little or no changes in these engines. On the other hand, incomplete combustion can be a critical problem when biodiesel fuel derived from any vegetable oil is directly used in a diesel engine [45]. This is the main limitation of vegetable oils.

Lastly, other remarkable feed stocks for first generation biofuels are peanuts [46], rapeseed [47] and sugar beets [48]. Nevertheless, they also have several limitations despite their low usage than main feed stocks. Firstly, food chain is negatively affected when these sources are used as feed stocks for biofuel production. In addition, carbon emission increases when biofuels derived from these sources are utilized [8].

2.2.1.2. Second Generation Biofuels

Since the feed stocks used for the first generation biofuels constitute food, the need to utilize second generation biofuels arose. The primary distinction between the first and second generation biofuels is the source. The food crops which are sources of first generation biofuels are not normally sources of second generation biofuels. For instance, vegetable oil is a source for first generation biofuels. However, waste vegetable oil (WVO) is utilized to produce second generation biofuels. The only situation that food crops are resources of second generation biofuels is when a food is not desired to meet human's need [49]. Some of the most common feed stocks for second generation biofuels are grasses, lignocellulosic biomass, waste vegetable oil and some seed crops especially jatropha [8].

Lignocellulosic biomass, which is the biggest source of second generation biofuels mainly ethanol [50], is obtained from plant biomass consisting of cellulose and lignin. Cellulose is one kind of a sugar, and it is found in walls of plants as a main segment. Lignin improves hardness of plant walls by filling the spaces between cellulose molecules. Carbon, hydrogen and oxygen are found in lignocellulose that can be utilized to produce biofuel especially ethanol [8]. There are some positive sides of lignocellulosic biomass as a source for biofuel production. Primarily, lignocellulose cannot be eaten hence it is an insignificant part of the plants for humans' need. As another advantage, producing ethanol from lignocellulose has positive effects on the environment. Because, huge amounts of lignocellulosic biomass is produced and wasted every year in the USA. This quantity is sufficient to meet the need for oil in the USA annually. In cases which this lignocellulose is not converted into biofuel, it can decompose into methane which is 21 times harmful for the environment than CO_2 [8]. Furthermore, ethanol generated from lignocellulosic biomass can produce more energy up to 5 times than ethanol generated from corn, and this kind of ethanol can decrease greenhouse gas emissions up to 115% [8].

Jatropha is the second important feed stock for second generation biofuels [8]. Oil extraction from seeds of jatropha is high, and this amount is around 50% [51]. Besides, different biofuels can be obtained by using different parts of jatropha. Usually, biodiesel is derived from seeds. The remaining parts of jatropha can be used to obtain solid biofuels and syngas [8]. The most important advantage is that jatropha can be grown up in all kinds of terrain, and it can be cultivated in lands where most of the food crops cannot be cultivated. This emphasizes that biofuel production from jatropha which is non-edible

oil does not threaten the food supply of the world [52]. However, oil extraction amount reduces fairly as the quality of the land decreases. Additionally, greenhouse gas emissions rise when the biofuel derived from jatropha is used [8].

Like jatropha, camelina which is a seed crop can be used to obtain second generation biofuel mostly biodiesel and jet fuel [53]. Nevertheless, there are some limitations about camelina. Greenhouse gas emissions raises when the biofuel derived from camelina is utilized. Besides, double lands are needed for camelina to get the same amount of biofuel as the amount of biofuel from jatropha [8].

Some other seed crops like rapeseed and palm oil can be used to produce second generation biofuel. Yet, they have almost the same problems like camelina and jatropha [8]. However, these disadvantages can be equilibrated by the demand to use crop area to get acceptable yields.

For a while, biofuels derived from waste vegetable oils have been utilized in diesel engines. They are also second generation biofuels. Because, they do not damage the humans' food chain as a result of already completing the utility as a source for food. Besides, the main advantages of WVOs are easy conversion to biodiesel, availability in all regions in the world and easy adaptability to diesel engines [54, 55]. Even, they can be directly utilized in diesel engines. Contrarily, the need for filtering which increases the cost is a disadvantage for WVOs. If they are properly refined and perfectly blended with conventional diesel fuel, these kind of fuels can be the most promising biofuels in order to meet the need for fuel [8].

2.2.1.3. Third Generation Biofuels

Some important disadvantages of first generation and second generation biofuels such as breaking the food chain, large amount of water usage and raising the pollutant emissions led researchers to develop new kinds of biofuels [8]. In this way, the third generation biofuels emerged. Algae and microbes such as yeast, microalgae and fungi can be utilized to produce third generation biofuels [30]. However, the majority of third generation fuels are produced from algae.

Algae has a lot of advantages as a resource for biofuel generation. Firstly, algae can cultivated in different systems such as open ponds, closed-loop systems, photobioreactors and algae scrubbers. In open ponds, cultivation of algae is realized in open air.

This process is simple and cheap [8]. However, it takes long time to grow algae with this method [56]. Other drawback of this technique is the probability of algae being damaged by other organisms which can contaminate the ponds [57]. Closed-loop systems are similar to open ponds. The main distinction is that closed-loop systems have no interaction with the open atmosphere as open ponds [8]. These kinds of systems use barren carbon dioxide sources. The primary advantage of closed-loop systems over open ponds is that they have a direct connection with the source of CO_2, and they are able to use the gas before releasing it to the environment [58]. Like closed-loop systems, photobioreactors (PBR) are closed systems. A PBR is a bioreactor which uses a light source to cultivate algae. These organisms utilize photosynthesis to produce biomass from the light and CO_2. Although running a PBR is difficult and expensive, productivity of this process is higher than open ponds and closed-loop systems [59, 60]. Besides, algae can be grown in an algae scrabber which is a system designed mainly to remove contaminants and nutrients from water by utilizing algal turfs. Algae can be harvested in 5-15 days with this method [61], and 18000 kg of algal biomass (dry weight) can be cultivated in a hectare per year [62]. Besides, the cost can be very low for algae scrubbers [62]. These processes show that algae cultivation is possible at nearly everywhere. The only condition to produce algae is warm temperature [8]. Also, there is no threat for farm lands because of the production of algae. Algae can be cultivated by closed-loop systems and photobioreactors in deserts [63]. Even, they can be produced in waste water [64].

Secondly, energy density of biofuel derived from algae is high. For example, energy density of third generation biofuels can achieve up values to 123 MJ/kg while first and second generation biofuels can have values up to 48 MJ/kg and 38 MJ/kg, respectively [8]. Thirdly, algae can catch carbon dioxide emitted from power plants, industry or other carbon dioxide resources [30].

On the other hand, algae have some drawbacks to be overcome in order to fully make use of. First of all, algae cultivation requires high amount of nitrogen, waste water and fertilizer [65]. Also, greenhouse gas emissions rise when producing this large amount of fertilizer above the levels recovered by algae. However, this situation normally happens for large scale operation. For instance, in order to obtain 38 billion liters of third generation biofuel from algal resources, 6 million metric tonnes of nitrogen and around 125 billion liters of water are required [8]. Therefore, huge amounts of fertilizer production are required to cultivate algae well. Producing huge amounts of fertilizer would eventually rise the pollutant emissions which algae cannot recover. Namely, energy needed to

grow algae is more than the energy obtained from them. In case of small scale operation, the situation is opposite. Nitrogen can be obtained from the waste water with recycling that can provide major portion of the nitrogen required [8]. This reduces the increase in greenhouse gas emissions. In addition to this disadvantage, biofuel derived from algae is less stable when compared the first and second generation biofuels. When compression-ignition and sprak-ignition engines are operated with algal biofuels, some engine parts may be damaged [8].

2.2.2. Production Methods of Liquid Biofuels

All kinds of liquid biofuels are derived from biomass feed stocks. In the followings of this section, first generation biofuels will be named as conventional biofuels while second and third generation biofuels will be named as advanced biofuels regarding to resource type used and variations in production methods. Conventional liquid biofuels cover biodiesel obtained from vegetable oils and even waste cooking oils, which are produced for commercial purposes in many countries, and bioethanol derived from plants having sugar and starch. On the other hand, advanced biofuels include biofuels obtained from lignocellulosic biomass or algae. Below, both conventional and advanced biofuel production technologies will be explained.

2.2.2.1. Traditional Technologies for Biofuel Production

Ethanol and biodiesel are the most well-known conventional biofuels. Ethanol is alternative for gasoline, and biodiesel is alternative for diesel fuel. Figure 2.2 shows conventional biofuel production techniques.

Ethanol is produced via three consecutive processes which are respectively pre-treatment, fermentation and distillation [8]. First process is pre-treatment process which commonly consists of wet and dry milling. In wet milling, crops are chemically subdivided into starchy parts. In dry milling, granules are obtained by grinding the unprocessed seeds. Then, fermentation process takes place, and ethanol-water mixture is obtained. Following the fermentation process, distillation process is applied to remove the water from ethanol. Thence, ethanol is made ready to be blended with gasoline.
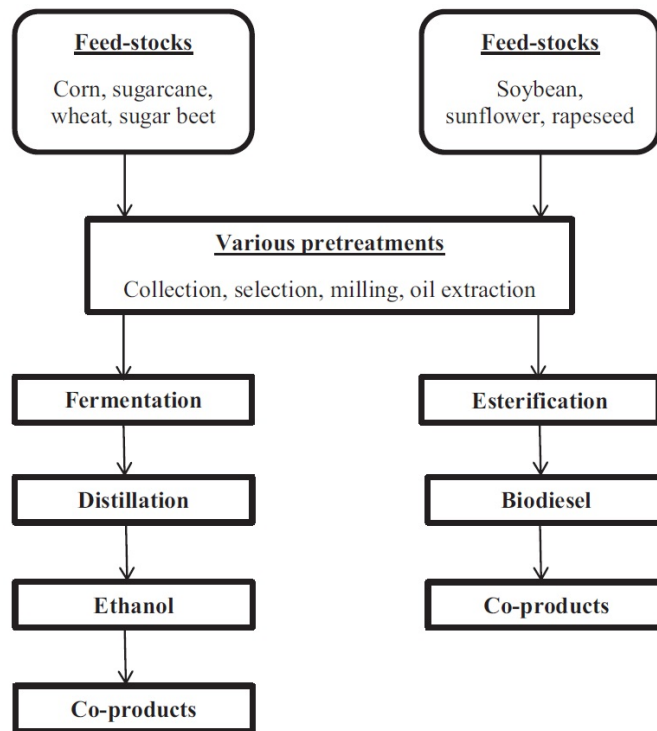
Figure 2.2. Processes for conventional biofuel production [8].

Biodiesel production method is transesterification process. In this process, feed stock such as vegetable oil or animal fat is combined with alcohol to produce biodiesel fuel in the presence of catalysts such as KOH, NaOH, etc. Mostly, methanol is utilized to produce biodiesel. Other alcohols such as ethanol, propanol and butanol can also be utilized [16, 17]. Detailed information about transesterification process, which is the method applied in this study, will be given in Section 3.1.

2.2.2.2. Advanced Technologies for Biofuel Production

Feedstocks for advanced biodiesel fuels are non-food feedstocks. There are several processes to convert these feed stocks into fuel. These processes can be grouped as bio-chemical and thermo-chemical processes [66]. Figure 2.3 shows the summary of advanced technologies for biofuel production.

Two methods which are fermentation and anaerobic digestion are bio-chemical conversion processes [66]. In anaerobic digestion, bacteria is utilized to convert the feed stock into gaseous fuels. In fermentation process, cellulose of lignocellulosic feed stock
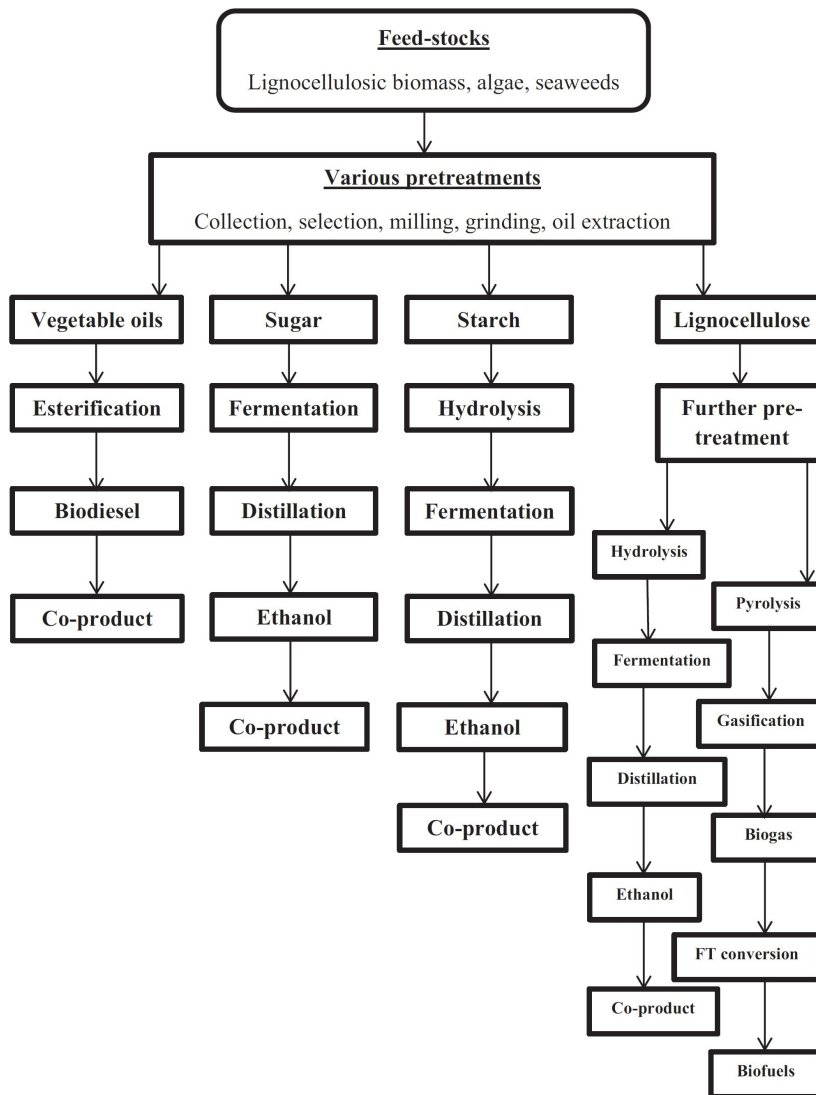
Figure 2.3. Advanced technologies for biofuel production [8].

is firstly converted into sugars which are then transformed into ethanol by using yeasts. As it is seen in Figure 2.3, pre-treatment is required before the fermentation process in order to remove lignin. However, this lignin is not a waste, but a by-product that can be utilized in power generation [8].

In thermo-chemical conversion processes, pyrolysis, gasification and liquefaction can be applied to produce biofuels [66, 67]. Different biofuels can be produced with different techniques from various biomass feedstocks. Besides, all processes require different pre-treatment steps for the feedstocks and varied operating conditions. Also, some methods can have various upgrading processes to obtain biofuels. Gasification process can be used to produce liquid biofuels. Firstly, syngas is obtained in this process.

However, syngas must be upgraded. Fischer-Tropsch (FT) synthesis is a well-established method to convert the syngas into biofuels such as diesel, gasoline and jet fuel [8]. Low temperature FT process is used in order to obtain jet fuel and diesel fuel while high temperature FT process is utilized to obtain gasoline. Also, different products such as hydrogen, ethanol or methanol can also be obtained from syngas. Besides that, it is possible to produce bio-oil in the gasification stage. When temperature reaches to 300 °C in the gasification stage, process can be stopped then bio-oil can be obtained [8]. An alternative method to produce biofuels is liquefaction. Algae can be feed stock for hydrothermal liquefaction [68]. Wet algae is processed in this process, and crude oil is obtained from algae. After refining this crude oil, different biofuels can be obtained including diesel, gasoline and jet fuel. Pyrolysis method is another process to produce biofuels. It is a thermal decomposition of biomass feedstocks in the absence of oxygen. Liquid, solid and gaseous products can be obtained with different chemical reactions. These products in three different phases are every time produced yet their proportions can be different from process to process depending on the operating conditions [66]. Different pyrolysis technologies are available, such as fast, slow, intermediate, flash, vacuum and ablative pyrolysis [69, 70, 71, 72]. Fast pyrolysis process is nowadays of attention because the liquids obtained as a result of fast pyrolysis could be stored, transported and utilized for different purposes such as being fuels for transportation, carrying energy or becoming chemicals [66]. In this process, biomass decomposes into vapour, gas and charcoal. After condensation of this gas, bio-oil is obtained. Then, this bio-oil can be converted into biodiesel fuel by refining it.

2.2.3. Summary on Biodiesel Fuels

Biodiesel is an alternative fuel for diesel engines. Biodiesel fuels can be originated from first, second, and/or third generation feedstocks. Plenty of vegetable or animal resources can be used as feedstocks for biodiesel production. Some of the feed stocks are vegetable oils like corn oil and canola oil, animal fats, lignocellulosic biomass, jatropha, camelina, waste vegetable oils, algae, etc.

Several different processes can be employed for biodiesel production as explained in Subsection 2.2.2. Among the available techniques, transesterification is the most common method owing to being cheap and simple.

In transesterification, ester bonds occur as a result of esterification of vegetable oil or animal fat with alcohols in the presence of a catalyst. Although different alcohols can be utilized for biodiesel production, methanol is the most common alcohol for biodiesel production. Also, ethanol can be a good alternative instead of methanol. Biodiesel fuels derived from methanol and ethanol are called as methyl ester and ethyl ester, respectively. Moreover, higher alcohols such as propanol and butanol can also be used to generate biodiesel fuel.

The generation does not depend on the production method of biodiesel fuel. For example, first, second and third generation biodiesel fuels can be produced through transesterification. Biodiesel fuel derived from edible oil is first generation biofuel while biodiesel fuel derived from waste vegetable oil is second generation biofuel. Besides, biodiesel fuel can be obtained by transesterification of algal oil. This type of fuel is an example for third generation biofuels.

2.3. Essential Features of Combustion Process in Diesel Engines

In a diesel engine's cylinder, fuel is directly injected by an injector to combustion chamber which is filled with air towards the end of the compression stroke. Then, fuel vaporizes and mixes with the air. Load control is provided by injection quantity per each cycle. During the compression stroke, pressure and temperature of air rises beyond the fuel's ignition point. Once this point is reached, sudden combustion starts, and it continues up to early stages of expansion stroke. Heat is released as a consequence of combustion process, and pressure inside the cylinder increases. Sharp increase can be observed in heat release rate and in-cylinder pressure. Afterwards, flame quenches and combustion event is completed. Figure 2.4 shows the pressure variation in the cylinder against the crank angle [6].

Combustion in a diesel engine is a complex process. It is heterogeneous, three-dimensional and unsteady combustion. Fuel properties, characteristics of injection system and combustion chamber design affect the process. Therefore, complete explanation of the diesel combustion cannot be expressed although understanding at a good level has been reached [6].

However, compression-ignition engines have some advantages over spark-ignition engines to make them desirable. These advantages are as follows:
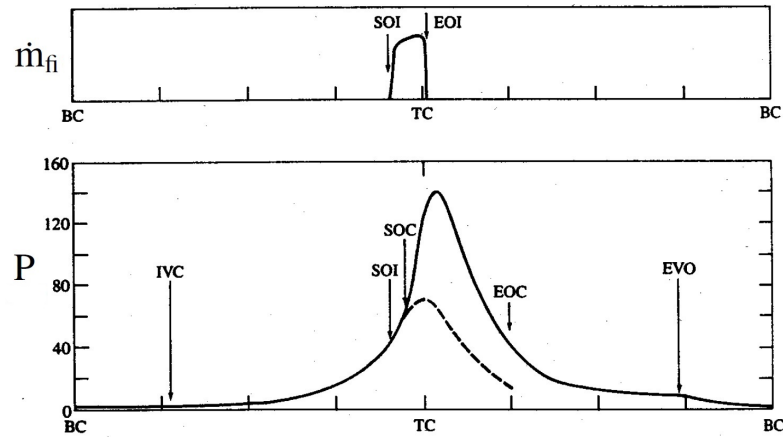
Figure 2.4. Events in the compression and expansion strokes. Injection rate of fuel $\dot{m}_{fi}$, in-cylinder pressure P (dashed line: motored cycle, solid line: firing cycle) diagrams are plotted versus crank angle degree. SOI: start-of-injection, EOI: end-of-injection, IVC: intake valve closing, EVO: exhaust valve opening, SOC: start-of-combustion, EOC: end-of-combustion [6].

- Knock can not occur in a diesel engine because combustion starts as soon as the fuel is injected into the cylinder. Thence, higher compression ratios can be utilized in CI engines resulting in higher thermal efficiencies than those of spark-ignition engines.

- The load thus the torque output of diesel engines is determined by the injection quantity. Therefore, throttles which lead pumping work are not needed.

- Normally, diesel engines operate with lean mixtures of fuel-air [6]. Therefore, the effective value of specific heat ratio γ (c_p/c_v) is higher than as it is in a spark-ignition engine. This is another reason why CI engines have higher fuel conversion efficiencies than SI engines.

2.3.1. Combustion Phases

Combustion phases are defined in order to better explain the combustion process. These phases can be shown in a typical heat-release-rate diagram versus crank angle degree as it is seen in Figure 2.5. Combustion phases in a diesel engine are divided into 4 groups which are ignition delay period, premixed combustion phase, mixing-controlled combustion phase and late combustion phase.
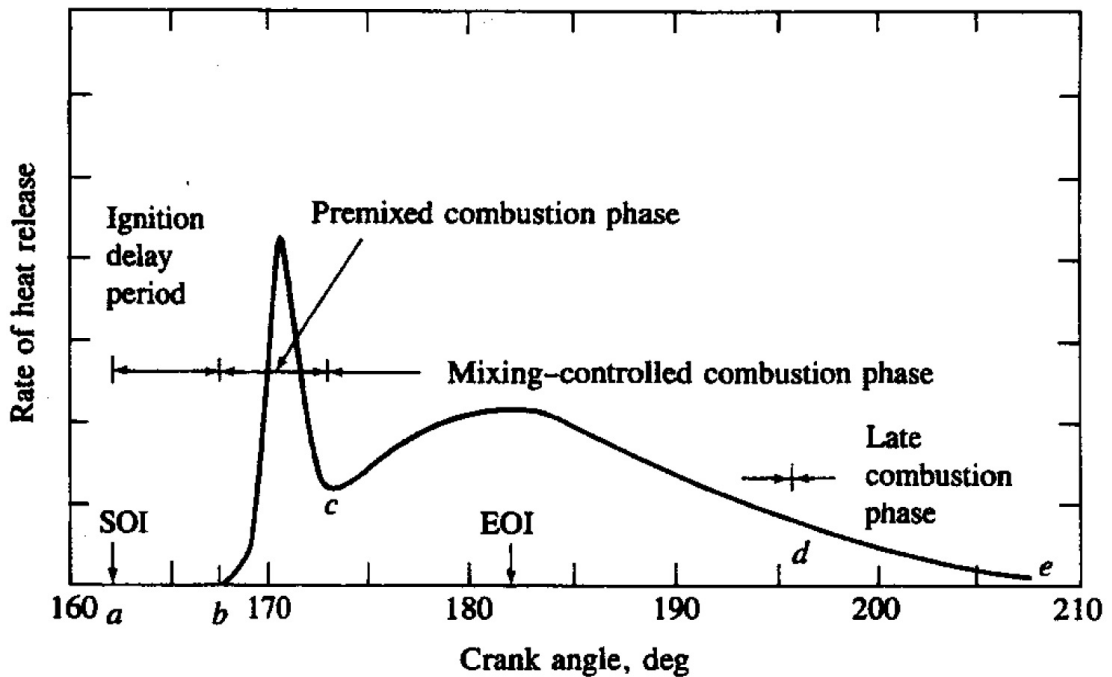
Figure 2.5. General heat-release-rate diagram indicating the combustion phases in a CI engine [6].

- Ignition delay period: It is the period between the first droplet of fuel enters the cylinder and the first flame is seen. Namely, it is the duration between start of injection and start of combustion.

- Premixed combustion phase: When the temperature inside the cylinder reaches the fuel's ignition point, the fuel-air mixture prepared in the ignition delay period is burned in a few crank angle degrees. Rapid increase in heat release rate is achieved. Most of the power is produced in this phase.

- Mixing-controlled combustion phase: After bulk of fuel-air mixture is burned, heat release rate is controlled by the mixture available for burning. Mainly, the fuel vapor-air mixture controls the burning rate [6]. Heat-release-rate might have a second peak which is lower than the peak in the premixed combustion phase or any second peak might not be observed.

- Late combustion phase: During the expansion stroke, heat release may continue lowly because of the following reasons: there may be still unburned fuel available for combustion, and/or fuel-rich combustion may have a fraction of energy and may release this energy [6].

2.4. Emissions from Diesel Engines

Compression-ignition engines are one of the significant sources of air pollution. Important pollutants are nitric oxides, unburned hydrocarbons and soot. Formation of these pollutants depends on different parameters such as engine design, fuel properties, operation parameters, etc. This section explains the pollutant emissions from diesel engines in terms of formation mechanisms.

2.4.1. NO$_x$

Nitric oxides (NO$_x$) are referred to both nitric oxide (NO) and nitric dioxide (NO$_2$). However, NO is the dominating one [73, 74]. Three different reasons cause the NO formation. The first and the most dominant one is the **thermal formation of NO**. Nitrogen does not normally react with oxygen yet it oxidizes at higher temperatures (above 1800 K) [75]. NO formation mechanisms were explained by Zeldovich [74] (Equations 2.1 and 2.2) and Lavoie [6] (Equation 2.3) as follows:

$$O + N_2 = NO + N \tag{2.1}$$

$$N + O_2 = NO + O \tag{2.2}$$

$$N + OH = NO + H \tag{2.3}$$

Secondly, **prompt formation of NO** is also important mechanism in fuel-rich combustion processes at low temperatures this once. Prompt mechanism which is shown in Equations 2.4 and 2.5 is also known as Fenimore mechanism [73, 76]. Fenimore states that free radicals in flame front cause the formation of NO in a rapid way. Prompt NO is less significant compared to thermal formation of NO. However, major quantities of NO are occured by prompt mechanism when biodiesel is used [73]. Prompt mechanism is as follows:

$$C_2 + N_2 = 2CN \tag{2.4}$$

$$CN + O_2 = NO + CO \tag{2.5}$$

Thirdly, NO can be formed from **N₂O pathway** [73]. This mechanism is observed at elevated pressure when lean fuel-air mixtures are used. The mechanism begins with Equation 2.6:

$$O + N_2 + M = N_2O + M \tag{2.6}$$

where M is any molecule that is needed to accomplish the reaction. Then, N_2O is converted to NO by the following reaction (Equation 2.7):

$$N_2O + O = NO + NO \tag{2.7}$$

Although NO is the dominant pollutant among nitric oxides, NO_2 is also important for diesel engines [6]. Nitric oxide can be converted to nitric dioxide during the combustion as it is seen in Equation 2.8.

$$NO + HO_2 = NO_2 + OH \tag{2.8}$$

If NO_2 formed within the flame is not extinguished with a cooler fluid, this NO_2 is subsequently converted to NO through:

$$NO_2 + O = NO + O_2 \tag{2.9}$$

This expression is coherent with the biggest NO_2/NO ratio happening in diesel engines operating with higher loads, when cooler regions that can lead the conversion of NO_2 to NO are widely present.

2.4.2. Particulate Matters

Particulate matters (PM) are very critical for diesel combustion. Particulates are divided into three groups which are soluble organic materials, sulphate particles and most widely soot [2].

Soot forms in the core of fuel spray in combustion environment at temperatures varying between 1000 and 2800 K [6]. Several stages are involved for soot generation, and they can be explained as follows:

- The first step is particle formation. Oxidation of fuel molecules constitute the first condensed material. Also, pyrolysis products which are unsaturated hydrocarbons can lead the formation of the first condensed material. These first particles are very small in diameter (d<2 nm) [6]. Nonetheless, they are grown-up in the later stages.

- Particle growth consists of surface growth, coagulation and aggregation [6, 77]. Gas-phase species attached to the surface of particulates, which is known as surface growth. Increase in the amount of soot is observed by the surface growth reactions while the number of particles are constant. Reverse is valid for growth by coagulation in which particles collide and coalesce. In this once, the amount of soot is constant while the number of particles decreases.

Total amount of soot emission depends on the balance between formation and burnout. Then, further mass addition to the emitted soot takes place in the exhaust system, and new particles occur by the adsorption into soot particle surface.

2.4.3. Unburned Hydrocarbons

Unburned hydrocarbons (HC) form in places where flame quenches on piston bowl or combustion chamber walls [6]. Namely, incomplete combustion causes hydrocarbon emissions. Different hydrocarbons can be emitted from a CI engine, which are paraffins, olefins, acetylene, aromatics, etc. [6]. Fuel composition directly affects composition of HC emissions. Two different significant reasons also cause HC emissions: (1) leaner mixtures than the diesel operating mixtures, (2) some portions of fuel may leave the nozzle after bulk of the fuel has burned. As a consequence of first reason, over lean mixtures decrease the possibility of autoignition resulting in incomplete combustion.

2.4.4. Carbon Monoxide

Carbon monoxide (CO) emissions are related with fuel/air equivalence ratio. Gasoline engines often operates with rich mixtures at full load. Whereas, diesel engines operate

with lean mixtures. Therefore, CO emissions are significant for gasoline engines while diesel engines emit low levels of CO [6]. Hence, formation of CO emissions in diesel engines will not be explained further.

2.5. Spray Formation in Diesel Engines

Spray investigation is crucial for diesel engines. Because, spray directly affects the performance, fuel consumption and emissions. Measuring spray parameters can help researchers understand how any fuel propagates in the cylinder, and how it mixes with air depending on the physical properties of that fuel. Therefore, researchers have focused on this topic while developing new fuels. In this section, fundamentals of diesel sprays are explained.

2.5.1. Injection System

The purpose of an injection system is to vaporize fuel in a higher degree in order to achieve a good fuel-air mixture thus the combustion. Nowadays, two different high-pressure injection systems are available for diesel engines. These are common rail injection system and unit injection system. Among them, common rail injection system is more widespread [78].

For common rail injection systems, injection system consists of a fuel tank, low and high pressure pumps, delivery pipes, a common rail and fuel injectors as it is seen in Figure 2.6. Number of the injectors depends on design of the engine. In general terms, fuel tank stores the fuel to be used. Then, fuel goes through low pressure pump connecting with high pressure pump via delivery pipes. The reason why two pumps are utilized is to prevent vaporization of fuel in injection system. Namely, fuel can vaporize when pressure suddenly changes. It needs to be increased step by step. Low pressure pump increases the pressure of the fuel to a level. Then, fuel goes through the high pressure pump which supplies the fuel to common rail. The common rail distributes the fuel to different injectors at the desired pressure level. Consequently, injector releases the fuel into the cylinder. Moreover, excess fuel from both the injector and the common rail goes to the fuel tank via return lines.
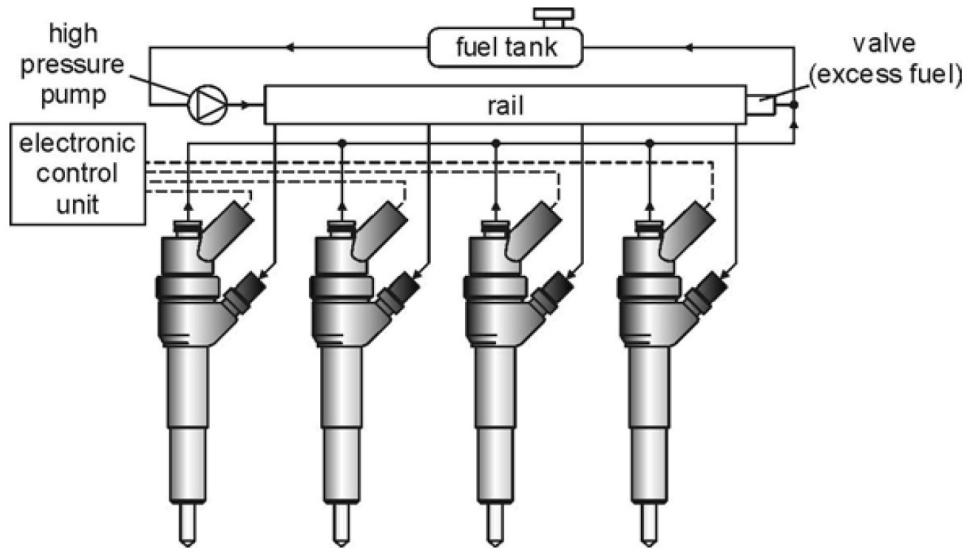
Figure 2.6. Schematic sketch of a common rail injection system [78].

Two different injector types are available for diesel engines that have a common rail system, which are solenoid injector and piezoelectric injector. Schematic sketches of solenoid and piezoelectric injectors are given in Figures 2.7, 2.8 and 2.9. Both of them have advantages and disadvantages. The technology behind solenoid injectors are traditionally reliable, cost-effective, and the physical unit of a solenoid injector is smaller than the physical unit of a piezoelectric injector [79]. Against, piezoelectric injectors vibrate less than solenoid injectors thence creating less noise [80]. Less power is required to operate a piezoelectric injector [79]. Moreover, the dynamic response of a piezoelectric injector is better than a solenoid injector [81].

For a solenoid injector (see Figure 2.7), injection event takes place by a needle inside the injector. Needle movement of the injector is hydraulically controlled by a solenoid valve [78]. The needle of injector is kept close by the spring force (F_{spring}) and the hydraulic force (F_1) of fuel located at control chamber. The summation of F_{spring} and F_1 is bigger than the hydraulic force (F_2) caused by fuel located in the circular ring area above the needle. When the valve is opened, the pressure above the control rod thus F_1 gets smaller resulting in opening of the needle. Then, fuel leaves the injector from its nozzle, and injection event starts. Excess fuel inside the injector to be recirculated goes to fuel tank through the return of the injector. After the required amount of fuel is injected, valve closes the needle. In addition, the opening and the closing speeds of the needle are influenced by the size of throttle [78].
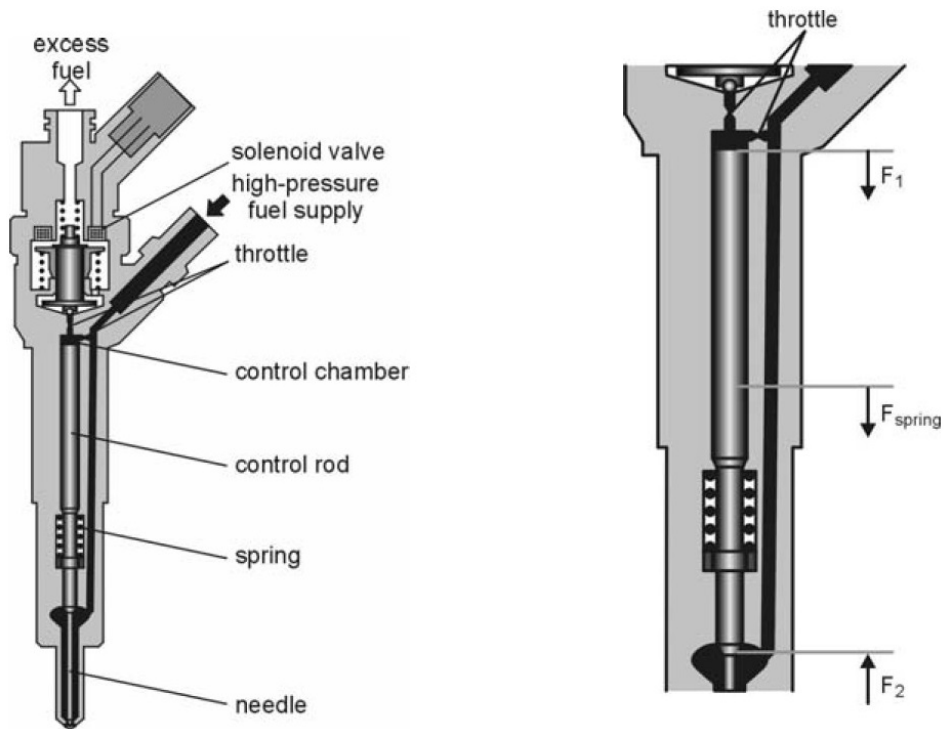
Figure 2.7. Schematic sketch of a typical solenoid injector [78].

For piezoelectric injectors, two different concepts can be applicable, which are indirect and direct needle control [78]. First type is the piezoelectric injector with indirect needle control (see Figure 2.8). The injector consists of four main components that are piezo stack, hydraulic coupling device, control valve and the nozzle module. Firstly, common rail system continuously delivers fuel at high pressures to the injector tip which is closed by a needle. Also, this high pressure fuel is delivered to top of the needle, causing a force that keeps this needle closed. Next, the elongation of the piezo stack is amplified, and piezo stack is then transferred to the control valve by the hydraulic coupling device. Then, control valve opens, and high pressure fuel at top of the needle goes to fuel tank through return line. As the pressure above the needle decreases, the needle moves upwards, opens the injector tip, and fuel is injected into the cylinder. After the required amount of fuel is injected, the piezo stack is de-energized, and the control valve closes. Then, pressurized fuel pushes the needle to its initial position. Additionally, this injection technique can achieve up to five injections in one cycle with variable timings, and very small amounts of fuel can be injected [78].

Piezoelectric injectors with direct needle control can achieve more flexibility, because it is easy to realize partial needle lifts [78]. Such an injector is presented in Figure
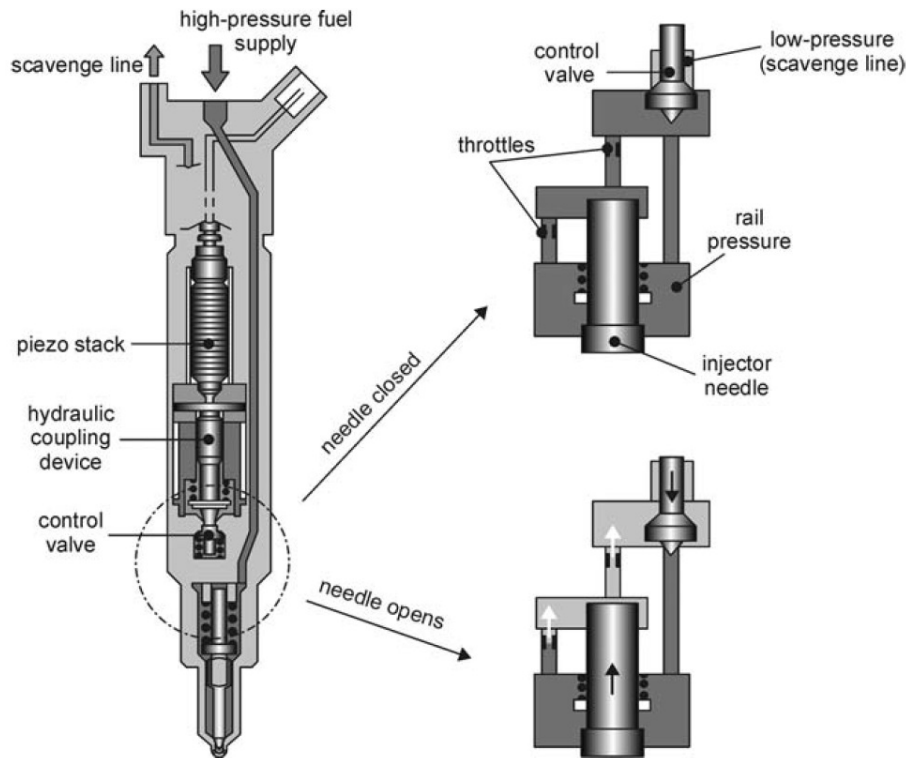
Figure 2.8. A piezoelectric injector with indirect needle control [78].

2.9. In these types of injectors, piezo stack is directly connected to injector needle with a connecting rod. Therefore, the needle lift can be directly proportional to the voltage, and partial lift can be achieved by adjusting the voltage between zero and a maximum value. This maximum value is determined by the maximum elongation of the piezo stack. Besides, different injection rate shapes can be realized by controlling the voltage accordingly [78].
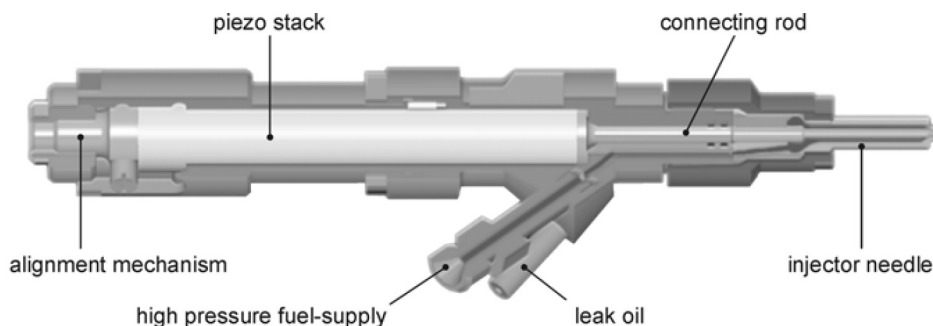
Figure 2.9. A piezoelectric injector having direct needle control [78].

2.5.2. Break-up Regimes of Liquid Jets

Break-up length is the length between the nozzle tip and the point where the first droplet forms. Different mechanisms cause a liquid jet to disintegrate depending on the properties of the fuel and air. Reitz and Bracco stated that break-up regimes could be divided into the Rayleigh regime, the first wind-induced regime, the second-wind induced regime and the atomization regime [82]. Figure 2.10 shows these regimes on Ohnesorge diagram which is derived from Reynolds number (Re) and Ohnesorge number (Z). Reynolds number is

$$Re = \frac{u_l D \rho_l}{\mu_l} \tag{2.10}$$

where u is the jet velocity, D is the characteristic length (which is nozzle hole diameter in this case), ρ is the fuel density, μ is the fuel viscosity, and l indicates the liquid phase. Ohnesorge number is

$$Z = \frac{\mu_l}{\sqrt{\sigma \rho_l D}} \tag{2.11}$$

where σ is the surface tension at the interface (liquid-gas). On the Ohnesorge diagram, regime changes from the Rayleigh regime to the atomization regime when Re increases.
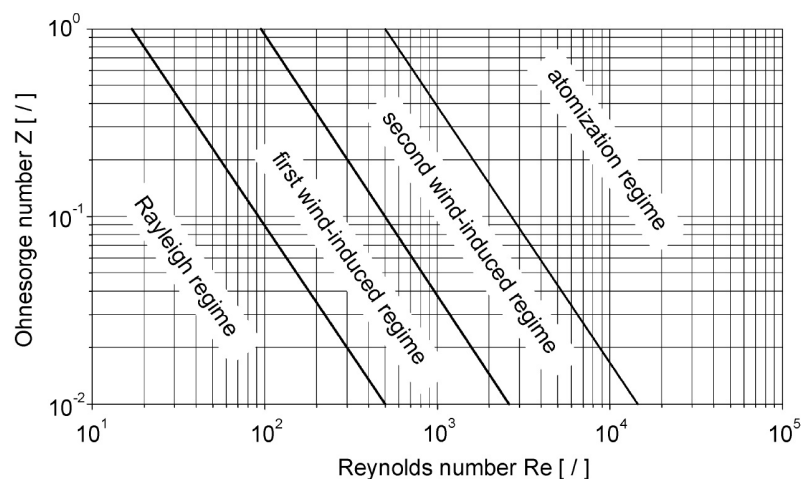
Figure 2.10. Ohnesorge diagram indicating the break-up regimes of liquid jets [78].

Firstly, drip flow is observed at very low velocities, and no jet is observed. As the velocity of liquid fuel increases, jet is formed. Then, some droplets are disintegrated from the unbroken jet. This break-up is called as Rayleigh break-up [78]. Rayleigh regime is observed at low velocities. Surface tension forces and fuel inertia causes the axisymmetric oscillations in the liquid jet resulting in break-up. The droplets are larger than the diameter of the nozzle.

As the jet velocity increases more, break-up length decreases but it is still larger than diameter of the nozzle. On the other hand, droplet sizes are comparable to nozzle diameter. This regime is called as the first wind-induced regime. The forces acting in the Rayleigh regime are amplified by aerodynamic effects [82].

A further increase in flow velocity makes the liquid jet turbulent. Surface waves are initiated unstably by turbulence and amplified by aerodynamic forces [78]. Then, jet break-up occurs as a consequence of surface waves. This regime is named as the second wind-induced break-up regime [82]. In this regime, droplet sizes are smaller than the nozzle diameter. Besides, a raise in Reynolds number shortens the break-up length.

The last regime is the atomization regime [78] in which the break-up length approaches to zero. A conical spray occurs, and this spray is initiated when the fuel jet leaves the nozzle. Fuel mixes with air then vaporizes. Droplets developed in this regime are much smaller than the nozzle diameter. Furthermore, liquid phase may still be in the spray core.

a) Rayleigh   b) First wind induced   c) Second wind induced   d) Incomplete atomization   e) Complete atomization
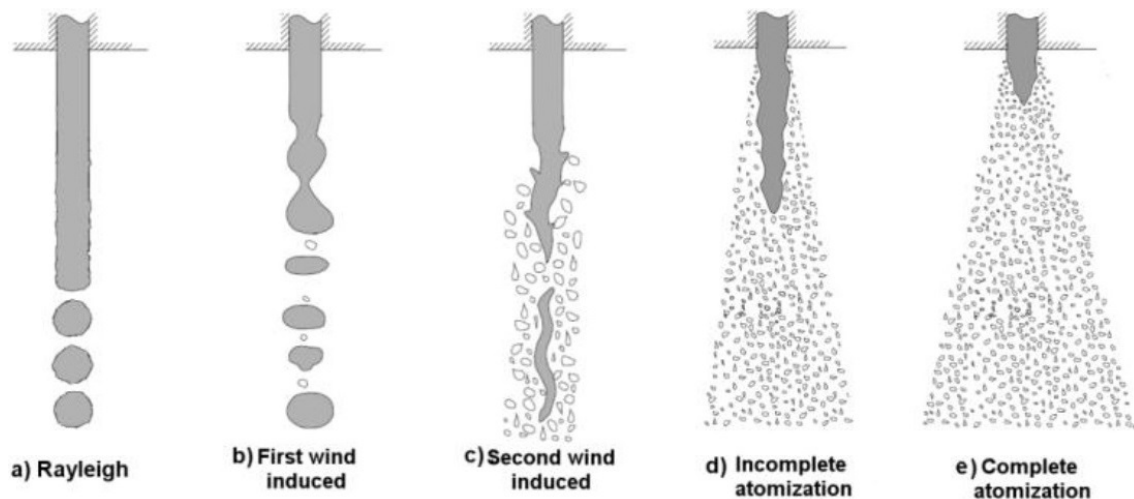
Figure 2.11. Jet break-up regimes [83].

All regimes are shown in Figure 2.11. The atomization regime is the regime in which the fuel most propagates inside the cylinder. Therefore, the atomization regime is the most proper regime for a diesel spray to achieve a good fuel-air mixture.

2.5.3. Break-up Regimes of Liquid Drops

Break-up of liquid drops occurs by friction and pressure [78]. Relative velocity between droplet and the gas, u_{rel}, causes these aerodynamic forces resulting in developing of waves on the interface. Consequently, disintegration takes place to form smaller droplets which are then again induced break-up by aerodynamic forces. Conversely, surface tension forces try to prevent the droplets being deformed. The surface tension force has a relationship between the curvature of droplet surface. When the size of droplet is small, the surface tension effect gets larger thus the relative velocity that causes to disintegration. Weber number in the gas phase describes this behaviour. This number depends on the droplet diameter (d) and the gas density (ρ_g). Equation 2.12 [78] shows the gas phase Weber number:

$$We = \frac{(\rho_g u_{rel}^2 d)}{\sigma} \qquad (2.12)$$

where σ is the surface tension between the liquid and surrounding gas. In other words, the Weber number symbolizes the ratio of aerodynamic forces to the surface tension effects.
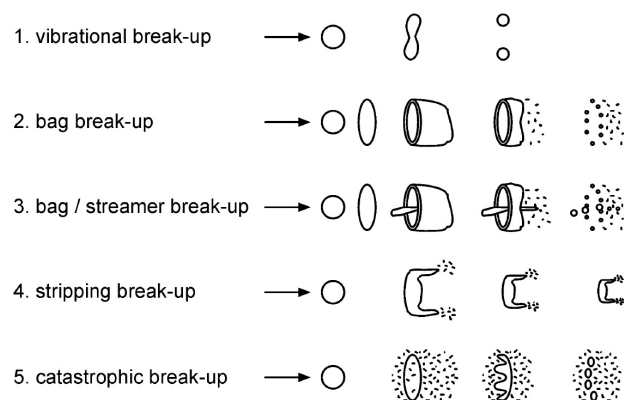
Figure 2.12. Break-up regimes of liquid drops [78].

Experimental investigations showed different break-up mechanisms [78, 84, 85], and Figure 2.12 gives a summary about these drop break-up regimes. All of these mechanisms are observed in a diesel spray. Disintegration process is mostly observed near the nozzle tip at large Weber numbers, on the other hand, Weber number decreases away from the nozzle. Because, evaporation, previous break-up and drag forces negatively affect the Weber number.

2.5.4. Structure of a Full-Cone Spray

An example of a full-cone diesel spray is shown in Figure 2.13. As it is seen in the figure, the maximum length between the injector nozzle, and the farthest point on the spray axis is called as spray penetration length, and the angle between the nozzle and two farthest apart points on the outer spray boundary is called as spray cone angle. These two parameters are so important to observe how much spray spreads in the cylinder.
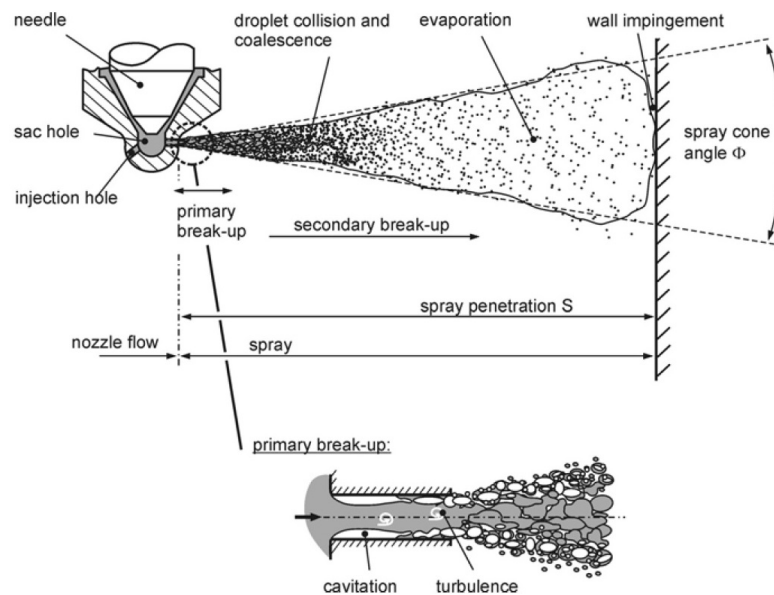
Figure 2.13. Structure of a full-cone spray [78].

When the fuel spray enters into the combustion chamber, it begins to break-up and forms a conical shape. This first formation of the liquid break-up is called as primary break-up. Turbulence characteristics of flow and cavitation are the main-break up mechanisms for primary break-up. Then, new droplets occur from the existing ones because of
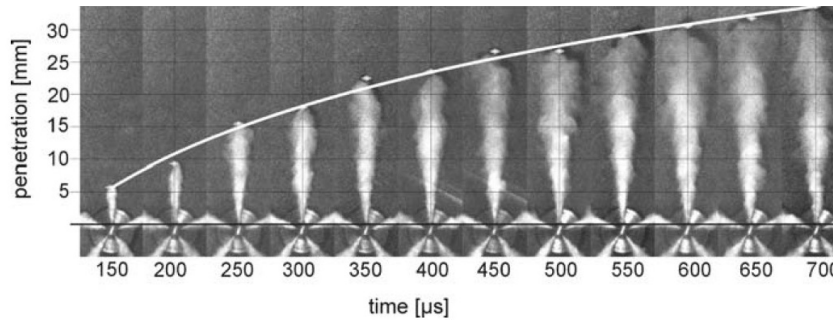
Figure 2.14. Example spray development where rail pressure and back pressure are respectively 70 and 5 MPa, and air temperature is 890 K [78].

the aerodynamic forces. This break-up is called as secondary break-up. The droplets of secondary break-up are smaller than the primary one.

Droplets are decelerated by aerodynamic forces. The strongest drag force thus the largest deceleration is experienced at the spray tip. Therefore, new droplets are replaced with the new droplets at the spray tip, and spray penetration length (S) continuously increases as it is seen in Figure 2.14 [78]. The outer spray region is formed by droplets having low kinetic energy because they are pushed aside. Then, a conical spray is formed, which has an angle called as spray cone angle (ϕ). Besides, most of the fuel vapour is concentrated at the outer region while the inner region contains more amount of liquid mass and less fuel vapour, see Figure 2.15.
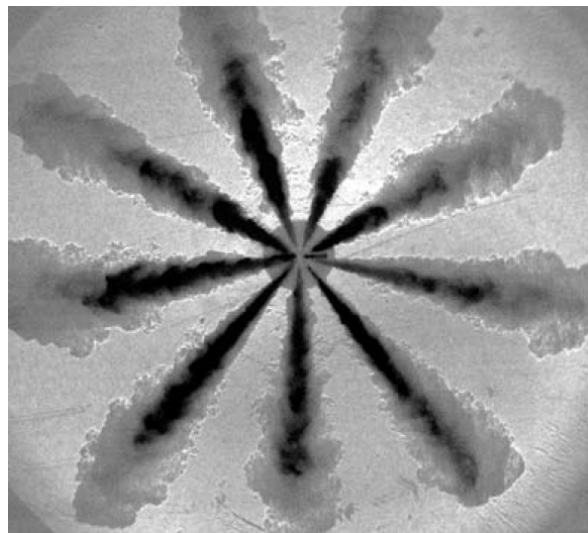
Figure 2.15. Vapor (gray) and liquid (black) phases of a spray [78].

Furthermore, boundary conditions affect the spray propagation. These boundary conditions are gas density and temperature, gas flow (swirl and tumble) and the distance between the nozzle tip and piston bowl [78]. Spray can impinge on the spray bowl, which can negatively affect the engine's performance output and emissions in the case of higher injection pressures or longer injection duration. Additionally, low densities of surrounding gas due to early injection may lead the spray to impinge on the wall.

Finally, many researchers have investigated the spray parameters. According to Hiroyasu and Arai [86], important parameters of a full-cone diesel spray are spray penetration length, spray cone angle, break-up length and average droplet size. And, these parameters are dependent on boundary conditions.

2.5.4.1. Disintegration of a Full-cone Spray

Here, disintegration mechanisms of a full-cone diesel spray is explained, including the primary and secondary break-up. Possible primary break-up mechanisms are growth of surface waves due to aerodynamic forces, turbulence, cavitation and relaxation of the velocity profile [78]. Figure 2.16 shows these mechanisms.
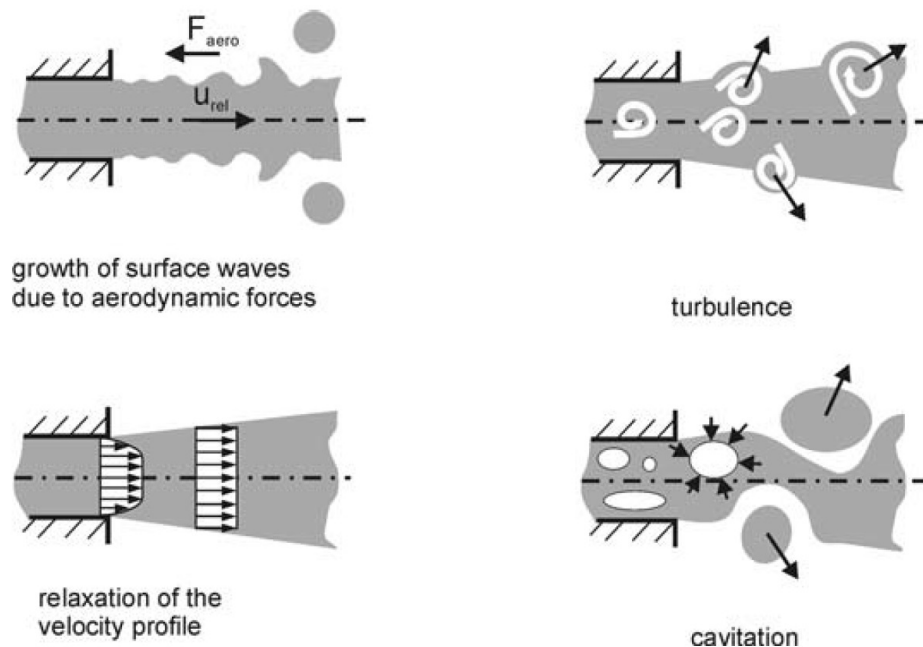
Figure 2.16. Primary break-up mechanisms [78].

The first primary break-up mechanism is the formation of surface waves due to aerodynamic shear forces which is generated at the liquid jet and gas interface due to relative velocity [78]. Turbulence inside the nozzle generates surface waves which are then amplified by the aerodynamic shear forces. Afterwards, these surface waves become unstable and are separated from the jet. By this way, first droplets are formed. In addition, aerodynamic forces can not affect the inner structure of the spray, can only influence the outer regions.

Secondly, turbulence-induced disintegration is also possible [78]. Inside the nozzle turbulent eddies can be generated, and can overcome the surface tension to form droplets in case they are strong enough. This is one of the primary break-up mechanisms for a high-pressure full-cone spray.

Thirdly, the relaxation of the velocity profile can be a primary break-up mechanism. By assuming fully developed pipe flow (in case of turbulent flow without cavitation, and large length/diameter ratios), the velocity profile may relax when the jet is presented into the cylinder [78], and no slip boundary condition expires due to the absence of wall no more. Also, an acceleration is observed at the outer region of the spray. After gaining acceleration, velocity profile turns into a block profile from a parabolic profile. This situation may cause instabilities thence break-up at the outer region of the liquid jet. This break-up mechanism is only valid for the given assumptions above. In case of high injection pressures, cavitation can occur, and the possibility of development of velocity profile explained above is unlikely.

Lastly, another important possible primary break-up mechanism is the cavitation induced break-up of the spray [78]. Cavitation can occur as a result of reduced static pressure due to a raise in the acceleration and the velocity of the fuel [78]. In addition, cavitation depends on the nozzle geometry and the pressure inside the cylinder. Furthermore, experimental studies showed that spray cone angle increased as the flow moves on the cavitating flow inside the nozzle from the turbulent flow [87, 88, 89]. Cavitation bubbles implode inside the nozzle hole resulting in an increase in the turbulence level therefore the spray disintegration. Cavitation and turbulence are the most important break-up mechanisms for diesel sprays, and clear separation of these mechanisms from each other is difficult [78].

Moreover, aerodynamic effects induce the secondary break-up of the liquid droplets. Break-up mechanisms which were described in Section 2.5.3 are valid for secondary break-up of a diesel spray.

2.5.4.2. Phases of Injection Event

Typical development of a diesel spray can be explained in three phases [78]. The first phase is needle opening. Fuel mass flow rate is controlled by the needle movement. Namely, the main throttle is determined by the small cross-sectional area inside the injector. Spray structure near the nozzle is dependent on the needle speed. Larger spray angles are occured when the needle opening is very slow, or vice versa [78].

When the cross-sectional area at the needle seat is bigger than the total areas of nozzle holes, the main throttle is now the holes of the nozzle, and spray disintegration as a consequence of cavitating flow depends on the nozzle geometry [78]. The stronger cavitating flow in the nozzle, the bigger the spray cone angle. Injection duration is also important because spray penetration length gets longer with time owing to presenting new droplets having high kinetic energy into the cylinder.

At the end, the needle closes and the injection event comes to an end. Injection velocity reaches to zero. As the flow velocity decreases, droplet sizes get bigger, and atomization reduces. In order to prevent this situation, rapid closing of the needle is required [78].

2.5.5. Spray Impingement on Walls

Spray can impact combustion chamber wall or piston bowl in case of high injection pressures or low gas densities resulting in increased spray penetration. Two primary processes can be observed, which are wall-spray evolution and wall film development [78]. Both of them affects the performance, fuel consumption and emission levels.

Positive and negative effects can be observed as a result of spray-wall interaction. For example, wall temperature is relatively lower than normal operating conditions under cold starting conditions, which causes slow evaporation resulting in a rise in the hydrocarbon and soot emission levels [78]. This is the negative effect of spray impingement on wall. On the other hand, evaporation can be improved in the case of hot wall interaction. For instance, MAN developed a technique called as M-combustion [78, 90]. In this technique, the aim is to obtain a liquid film on the hot piston bowl by injecting the fuel on the bowl. Then, fuel vaporizes and combustion starts. Control of the combustion is provided by the amount of fuel on the piston bowl.

2.6. Spray Measurement Techniques

It is important to study mixture formation in order to understand the combustion phenomena. To conduct these kinds of studies, several test rigs have been utilized. These are optical research engine (ORE), rapid compression and expansion machine (RCEM), constant pressure flow rig (CPFR), and constant volume combustion chamber (CVCC) [18]. Oren et al. [91] and Baert et al. [92] gave summaries about the advantages and disadvantages of these test rigs. Among these techniques, CVCC has a very wide range of gas temperatures and pressures [18]. An example for a CVCC is given in Figure 2.17. A CVCC can be used for spray measurement or combustion simulation.
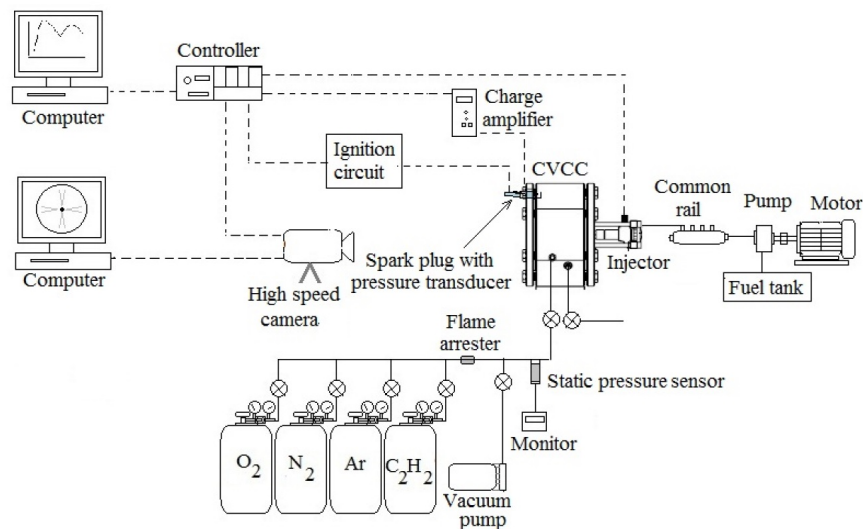
Figure 2.17. An example for a constant volume combustion chamber (CVCC) [18].

In order to measure the spray characteristics, the chamber is filled up with a non-flammable gas, usually nitrogen. Chamber pressure can be adjusted by the amount of gas presented in the chamber. Then, fuel is directly injected into the chamber. Spray is viewed by an optical setup which is explained in Section 2.6.1.

Secondly, CVCC can also be used to simulate the combustion of a fuel with a pre-combustion technique. Figure 2.18 represents the pre-combustion technique for a CVCC in order to simulate a real engine. A gaseous mixture which consists of e.g. C_2H_2, O_2, Ar and N_2 is presented into the chamber. This mixture is then ignited by a spark plug in order to rise the temperature and pressure inside the chamber. Afterwards, test fuel is
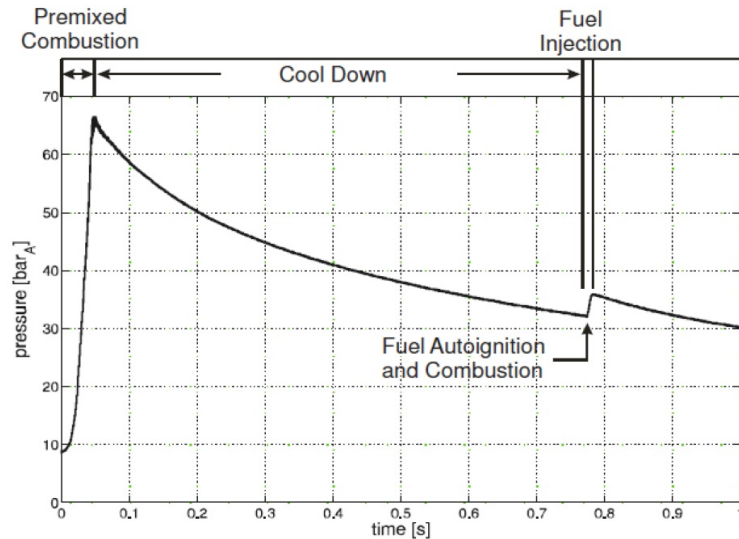
Figure 2.18. Principle of the pre-combustion technique for a constant volume combustion chamber [18].

injected by an injection system when pressure inside the chamber decreases to the target values. Because the temperature inside the chamber is higher than the fuel's ignition point, spontaneous combustion starts. However, this pre-combustion technique is used when the combustion simulation of the tested fuel is required. It is not suitable to be used when the spray characteristics are required.

2.6.1. Optical Diagnostics

The injection process consists of 4 different stages which are fuel injection, atomization, vaporization and mixing with air. Performance of an engine is influenced by these stages. Thence, researchers need to visualize the injection for a better understanding of the effects of injection on engine performance and emissions. Visualization can be possible by optical diagnostics. Some of the methods are explained below.

- Schlieren Technique: Schlieren system is an optical system which "projects line-of-sight information onto a viewing screen or camera focal plane" [93]. Figure 2.19 shows an example of a simple Schlieren technique. This system needs a light source and lens. Lens is required to focus the light which passes through the test region to a high-speed camera.
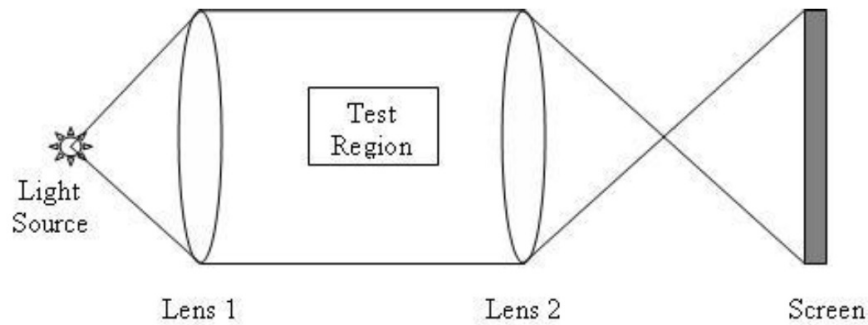
Figure 2.19. Schematic sketch of a simple Schlieren technique [2].

- Shadowgraph Technique: It is a simpler technique of Schlieren technique. It is not a focused technique thus is less sensitive. Figure 2.20 represents the schematic sketch of the shadowgraph technique.
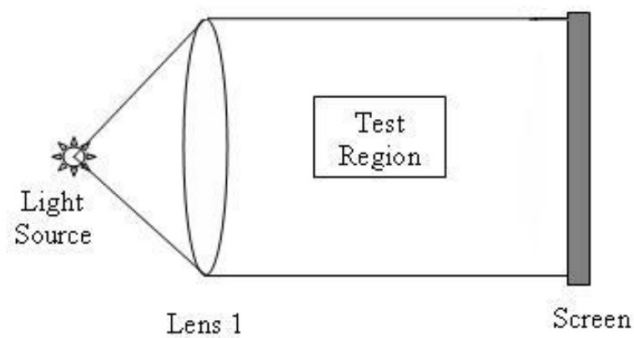
Figure 2.20. Shadowgraph technique [2].

- Laser Rayleigh Scattering: This method is an elastic process in which the wavelengths of the scattered light and the incident light are the same. The main drawback of this technique is that the scattered light from the chamber walls can interfere with the light scattered from the gas [2]. Also, this technique allows only detection of vapour phase in the absence of liquid drops [2].

- Mie Scattering: Mie scattering is another elastic process of scattered light as the laser Rayleigh scattering technique [2]. This technique allows researchers to detect liquid drops of a fuel. It depends on the particle size and requires no energy exchange, hence the scattered light is a good signal.

2.7. Biodiesel Fuel Application in Diesel Engines

There are many research concerning about the application of biodiesel fuels in diesel engines. Researchers have investigated the combustion characteristics, performance, emission levels and spray characteristics of biodiesel fuels in comparison with conventional diesel fuel. In this section, a review on the application of biodiesel fuels will be given, see Tables 2.3 and 2.4. (Note that biodiesel fuels which will be reviewed in this section are produced through transesterification process). Before explaining these parameters, it is required to compare some of the physical and chemical properties of biodiesel fuels with those of fossil diesel fuel, including density, viscosity, surface tension, calorific value and cetane number. Table 2.2 shows some important specifications for biodiesel fuels according to the USA and the EU standards. ASTM D6751 and EN 14214 standards are applied for biodiesel fuels in the USA and the EU, respectively. ASTM D6751 specifies biodiesel fuel as mono-alkyl esters of long chain fatty acids obtained from vegetable oils and animal fats, and the type of alcohol utilized to produce biodiesel is not specified. It can be methanol, ethanol, etc. However, EN 14214 applies only to mono-alkyl esters derived with methanol, i.e. fatty acid methyl esters (FAME).

Table 2.2. Biodiesel specifications in the USA and the EU.

Region →	United States				European Union			
Specification Type →	ASTM D975-14		ASTM D6751-12		EN 590:2013		EN 14214:2012	
	Diesel	Test Method	Biodiesel	Test Method	Diesel	Test Method	Biodiesel	Test Method
Density @ 15 ^{o}C, kg/m^3, min-max					820 - 845	EN ISO 3675 EN ISO 12185	860 - 900	EN ISO 3675 EN ISO 12185
Viscosity @ 40 ^{o}C, mm^2/s, min-max	2.0 - 4.1	D445	1.9 - 6	D445	2 - 4.5	EN ISO 3104	3.5 - 5.0	EN ISO 3104
Cetane Number, min	40	D613	47	D613	51	EN ISO 5165	51	EN ISO 5165
Ester Content	5 vol.% (max)				7 vol.% max	EN 14078	96.5 wt.% (min)	EN 14103

Data source: [94, 95, 96, 97, 98].

Besides, Table 2.3 gives a review about the studies which investigate the combustion characteristics, performance and emission levels of biodiesel fuels. Table 2.4 shows a summary about the studies that examine the spray characteristics of biodiesel fuels in terms of spray penetration length, spray cone angle and break-up length. Both tables compare the characteristics with those of fossil diesel fuels. Also, some important physical and chemical properties are included to make a better understanding. Additionally, test equipment is explained.

2.7.1. Physical and Chemical Properties of Biodiesel Fuels

Although physical and chemical properties of biodiesel fuels vary from feedstock to feedstock, a general inference may be made according to Table 2.2 and studies available in the literature.

Firstly, many research studies show that density values of biodiesel fuels are higher than the density of conventional diesel fuel [99, 100, 101, 102, 103, 104, 105, 106]. For example, Qi et al. [99] produced biodiesel from soybean oil, and found that density of biodiesel fuel was 6.1% higher than the conventional diesel fuel. Next, Nirmala et al. [102] produced biodiesel fuel from algal oil, and showed that biodiesel fuel had 7.93% higher density than diesel. Besides, Patel et al. [103] produced biodiesel fuel from jatropha, and this biodiesel fuel had 3% higher density than the reference diesel fuel.

Secondly, viscosity of biodiesel fuels is larger than the viscosity of diesel fuels [106, 107, 108, 109, 110, 111]. For instance, Das et al. [106] used castor oil biodiesel in their experiments, and this biodiesel fuel had 5.7 times larger viscosity than the reference diesel fuel. Next, Mistri et al. [109] used karanja biodiesel having 2.3 times bigger viscosity than fossil diesel fuel.

Thirdly, biodiesel fuels have bigger surface tension values than fossil diesel fuel [112, 113, 114]. For example, Patel et al. [112] used jatropha biodiesel having approximately 15% higher surface tension than fossil diesel fuel. Moreover, Kuti et al. [114] utilized biodiesel from palm oil in their studies, and this biodiesel fuel had 6.5% larger surface tension than reference diesel fuel.

Next, calorific value of biodiesel fuels are lower than conventional diesel fuels [101, 103, 104, 105, 106, 115]. For instance, Shrivastava et al. [101] produced biodiesel fuel from roselle oil, and calorific value of this biodiesel fuel was 8.75% lower than standard diesel. Furthermore, Soto et al. [105] used sugarcane biodiesel having 14.8% lower calorific value than the calorific value of conventional diesel fuel.

Finally, cetane number is larger for biodiesel fuels than standard diesel fuels [100, 101, 104, 105, 107, 109, 112, 115]. For example, Raman et al. [107] produced biodiesel fuel from rapeseed oil, and cetane number of this biodiesel fuel was approximately 5.9% higher than conventional diesel fuel. Next, Nabi and Rasul [104] used biodiesel derived from waste cooking oil, and this biodiesel fuel had approximately 9.94% higher cetane number than reference diesel fuel.

Table 2.3. Research concerning on performance and emission characteristics of biodiesel in the literature.

Reference	Properties of the Tested Engine						Biofuel	Properties				Combustion Characteristics		Performance			Emissions			
	No of cylinder	Cooling	Aspiration	CR	RP (kW)	RS (rpm)		Density	Viscosity	CV	CN	In-cylinder pressure	HRR	BSFC	BTE	BP	NOx	HC	PM	CO
[99]	1	WC	NA	16.5:1	11.03	2000	Biodiesel (30%, 50%, 80% and 100%)	↑	↑	↓	-	↑	→	↑	↓	-	↑	↑	↓	→
[100]	1	AC	NA	17.5:1	7.4	1500	Biodiesel (5%, 10%, 20%, 30% and 100%)	↑	↑	↓	↑	→	→	↑	↓	-	↑	↓	↓	→
[101]	1	WC	-	17.5:1	3.5	1500	Biodiesel (10%, 20% and 100%)	↑	↑	↓	↑	→	→	↑	↓	→	↑	↓	→	-
[102]	1	WC	-	17.5:1	5.2	1500	Biodiesel (100%)	↑	↑	↓	-	-	-	↑	↓	→	↑	↓	↓	→
[115]	4	WC	NA	17:1	18	1500	Biodiesel (5% and 20%)	→	→	↓	↑	→	→	↑	→	→	↑	↑	↑	↑
[103]	1	WC	-	17.5:1	7.4	1500	Biodiesel (100%)	↑	↑	↓	↑	↑	↑	↑	↓	-	↑	↑	↓	↑
[104]	4	WC	NA	22.6:1	53.9	2600	Biodiesel (30% and 100%)	↑	↑	↓	↑	↑	-	↑	↓	-	↑	↑	↓	↑
[105]	4	-	TC, EGR	16.5:1	166	2400	Biodiesel (100%)	↑	↑	↓	↑	-	-	↑	↓	→	↑	↑	↓	↑
[116]	1	WC	-	17.5:1	5.2	1500	Biodiesel (20%, 30%, 40% and 100%)	-	-	-	-	↓	↓	↑	↓	-	↑	↑	↓	↑
[106]	1	WC	NA	variable (12-22)	5.73	1500	Biodiesel (5%, 10%, 20% and 100%)	↑	↑	↓	-	↑	↑	↑	↑	-	↑	↓	-	↑
[107]	1	WC	-	17.5:1	5.95	1500	Biodiesel (25%, 50%, 75% and 100%)	↑	↑	↓	↑	↓	↓	↑	↑	-	↑	↑	↑	↑
[108]	4	-	TC	18.5:1	78.3	4000	Biodiesel (7% and 100%)	↑	↑	↓	-	↑	↑	↑	-	→	↑	↑	↓	-
[109]	1	AC	TC	16.3:1	-	1500	Biodiesel (30% and 100%)	↑	↑	↓	↑	↓	↓	↑	-	→	↑	↑	↓	↑
[110]	8	AC	TC	16.5:1	190	2300	Biodiesel (15%, 20%, 25%, 30%, 35% and 40%)	↑	↑	-	↑	-	-	↑	-	→	↓	-	↓	-
[111]	4	WC	NA	18:1	40.4	3000	Biodiesel (20%)	↑	↑	↓	-	↑	↑	↓	↑	-	↑	↑	↓	↑
[117]	1	AC	-	18:1	8	3600	Biodiesel (5%, 20%, 50% and 100%)	↑	↑	↓	-	-	-	↓	↑	↑	↑	↓	-	→
[118]	1	WC	-	17.5:1	3.5	1500	Biodiesel (5%, 10% and 20%)	↑	↑	↓	-	-	-	↓	↑	↑	↓	↓	↓	-
[119]	1	WC	-	17.7:1	7.7	2400	Biodiesel (10%, 20%, 30% and 50%)	↑	↑	↓	↑	-	-	↓	↑	↑	↑	-	↓	↓
[120]	-	-	-	18:1	-	-	Biodiesel (10%, 20%, 30% and 50%)	↑	↑	↓	↑	↑	-	↑	↓	-	↑	-	↓	→

Abbreviations: WC: water cooled, AC: air cooled, NA: naturally aspirated, TC: turbocharged, EGR: exhaust gas recirculation, CR: compression ratio, RP: rated power, RS: rated speed, ↓: decrease, ↑: increase, →: similarity, -: no data available, CV: calorific value, CN: cetane number, HRR: heat release rate, BSFC: brake specific fuel consumption, BTE: brake thermal efficiency, BP: brake power, NOx: nitric oxides, HC: hydrocarbon, PM: particulate matters, CO: carbon monoxide.

Note: All biodiesel fuels are produced via transesterification process.

Table 2.4. Spray research studies on biodiesel fuels in the literature.

Reference	Test Equipment	Biofuel	Physical Properties			Spray Characteristics				
			Density	Viscosity	Surface Tension	LL	VL	SPL	BL	SCA
[112]	CVCC	Biodiesel (20% and 100%)	↑	↑	↑	–	–	–	–	↑
[113]	CVCC	Biodiesel (100%)	↑	↑	↑	–	–	↑	–	→
[121]	4S, optical single-cylinder diesel engine, CR: 16.5:1	Biodiesel (50% and 100%)	↑	↑	–	←	↑	←	–	→
[122]	CVCC	Biodiesel (40%, 60% and 100%)	↑	↑	–	–	–	–	–	→
[123]	CVCC	Biodiesel (20% and 100%)	↑	↑	–	–	–	←	–	→
[124]	Numerical methods	Biodiesel (10% and 20%)	↑	→	–	–	–	←	←	←
[125]	Optical single-cylinder diesel engine, CR: 17.4	Biodiesel (100%)	↑	↑	–	–	–	↑	–	←
[114]	CVCC	Biodiesel (100%)	↑	↑	↑	←	–	–	–	–
[126]	CVCC	Biodiesel (5%, 20% and 100%)	↑	↑	–	–	–	←	–	←
[127]	CVCC	Biodiesel (20% and 40%)	↑	↑	–	–	–	↑	–	↑
[128]	CVCC	Biodiesel (100%)	↑	↑	↑	–	–	←	–	→
[129]	A diesel engine	Biodiesel (10%, 20%, 30%, 40%, 50% and 100%)	↑	↑	–	–	–	←	–	→
[130]	CVCC	Biodiesel (100%)	↑	↑	–	–	–	↑	–	↑
[131]	4S, optical single-cylinder diesel engine, CR: 16.5:1	Biodiesel (50% and 100%)	↑	↑	–	–	–	←	–	↑
[132]	CVCC	Biodiesel (100%)	↑	↑	–	←	–	–	–	→
[133]	CVCC	Biodiesel (20%, 50%, 80% and 100%)	↑	↑	↑	–	–	→	–	→
[134]	CVCC	Biodiesel (100%)	↑	↑	–	←	↑	–	–	–
[135]	CVCC	Biodiesel (100%)	↑	↑	↑	–	–	←	–	→
[136]	Numerical methods	Biodiesel (5%, 10%, 15%, 20%, 25%, 50% and 100%)	↑	↑	↑	–	–	←	←	→

Abbreviations: CVCC: constant volume combustion chamber, 4S: four stroke, WC: water cooled, AC: air cooled, NA: naturally aspirated, TC: turbocharged, EGR: exhaust gas recirculation, CR: compression ratio, RP: rated power, RS: rated speed, ↑: increase, ↓: decrease, →: similarity, –: no data available, LL: liquid length, VL: vapour length, SPL: spray penetration length, BL: break-up length, SCA: spray cone angle.

Note: All biodiesel fuels are produced via transesterification process.

41

2.7.2. Combustion Characteristics of Biodiesel Fuels

Many researchers have investigated the combustion characteristics in terms of ignition delay, in-cylinder pressure and heat release rate. As it is seen in Table 2.3, different researchers used different test equipment with different diesel-biodiesel blend ratios. Some of them found similar results while some of them found different results.

2.7.2.1. Ignition delay

Several factors affect the ignition delay, such as injection timing, load, injection rate, engine speed, intake air temperature and pressure, cetane number of the fuel, etc. [6]. Among these parameters, cetane number is the only parameter affecting the ignition delay related with the fuel properties. Cetane number specifies the ignition quality of the fuel.

According to many researchers [99, 100, 101, 103, 104, 109, 111, 120, 122], ignition delay decreases with the use of biodiesel fuel. Most researchers agreed that the decrease of ignition delay depends on the high cetane number of biodiesel fuels than conventional diesel fuel [100, 101, 103, 104, 109, 111, 122]. Also, Lee et al. [122] concluded that higher oxygen content of biodiesel fuel results in reduced ignition delay. Additionally, Qi et al. [99], and El-Kasaby et al. [120] agreed that higher viscosity thus lower volatility of biodiesel fuel reduces the ignition delay period. This may be possible due to a rapid pre-flame chemical reactions that take place at relatively higher temperatures. Because of the high cylinder temperature during injection, thermal cracking of biodiesel fuel may occur. As a result of thermal cracking, lighter compunds are produced in the cylinder, which may ignite earlier.

2.7.2.2. In-cylinder Pressure

In-cylinder pressure is an important parameter for engines. It is necessary to know the peak pressure, and when this peak pressure occurs. In a diesel engine, the peak pressure is dependent on the fuel mass fraction which is burned in the premixed combustion phase, and in-cylinder pressure qualifies the ability of a fuel to mix with air, and to burn.

Many researchers [100, 101, 107, 109, 115, 116] found reductions in peak in-cylinder pressures for biodiesel fuels than reference diesel fuels. This can be explained by higher cetane numbers of biodiesel fuels resulting in shorter ignition delay thus reduced fuel-air mixing [100, 109]. Also, higher calorific value of diesel fuel plays an important role because diesel fuel releases more heat during combustion leading to higher pressure values under the same experimental conditions [115]. However, considerable number of researchers [99, 103, 106, 111] reported increase in peak cylinder pressures when biodiesel fuel was utilized. Qi et al. [99] and Agarwal et al. [111] concluded that increase in pressure may be related with the higher cetane numbers of biodiesel fuels. Ignition delays of biodiesel fuels are shorter, and combustion starts earlier. The peak cylinder pressure attains a larger value as it is closer to top dead center (TDC) in the power stroke. Also, higher density of biodiesel fuel can affect the peak pressure because more mass is injected under the condition of same injection duration [103]. Moreover, few researchers [104, 108] observed similar pressure values for both biodiesel and diesel fuels.

2.7.2.3. Heat Release Rate

Most researchers concluded that heat release rate (HRR) decreases when biodiesel used instead of conventional diesel fuel [99, 100, 101, 107, 109, 115, 116]. The main reason for this is the shorter ignition delay of biodiesel fuels compared to diesel fuel [99, 100, 101, 107, 109, 115, 116]. Shorter ignition delay causes accumulation of a lower quantity of fuel in the premixed combustion phase thus reduced peak heat release rate. In addition to this, higher volatility thus better mixing of traditional diesel fuel with air results in larger HRR [99]. Withal, lower calorific value of biodiesel fuels than that of diesel leads to decrease in HRR [107, 116]. On the other hand, several researchers concluded raise in HRR [103, 111]. For example, Agarwal and Dhar [111] used a biodiesel-diesel blend (20%-80%, respectively) at low engine loads, they observed significant increase in HRR. Additionally, Patel et al. [103] used a biodiesel having relatively low cetane number and viscosity compared to other biodiesel fuels. This fuel performed good mixing with air, and they observed higher peak HRR value than reference diesel fuel. Furthermore, Das et al. [106] and Özçelik et al. [108] found approximate heat release rate values for both biodiesel and traditional diesel fuels.

2.7.3. Performance of Biodiesel Fuels

Performance indicators for engines are brake specific fuel consumption (BSFC), brake thermal efficiency (BTE) and brake power (BP). Below, the effects of biodiesel fuels on performance indicators will be reviewed according to Table 2.3.

2.7.3.1. Brake Specific Fuel Consumption

Many researchers [99, 100, 101, 102, 103, 104, 105, 107, 108, 109, 110, 111, 115, 116] found that BSFC increases when biodiesel percentage increases in diesel-biodiesel blends as they are used in diesel engines. For example, Qi et al. [99] investigated the effects of different percentages of diesel-biodiesel blends on a diesel engine's performance. They found 6.91%, 8.01%, 9.71% and 12.4% increases for B30, B50, B80, and B100, respectively. Shrivastava [101] found 5.40%, 6.48% and 13.42% increases for B10, B20 and B100, respectively. Nirmala et al. [102] found 4.17% higher BSFC for 100% biodiesel fuel. Researchers [99, 100, 101, 102, 103, 104] provided several reasons for the increment of BSFC when using neat biodiesel or biodiesel-diesel blend in CI engines, such as higher density, larger viscosity and lower calorific value of biodiesel fuel than diesel. Whereas, few researchers [117, 118, 119] observed decrease in BSFC for biodiesel-diesel blends. Gümüş and Kaşifoğlu [117] found 0.48%, and 4.7% decrease in BSFC for B5, and B20, respectively. Ong et al. [119] used jatropha curcas biodiesel in a compression-ignition engine. They observed reduced BSFC values when B10 is used as a fuel.

2.7.3.2. Brake Thermal Efficiency

Slightly decreased or similar BTE values are obtained for biodiesel-diesel blends by many researchers [99, 100, 101, 102, 103, 104, 105, 106, 107, 115, 116]. For instance, Chauhan et al. [100] researched the performance, combustion and emission characteristics of Jatropha biodiesel, traditional diesel and their blends in the ratio of 5%, 10%, 20% and 30% in a single-cylinder, four-stroke, air-cooled, direct-injection compression-ignition engine with different loadings. As a result of this study, it was observed that increasing the biodiesel percentage in blended fuels lowered the BTE. Soto et al. [105]

used neat sugar cane biodiesel in a four cylinder, turbocharged, direct injection diesel engine. They found 1.3% loss in BTE. Qi et al. [99] utilized diesel, pure biodiesel and diesel-biodiesel blends in the ratio of 30%, 50% and 80%. Maximum BTE of diesel fuel was 0.35, and maximum brake thermal efficiencies of biodiesel and its blends were lower than diesel fuel with a very small margin. Researchers explained some reasons for lower BTE values, such as higher viscosity [101, 102, 116], higher density [99, 104], lower heating value [100, 103, 105, 107] and higher lubricity [8]. On the other hand, several studies showed higher BTE for biodiesel fuels compared to reference diesel [109, 111, 117, 118, 119]. Mistri et al. [109] used Jatropha and Karanja biodiesel fuels and their blends with diesel in the ratio of 30%. B100 and B30 performed 10.9% and 7.6% higher BTE, respectively. Next, Panwar et al. [118] utilized castor seed oil biodiesel with different blend ratios (5%, 10% and 20%). The maximum BTE was for B10, and this value was 14.14% higher than that of fossil diesel fuel. According to the opinions of researchers [117, 118, 119], higher BTE could be obtained owing to following reasons: higher oxygen content of biodiesel leading to improved combustion and higher lubricity resulting in reduced friction loss.

2.7.3.3. Brake Power

Smaller or greater reductions in brake power (BP) were found when pure biodiesel or biodiesel-diesel blends were utilized in diesel engines [101, 102, 105, 108, 110]. For instance, Chokri et al. [110] used biodiesel derived from waste vegetable oil in a 8-cylinder, air cooled, turbocharged, direct-injection diesel engine. They observed around 5% reduction in power for each 10% of biodiesel blend added comparatively to neat diesel. Özçelik et al. [108] found 4.97% and 14.39% decrease in BP for B7 and B100, respectively. Researchers explained several causes for the decrease of brake power, such as lower heating value [101, 108] and higher density [102]. However, few researchers found increase in BP when using biodiesel-diesel blends with biodiesel fuels of different origins [117, 118, 119]. For example, Gümüş and Kaşifoğlu [117] used apricot seed kernel oil biodiesel and its blends with traditional diesel. They found an increase in brake power with the raise in biodiesel content in blended fuels until the B20 blend. They argued two reasons for this increase: higher oxygen content leading to better combustion and higher density resulting in larger mass pumped to the combustion chamber for the

same fuel volume. Besides, Ong et al. [119] investigated the effects of jatropha curcas biodiesel fuel on performance and emission parameters in a single-cylinder, water-cooled, four-stroke, direct-injection compression-ignition engine under different engine speeds. They observed maximum brake power for B10 at 1900 rpm, and this value was 4.5% bigger than that of reference diesel fuel. They explained this higher BP value with higher oxygen content of the biodiesel fuel.

2.7.4. Emission Levels of Biodiesel Fuels

Emissions from diesel engines tend to decrease with the use of biodiesel-diesel blends [8]. But, emission levels vary from one cylinder to another cylinder and from one operating condition to another. Also, fuel quality and engine design are the other parameters which affect the emission levels. Below, a review of emission characteristics of biodiesel fuels are given. Table 2.3 documents the comparative results of different studies related with the emission investigation in the literature.

2.7.4.1. Hydrocarbons

The dominant point of view is that HC emissions from diesel engines reduce when diesel-biodiesel blends are used as fuel [100, 102, 103, 104, 106, 107, 108, 109, 111, 116]. For example, Asokan et al. [116] used juliflora biodiesel in a single-cylinder, water cooled, direct-injection compression-ignition engine with different blend ratios like 20%, 30%, 40% and 100%. They found approximately 6.6%, 9.1%, 13.2% and 17.4% reductions in HC emissions compared to fossil diesel fuel. Raman et al. [107] used rapeseed oil biodiesel, and found greater reductions in HC emissions at maximum brake power. These reductions were 15.4%, 26.7%, 32.2% and 42.1% for B25, B50, B75 and B100. Researchers found some important reasons for the decrease in HC emission levels, such as high oxygen content of biodiesel fuels leading to more complete combustion [100, 102, 106, 107, 108, 116], absence of aromatics in some biodiesel fuels [104, 105] and higher cetane number resulting in decreased ignition delay thus promoted reaction timing [8]. Yet, reverse result was observed by Seraç et al. [115]. In the study, different blends of soybean oil biodiesel and diesel (5% and 20%) were used, and more HC emis-

sions were produced with biodiesel compared to diesel fuel in the same power output of the tested engine. The researchers concluded that the introduction of rich fuel-air mixture into the engine caused higher HC emissions. Also, Ong et al. [119] found similar results. Although B10 emitted lower hydrocarbons than diesel, B20, B30 and B50 emitted higher hydrocarbons than diesel fuel at higher engine speeds. The authors explained this increase in HC emission levels with the higher viscosity of biodiesel fuel resulting in poor atomization and combustion at higher speeds.

2.7.4.2. Carbon Monoxide

Greater or smaller decreases in CO emissions were observed for the use of biodiesel fuels in diesel engines by many researchers [99, 100, 102, 104, 107, 109, 115, 116]. For example, Raman et al. [107] found 7.6%, 22.7%, 30.4% and 35.4% decrease in CO emission levels at maximum engine load for B25, B50, B75 and B100, respectively. Authors concluded that CO emissions decreased due to the higher oxygen content of biodiesel fuels. Next, Nabi and Rasul [104] observed 85%, 84% and 87% reduction in CO emissions for macadamia biodiesel-diesel blend, waste cooking oil biodiesel-diesel blend, and their triple blend. These researchers also explained the decrease in CO emissions with higher oxygen content of biodiesel fuels. In addition to this, they explained that the similarity of decrease levels for 3 different blended fuels were due to the similar oxygen content of these fuels. Researchers who found similar results with these two studies also agreed with the importance of oxygen content of biodiesel fuels leading to more complete combustion [100, 102, 115, 117]. Furthermore, Qi et al. [99] argued that less C\H ratio of biodiesel fuel than diesel fuel might lead to decrease in CO emission. In contrast, several researchers found no change [106, 111] or increase [103, 105] in CO emission levels. Patel et al. [103] used three different neat biodiesel fuels derived from waste cooking oil, jatropha oil and karanja oil. They observed increase in CO emissions, and explained that higher viscosity of biodiesel fuel led to poorer atomization thus less efficient combustion. Also, they explained that presence of long chain unsaturated fatty acid molecules in biodiesel fuels negatively affected the atomization hence combustion. Also, Soto et al. [105] observed rise in CO emissions from biodiesel fuels. They concluded that higher levels of CO may have been caused by different boiling characteristics of biodiesel fuels from reference diesel fuel.

2.7.4.3. Particulate Matters

It is a common conclusion that particulate emissions decrease with the use of biodiesel fuels in diesel engines instead of traditional diesel fuels [99, 100, 101, 102, 104, 105, 109, 110, 111, 115, 116, 117, 119]. For example, Shrivastava [101] used 2 different biodiesel fuels which are roselle and karanja biodiesel fuels, and their 10% and 20% blends with reference diesel fuel. A reduction in particulate emissions in the range of 7.9% to 15.8% was observed starting from a lower percentage of biodiesel content in the blended fuels to neat biodiesel. Namely, increasing the biodiesel percentage in the fuels decreased the smoke emissions. Next, Ong et al. [119] measured the smoke opacity for jatropha curcas, ceiba pentandra and calophyllum inophyllum biodiesel fuels. The most reduction in particulate emissions obtained for 50% biodiesel-diesel blends. The smoke opacity was found to be 22.88%, 21.46% and 20.57% for calophyllum inophyllum, ceiba pentandra and jatropha curcas biodiesel blends, respectively while smoke opacity of diesel was found to be 30.19%. Most researchers agreed that inbuilt oxygen content of biodiesel fuels decreased the particulate emissions by enhancing the combustion process [100, 102, 104, 105, 115, 117, 119]. Also, absence of aromatics in biodiesel fuels can reduce particulate emissions [101, 109]. However, Raman et al. [107] found 5.6% raise in particulate emissions when 20% biodiesel-diesel blend was used as a fuel, and this increase grew by up to 10.3% when neat biodiesel was used. Also, Patel et al. [103] observed increase in smoke emissions with the use of biodiesel fuels. Researchers [103, 107] agreed that inferior atomization as a result of higher viscosity of biodiesel fuels led to higher particulate emissions.

2.7.4.4. NO$_x$

Many studies showed that NO$_x$ emission increases when biodiesel fuels are used instead of neat diesel fuel [99, 100, 102, 104, 105, 107, 108, 109, 115, 117, 119]. As an example, Nabi and Rasul [104] reported around 27% higher NO$_x$ emission for blended fuels than neat diesel. Additionally, Raman et al. [107] used rapeseed oil biodiesel and its blends with fossil diesel in the ratio of 25%, 50% and 75% in a single-cylinder, water-cooled, four stroke, direct-injection diesel engine. They found higher NO$_x$ emissions, and increase in NO$_x$ emissions were found as 14.4%, 21.6%, 28.5% and 32.9% for B25, B50,

B75 and B100, respectively. Several reasons can be explained for higher NO_x emissions with the use of biodiesel fuels. Firstly, the most dominating one is the oxygen content of biodiesel fuels leading to two important consequences which are better combustion resulting in higher in-cylinder temperatures [99, 107, 108, 109, 115], and presence of excess oxygen that may react with nitrogen to form NO_x [108, 115, 117]. For example, Nirmala et al. [102] compared diesel fuel and two different biodiesel fuels derived from algal oil and waste cooking oil. In the study, NO_x emission from diesel fuel was the lowest, and algal oil biodiesel emitted more NO_x compared to waste cooking oil biodiesel. They concluded that oxygen content of algal oil biodiesel fuel may have been higher than the other biodiesel fuel. Next, authors of [104, 109] explained that the presence of long chain fatty acid molecules increases the level of unsaturation of biodiesel fuels which causes higher in-cylinder temperatures thus higher NO_x emissions. In addition, Ong et al. [119] reported that higher viscosity of biodiesel fuels reduced the injection timings thus increased the NO_x emissions. On the other hand, several researchers [101, 103, 110, 118] found decrease in NO_x levels with the use of biodiesel fuels, and few researchers [106, 111, 116] reported comparable NO_x levels of biodiesel fuels with traditional diesel fuels. According to Patel et al. [103] lower calorific value of biodiesel fuels led to lower heat release rates during pre-mixed combustion phase that decreased the in-cylinder temperatures resulting in reduction in NO_x levels. Also, Shrivastava et al. [101] observed lower in-cylinder temperatures for roselle and karanja biodiesel fuels, and they reported that NO_x levels were lower than reference diesel fuel by around 3.83%, 11.61% and 22.42% for the blends, B20, B10 and B100, respectively, at maximum load condition.

2.7.5. Spray Characteristics of Biodiesel Fuels

Biodiesel fuels are further investigated in terms of spray characteristics. Spray tip penetration length, spray cone angle and break-up length are important parameters. As it is seen in Figure 2.13, spray penetration length is the length between the nozzle and the farthest point of the spray boundary on the spray axis, and spray cone angle is the angle between the nozzle tip and two farthest apart points on the spray outline. Break-up length is the length between the nozzle exit and the point where first droplet occurs. Many researchers reported the spray tip penetration length by treating the spray as a whole structure without considering the vapour and liquid phases separately. Also, few

researchers investigated the penetration lengths of liquid and vapour phases, separately. Additionally, some researchers measured the break-up lengths of penetrating sprays.

In the followings, the effects of fuel properties on the spray characteristics will be explained. Besides the fuel properties, fuel injection pressure (FIP), ambient pressure and ambient temperatures are important parameters that affect the spray behaviour. The effects of FIP and ambient pressure on spray characteristics can be found in the following references [112, 113, 122, 123, 128, 133, 135]. In addition, references [132, 134] explained the effects of ambient temperature on spray characteristics.

2.7.5.1. Spray Penetration Length

Firstly, according to most researchers [113, 122, 123, 124, 126, 128, 129, 131, 135], spray penetration length increases with the use of biodiesel fuel instead of traditional diesel fuel. For instance, Lee et al. [122] investigated the effects of various blend ratios (40%, 60% and 100%) of biodiesel fuel derived from karanja oil on spray characteristics in a constant volume combustion chamber (CVCC). They reported increased spray penetration lengths for biodiesel fuels compared to traditional diesel fuel. Also, rising the biodiesel percentage in blended fuels extended the spray penetration lengths. Next, Agarwal et al. [126] studied the spray characteristics of karanja and jatropha biodiesel fuels, and their blends with diesel fuel in the ratio of 5%, 20% and 100% in a CVCC. They measured the spray tip penetration length for reference diesel fuel as 9.91 cm. Spray penetration lengths of karanja biodiesel and its blends were 10.15 cm, 10.87 cm and 12.19 cm for B5, B20 and B100, respectively. And, spray penetration lengths of jatropha biodiesel and its blends were 9.98 cm, 10.37 cm and 11.11 cm for B5, B20 and B100, respectively. Namely, biodiesel fuels penetrated longer than diesel fuel. Again, increasing the biodiesel percentage in blended fuels raised the spray penetration lengths. Next, Subramanian and Lahane [124] numerically predicted the spray characteristics by several models. First, they produced karanja biodiesel, and blended with conventional diesel fuel in the ratio of 10% and 20%. Then, they measured the injection and combustion characteristics in a four-stroke, air-cooled, single-cylinder, direct-injection diesel engine. Measured injection and combustion characteristics which were injection duration, in-line fuel pressure and in-cylinder pressure were used as inputs to the models. The numerical study was performed to obtain the spray characteristics of the biodiesel fuel against crank angle of

the engine for partial (75%) load and full load. As a result of the numerical study, they found that spray penetration lengths of blended fuels were respectively 4.3% and 2.64% higher for B10, and B20 than that of the reference diesel fuel. Various reasons can be shown for the increase in spray penetration lengths with biodiesel fuels, such as larger density [122, 128, 131], greater viscosity [113, 123, 126, 128] and higher surface tension [113, 123, 128] values of biodiesel fuels. Higher surface tension and viscosity of biodiesel fuels can help spray resist deformation thus retard the spray break-up, leading to increased penetration lengths [113, 128]. Also, droplets of biodiesel fuels can have bigger kinetic energies due to their bigger densities, leading to longer penetrations [128]. In addition, lower viscosity of diesel fuel compared to biodiesel fuel results in increased exit velocity from the injector nozzle which enhances fuel atomization thence reduces penetration lengths [123, 126].

Secondly, several researchers found similar spray penetration lengths for biodiesel and diesel fuels [112, 125, 127, 130]. For example, Patel et al. [125] investigated the spray characteristics of different biodiesel fuels derived from waste cooking oil, jatropha oil and karanja oil in an optical single-cylinder diesel engine. They found no significant differences in spray penetration lengths of all fuels at FIPs of 40, 80 and 120 MPa. Similar result was found by Y. Lin and H. Lin [130] for waste cooking oil biodiesel in a constant volume combustion chamber.

On the other hand, Xie et al. [133] found decrease in spray penetration length of biodiesel fuel compared to reference diesel fuel. They used drainage oil biodiesel with different blend ratios (20%, 50%, 80% and 100%), and examined the spray characteristics of these fuels in a CVCC. They found that increasing the blend ratio of biodiesel fuel decreased the spray tip penetration length compared to that of conventional diesel fuel. They explained short penetration lengths of neat biodiesel and blended fuels with the higher viscosity and surface tension of biodiesel fuel than those of diesel fuel, which enhanced the friction between the fuel and the injector nozzle thence reduce the exit velocity.

Furthermore, several studies investigated the liquid and vapour penetration lengths separately [114, 121, 132, 134]. For example, Mancaruso et al. [121] investigated pure rapeseed oil biodiesel and its blend (50%) with diesel in an optical single-cylinder diesel engine. They observed higher liquid penetrations for biodiesel fuels. Even in low speeds wall impingement was observed when using biodiesel fuel. They explained this situation with lower volatility of biodiesel fuel than diesel fuel leading to late start of vaporization

process. However, they found no significant differences in vapour phase penetration for all fuels. Similar results were found by Nerva et al. [134]. They compared the spray characteristics of soy biodiesel fuel with conventional diesel fuel in a CVCC. They observed faster liquid penetrations for biodiesel fuel, similar vapour penetration lengths for both fuels. They explained that higher liquid penetrations for biodiesel fuels were possible by having higher spray momentums. Besides, Kuti et al. [114] and Hwang et al. [132] also observed higher liquid penetration lengths for biodiesel fuels.

2.7.5.2. Spray Cone Angle

Many researchers [113, 121, 122, 123, 128, 129, 132, 133, 135, 136] observed significant or slight reductions in spray cone angle for biodiesel fuel sprays. For example, Mohan et al. [123] investigated the spray characteristics of waste cooking oil biodiesel and its blend with conventional diesel fuel in the ratio of 20% in a CVCC. They observed narrower spray shapes thus smaller spray cone angles for biodiesel fuels. Also, they explained that pure biodiesel fuel showed darker spray images than those of diesel fuel due to weak light scattering from neat biodiesel spray. This was because of the poor atomization of biodiesel fuel. Next, Yu et al. [113] experimentally studied the diesel and biodiesl spray characteristics emerging from equilateral triangular orifice. They found significantly smaller spray angles for biodiesel fuel under all experimental conditions. Particularly, they found that average spray cone angle for biodiesel fuel was 20.8% smaller than that of diesel fuel at 1 ms after SOI, under the backpressure of 3 MPa, and the injection pressure of 90 MPa. Researchers, who have conducted different studies and concluded that the spray angle for biodiesel is reduced, brought several reasons for this situation such as greater viscosity [113, 123, 128, 132, 133, 135, 136], higher surface tension [113, 128, 133, 135, 136] and bigger density [121, 132, 136] values of biodiesel fuels resulting in poor atomization, and higher evaporating temperature leading to reduced evaporation of biodiesel fuel spray [132].

Secondly, several researchers found similar values for spray cone angles of both biodiesel and diesel fuels [112, 127, 130, 131]. For example, Patel et al. [112] examined the spray characteristis of jatropha biodiesel fuel in a CVCC. They found no distinct difference in spray cone angles of biodiesel and reference diesel fuels, particularly at higher ambient pressures (10 bar and 20 bar).

However, few researchers found increase in spray cone angle when using biodiesel fuel instead of traditional diesel fuel [124, 125, 126]. For instance, Subramanian and Lahane [124] numerically predicted the spray cone angle for the blends of karanja biodiesel and diesel in the ratio of 10% and 20% under engine-like simulations. Although spray cone angle for the blended fuels was smaller than that of reference diesel fuel before TDC, it was larger than reference diesel at TDC. They explained that the possible reason for this was charge density which was directly related with the in-cylinder pressure. They showed that the increasing and reducing trend of spray angle followed as in-cylinder pressure pattern. Next, Agarwal et al. [126] investigated the spray angles of karanja biodiesel fuel in comparison with fossil diesel fuel. They found that spray angles were 19.30°and 20.98°for diesel and biodiesel fuel, respectively. They explained that this incrase might be basically due to the resistance of air to the incoming fuel droplets.

2.7.5.3. Spray Break-up Length

Few researchers measured the break-up length for biodiesel fuels in comparison to that of traditional diesel fuel [124, 131, 136]. For example, Lahane and Subramanian [136] calculated the spray break-up lengths for karanja biodiesel fuel and their blends (for blend ratios of 5%, 10%, 15%, 20%, 25% and 50%) with diesel fuel. They found that break-up lengths of neat biodiesel and diesel fuels were 13.9 mm, and 13.5 mm at the rated load. Also, increasing the biodiesel percentage in the blended fuels increased the break-up length. They explained that this increase caused by the higher density of biodiesel fuel. In addition, Mancaruso et al. [131] calculated the break-up times for diesel and biodiesel fuels from Hiroyasu, and Siebers correlations at 1500 rpm engine speed. Break-up times were calculated by Hiroyasu model as 143.7 μs and 146 μs for diesel and neat biodiesel, respectively. Namely, break-up occured later for biodiesel fuel. In addition, they compared the calculations with the experimental data by examining the spray images in detail, and reported that the data obtained from experiments showed a good agreement with the data obtained from theoretical calculations. That means the experiments also showed that spray break-up occured later for biodiesel fuel. As a result of the study, they explained that the increase in break-up time for biodiesel fuel was related with the higher boiling point of biodiesel than that of diesel fuel, which affected the evaporation process.

2.7.6. Comparison of Methyl Ester and Ethyl Ester

Limited amount of studies are available for ethyl ester type biodiesel fuels compared to methyl ester type biodiesel fuels in terms of combustion, performance and emission characteristics. According to many researchers [137, 138, 139, 140, 141, 142, 143, 144], combustion, performance and emission characteristics of ethyl esters are comparable with those of methyl esters. Namely, researchers found similar results or very little differences for both ethyl esters and methyl esters based on the same feed stock. Table 2.5 shows the studies which investigate the performance, emission and combustion characteristics of ethyl esters, and compares these characteristics with those of methyl esters. Furthermore, physical and chemical properties of both fuels are compared in the table to create a better understanding.

For example, Sanli et al. [137] investigated the performance, combustion and emission characteristics of methyl ester and ethyl ester derived from waste frying oil in a six-cylinder, four stroke, water cooled, turbocharged, direct injection diesel engine. Firstly, when the physical and chemical properties of fuels are compared, it would be seen that these properties are very similar with small differences. Density of ethyl ester is 0.1% smaller than that of methyl ester. Viscosity, calorific value and cetane number of ethyl ester are 8.8%, 0.58% and 2.5% are higher than those of methyl ester, respectively. Secondly, they compared the performance characteristics of these fuels in terms of BSFC and BTE. On average, ethyl ester performed 2.38% decrease in BSFC, and 1.98% increase in BTE. They explained that this difference was caused by the relatively higher calorific value of ethyl ester. Next, they investigated the combustion characteristics of ethyl ester in terms of in-cylinder pressure in comparison with that of methyl ester. They found very close values for both types of fuels. They realized that combustion of methyl ester started slightly earlier than that of ethyl ester. Authors of the article explained that this situation might be a result of relatively high cetane number of methyl ester over ethyl ester. Finally, they compared these fuels in terms of exhaust emission characteristics. On average, ethyl ester emitted 8% less CO and 12.74% less HC than methyl ester. NO_x emissions were very close to each other for both fuels. Authors explained that less CO emissions of ethyl ester caused by more calorific value of ethyl ester resulted in higher air-fuel ratios for ethyl ester type of biodiesel fuel. As a conslusion to this study, ethyl ester had slightly better results in terms of performance and combustion characteristics when compared to those of methyl ester.

Table 2.5. Performance and emission investigations of ethyl ester in comparison to methyl ester from the literature.

Reference	Properties of the Tested Engine						Ethyl Ester (and blends with diesel)	Properties				Combustion Characteristics		Performance			Emissions			
	No of cylinder	Cooling	Aspiration	CR	RP (kW)	RS (rpm)		Density	Viscosity	CV	CN	In-cylinder pressure	HRR	BSFC	BTE	BP	NO$_x$	HC	PM	CO
[137]	6	WC	TC	16.4:1	136	–	20% and 100%	↓	↑	↑	↓	↑	–	↓	↑	–	↑	↓	–	↓
[138]	4	WC	TC	18.45:1	7.4	1500	100%	↑	↑	↑	↓	↑	↑	↑	↑	–	–	–	–	–
[139]	1	AC	NA	17.5:1	7.4	1500	10%, 20% and 100%	↓	↑	↑	↓	–	↓	↑	↓	–	↑	↑	↑	↑
[140]	1	WC	–	–	5.2	–	20%, 40%, 60%, 80% and 100%	↓	↓	→	–	↑	↑	–	↑	–	↑	–	↑	–
[141]	1	WC	–	17.5:1	5.9	1500	5% and 10%	↑	↑	↑	↑	–	–	↓	↑	–	↑	↑	↑	↑
[142]	4	–	–	–	65	–	20% and 50%	↓	↑	–	–	–	–	–	–	–	↓	–	–	–
[143]	1	WC	–	variable (12-18)	5.2	1500	10% and 20%	↓	↓	↑	–	–	–	↓	↑	–	↓	↑	–	↑
[144]	1	–	–	17.5:1	5.5	3000	100%	↑	↑	–	–	–	–	↑	–	↑	↑	–	↑	↑

Abbreviations: WC: water cooled, AC: air cooled, NA: naturally aspirated, TC: turbocharged, CR: compression ratio, RP: rated power, RS: rated speed, ↑: slight increase, ↓: slight decrease, →: similarity, –: no data available, CV: calorific value, CN: cetane number, HRR: heat release rate, BSFC: brake specific fuel consumption, BTE: brake thermal efficiency, BP: brake power, NO$_x$: nitric oxides, HC: hydrocarbon, PM: particulate matters, CO: carbon monoxide.

Note: All ethyl esters are produced via transesterification process.

55

Besides, Alptekin et al. [138] compared the performance and combustion characteristics of ethyl ester and methyl ester derived from waste frying oil. Fuels had similar physical and chemical properties with small distinctions. They found comparable BSFC and BTE values for both fuels. The average difference between ethyl ester and methyl ester in terms of BTE and BSFC was lower than 1.2% and 1%, respectively. Besides, they found comparable maximum cylinder pressures for ethyl ester and methyl ester. Numerically, maximum cylinder pressures of ethyl ester and methyl ester were 3.6% and 3% higher than that of reference diesel fuel. Additionally, there was a relative difference in heat release rates of these fuels, and this difference was around 2%.

Moreover, Gautam et al. [139] investigated the combustion, performance, emission characteristics of methyl ester and ethyl ester derived from jatropha oil and their blends with traditional diesel fuel in the ratio of 5%, 10%, 20% and 30% in a single-cylinder, direct injection compression ignition engine under variable loads. First of all, ethyl ester had 1% less density, 5.3% more viscosity and 0.8% more calorific value compared to methyl ester. They found that ethyl ester and methyl ester performed comparable combustion property, and that the optimum blend ratio was 20%. BSFC values of B20 of methyl ester and ethyl ester were 9.8% and 8.6% lower than that of diesel fuel, respectively. BTE values of B20 of methyl ester and ethyl ester were 11% and 9.3% higher than that of diesel fuel, respectively. Besides, NO_x, CO, HC and PM emissions were very close to each other for both ethyl and methyl esters.

These three studies and references [140, 141, 142, 143, 144] showed that there were no significant differences in combustion, performance and emission characteristics of ethyl esters and methyl esters. Researchers suggested that both ethyl ester and methyl ester can be alternative fuels for fossil diesel fuel.

Moreover, there is no published research available in the literature while this study is being conducted, which compares the spray characteristics of ethyl ester type biodiesel fuels with those of methyl ester type biodiesel fuels. Considering the importance of spray investigation, this gap in the literature is a necessary topic to be pointed out.

CHAPTER 3

EXPERIMENTAL DESIGN AND METHODOLOGY

3.1. Biodiesel Production

In this study, biodiesel fuels were produced through transesterification process. Biodiesel production will be explained in two steps. Firstly, theory of transesterification will be explained briefly. Then, methodology of biodiesel production utilized in the study will be expressed.

3.1.1. Theory of Transesterification

Transesterification is the process of converting a carboxylic acid ester into a different carboxylic acid ester. In the most common method, the reaction of ester occurs with an alcohol such as methanol, ethanol, etc. in the presence of a catalyst such as alkaline metal hydroxides, acids, carbonates, etc. For the production of biodiesel, relevant lipids from vegetable oil are triacylglycerols (TAGs) and free fatty acids (FFAs) [145]. In the stoichiometric reaction, 1 mol of a TAG reacts with 3 mol of alcohol. Whereas, excess amount of alcohol is generally used in order to increase the biodiesel yield [146]. Figure 3.1 shows the stoichiometric reaction of transesterification of vegetable oils for biodiesel production. As a result of the reaction, biodiesel is obtained as the main product, and glycerol is obtained as a by-product.

$$
\begin{array}{cccccc}
CH_2\text{-}OOC\text{-}R_1 & & & R_1\text{-}COO\text{-}R' & & CH_2\text{-}OH \\
| & & \text{Catalyst} & & & | \\
CH\text{-}OOC\text{-}R_2 & + & 3\ R'OH \longleftrightarrow & R_2\text{-}COO\text{-}R' & + & CH\text{-}OH \\
| & & & & & | \\
CH_2\text{-}OOC\text{-}R_3 & & & R_3\text{-}COO\text{-}R' & & CH_2\text{-}OH \\
\text{TAG} & & \text{Alcohol} & \begin{array}{c}\text{Alkyl-ester}\\\text{Biodiesel}\end{array} & & \text{Glycerol}
\end{array}
$$
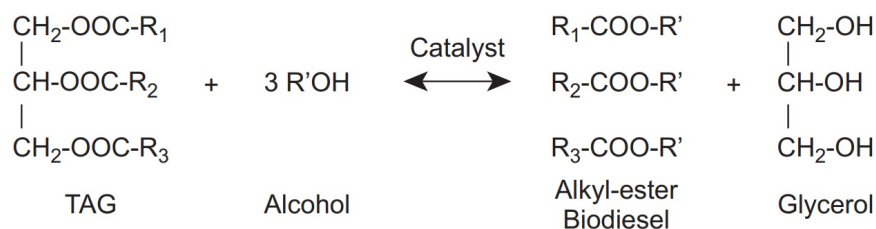
Figure 3.1. Transesterification of vegetable oils [145].

$$ROH + B \rightleftharpoons RO^- + BH^+ \qquad \text{(a)}$$

R'COO—CH₂
R"COO—CH   +   ⁻OR   ⇌
H₂C—OCR'''
        ‖
        O

R'COO—CH₂
R"COO—CH   OR
H₂C—O—C—R'''
        |
        O⁻   (b)

R'COO—CH₂
R"COO—CH   OR
H₂C—O—C—R'''   ⇌
        |
        O⁻

R'COO—CH₂
R"COO—CH   +   ROOCR'''   (c)
H₂C—O⁻

R'COO—CH₂
R"COO—CH   +   BH⁺   ⇌
H₂C—O⁻

R'COO—CH₂
R"COO—CH   +   B   (d)
H₂C—OH
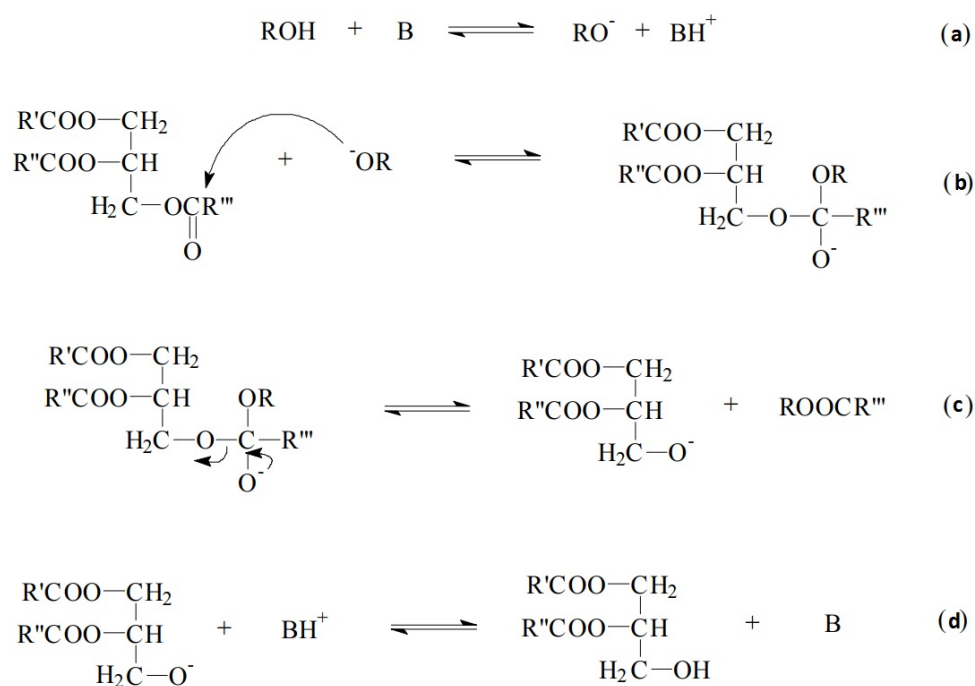
Figure 3.2. Mechanism of the base-catalyzed transesterification of vegetable oils [146]. (B indicates the base catalyst.)

In the production process of biodiesel fuels used in this study, KOH, which is base, was used as the catalyst. Therefore, the reaction mechanism of the base-catalyzed transesterification of vegetable oils is explained in the followings, see Figure 3.2. This reaction mechanism is valid for any alcohol to be used.

In the first step (Figure 3.2a), base catalyst reacts with the alcohol, and protonated catalyst and an alkoxide are produced. In the second step (Figure 3.2b), a tetrahedral intermediate occurs by the nucleophilic attack of the alkoxide at the carbonyl group of the triglyceride, where the corresponding anion of the diglyceride and alkyl ester are formed (Figure 3.2c). The latter cleans the catalyst from the proton, producing active species that can now react with a second alcohol molecule (Figure 3.2d), thereby initiating another catalytic cycle. Diglycerides and monoglycerides which are obtained before are converted into a mixture of alkyl esters and glycerol by the same mechanism [146].

At the end of the transesterification process, the by-product glycerol must be removed from the biodiesel-glycerol mixture. Additionally, biodiesel must be purified to improve its quality by removing excess contaminants such as alcohol, catalyst etc., and impurities such as soap, wax etc. [147]. In conventional transesterification process, purification method is called as washing process. Wet washing is the most widespread method

for purification of biodiesel fuels [148]. In wet washing, water which has a potential to supply a means for addition of acid in order to neutralize the unreacted alkali catalyst is used. Wet washing process can simply remove the salt products formed during the transesterification process.

3.1.2. Procedures for Biodiesel Production

Biodiesel fuels were produced in Renewable Energy and Hydrogen Research Laboratory of the Department of Chemical Engineering in Izmir Institute of Technology.

In this section, procedures utilized in the study to produce biodiesel fuels will be explained. Before the production of biodiesel, some calculations were needed to obtain the required amount of alcohol and catalyst to be used. These calculations and some important properties like chemical formula, density, molecular weight of alcohols and vegetable oils used in the study are given in Appendix A.

First of all, it is needed to provide some information regarding the process conditions for the production of biodiesel. For methyl ester production, molar ratio of methanol to lipid was 6, and 1 wt% KOH was used as the catalyst. For ethyl ester production, molar ratio of ethanol to lipid was 24, and 0.1 wt% KOH was used as the catalyst. The reaction time was 240 minutes. The reaction temperature was 50 °C. Besides, all reactions were carried out using a magnetic stirrer with a thermometer as shown in Figure 3.3.

Apart from the alcohol and catalyst ratios used, the method used for the production of both methyl ester and ethyl ester was not changed. Therefore, both methanol and ethanol will basically be referred to as alcohol during explaining the biodiesel production method. Firstly, catalyst which was KOH was added to alcohol at room conditions. Then, the solution started to be stirred at 1100 rpm, and its temperature was increased to 50 °C. At the same time, vegetable oil was heated up to 50 °C. After the temperature of alcohol-catalyst solution reached 50 °C, this solution was stirred at 1100 rpm for a further 10 minutes. In the next step, vegetable oil at 50 °C was added into the alcohol-catalyst solution at 50 °C, and this mixture was stirred at 1100 rpm for 240 minutes. After the reaction, the mixture was waited until formed glycerol precipitation completed. Then, biodiesel was separated from the glycerol.

After obtaining the biodiesel, washing step was applied to improve the biodiesel quality. 5 vol% acetic acid solution in water was prepared, and pH of acetic acid solution
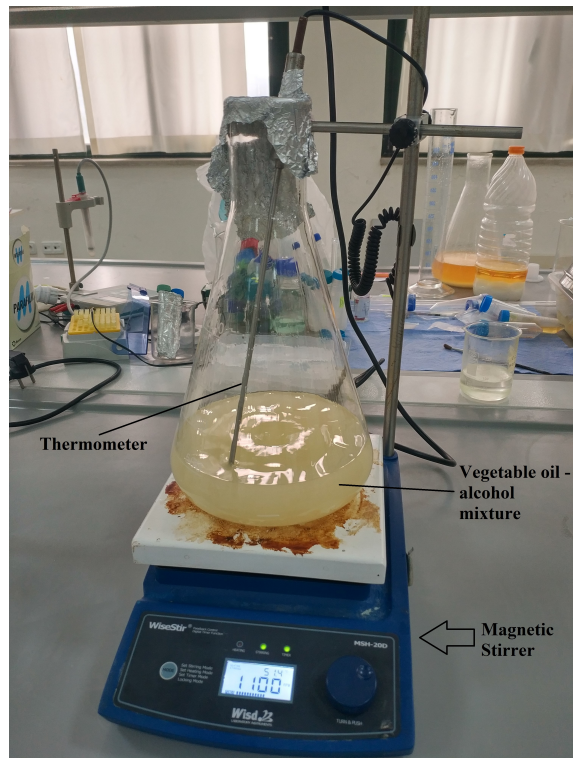
Figure 3.3. Biodiesel production process in the laboratory.

was measured. Then, 1/3 vol% acetic acid solution was added into the biodiesel so that the ratio of acetic acid solution and biodiesel to be washed was 1/3 in volume. Next, this mixture was stirred at 500 rpm for 60 minutes. After 60 minutes, water was separated from biodiesel. These steps were repeated until pH of acetic acid solution in water removed from biodiesel washed was the same as the bulk acetic acid solution. After reaching the required pH value, the washing process was finished. In the next step, samples were dried at 75 °C at vacuum for 24 hours in order to remove remaining water molecules. Finally, biodiesel fuel was prepared for use.

3.2. Fuel Properties

Four methyl ester samples were prepared from corn oil, canola oil, sunflower oil and cotton oil; two ethyl ester samples were prepared from corn oil and sunflower oil; and fossil diesel fuel was used as a reference fuel. Methyl esters are referred to as CORME, CANME, SUNME and COTME due to their feed stocks which were corn oil, canola oil,

sunflower oil and cotton oil, respectively. Ethyl esters are named as COREE and SUNEE due to their feed stocks which were corn oil and sunflower oil, respectively. Before giving the properties of the fuels, density, viscosity and contact angle measurement methods utilized will be explained.

The densities of fuels were measured by using a calibrated pycnometer. The full volume of the pycnometer is 25.066 ml, and it is calibrated with 0.001 ml sensitivity with its lid. Now, it will be explained how the densities of the fuels were measured. Firstly, temperature of fuels brought to room temperature. Secondly, the mass of the empty pycnometer was weighed on a precision scales. Thirdly, first fuel was added into the pycnometer. After that, the lid of the pycnometer was closed, and excess fuel overflowed. Then, the outer surface of the pycnometer was cleaned with acetone from excess fuel. Next, the mass of the pycnometer which was filled with a fuel was weighed 10 times, and the mass of empty pycnometer was subtracted from the average mass of fuelled pycnometer thus the mass of the fuel in the pycnometer was found. Finally, the density of the first fuel was found by dividing the mass of the fuel by the volume of the pycnometer. After calculating the density of first fuel, pycnometer was drained, and was cleaned with acetone in order to ensure that the density of another fuel could be measured accurately. These steps were repeated for all fuels.

Besides, the viscosities of the fuels were measured using AR 2000ex rheometer, which is developed by TA Instruments. Table 3.1 shows some properties of the rheometer. The rheometer was used in controlled rate mode. The angular velocity of the rotating plate in the rheometer was given to the system as 10.5 rad/s, and the temperatures of the plates were adjusted so that the temperature of the fuel was 40 °C. Additionally, 1 data was received in 5 seconds, and 60 data were obtained for each experiment in total.

Table 3.1. Properties of the rheometer used in this study. (Data source: [149]).

Property	Value
Minimum Torque Oscillation	0.03 μN.m
Minimum Torque Steady	0.05 μN.m
Maximum Torque	200 mN.m
Torque Resolution	1 nN.m
Angular Velocity Range	0 to 300 rad/s
Step Change in Velocity	25 ms
Concentric Cylinder	-20 to 150 °C
Upper Heated Plate	-30 to 150 °C
Electrically Heated Plate	-80 to 400 °C

Table 3.2. Properties of the optical tensiometer used in this study. (Data source: [150]).

Property	Value
Contact Angle Measurement Range	0°-180°
Contact Angle Measurement Sensitivity	± 0.1°
Surface Tension Measurement Range	0.01 - 2000 mN/m
Surface Tension Measurement Accuracy	± 0.01 mN/m
Maximum Resolution	1984 x 1264 pixels
Maximum Measurement Speed	3009 fps

Moreover, the contact angles of all fuels were measured to predict the surface tension effects. They were measured by using Theta Optical Tensiometer that is developed by Attension. Table 3.2 shows some properties of the optical tensiometer. In addition, glass was used as the solid material to obtain the contact angles. Each fuel were tested three times at 25°, and values were calculated by taking the average of 3 experiments.

Table 3.3 shows the viscosity, density and contact angle values of the tested fuels. Diesel fuel has the lowest viscosity, density and contact angle values. Although all biodiesel fuels have higher density, viscosity and contact angle values than the fossil diesel fuel, they differ among themselves. When the biodiesel fuels produced from the same feed stocks are compared, the densities and contact angles of the ethyl esters are lower, and their viscosities are higher compared to those of methyl esters. For example, SUNEE has 1.7% lower density, 2.8% reduced contact angle and 13.2% higher viscosity than those of SUNME. Density, contact angle and viscosity values of COREE are 1.1% and 2.3% lower and 14.4% higher than those of CORME, respectively.

Table 3.3. Properties of the fuels tested in this study.

Test Fuel	Viscosity (mm^2/s)	Density (kg/m^3)	Contact Angle (°)
Diesel	3.07	829.55	14.71
Corn Oil Methyl Ester (CORME)	5.83	883.26	20.46
Sunflower Oil Methyl Ester (SUNME)	5.17	880.83	20.34
Canola Oil Methyl Ester (CANME)	5.12	873.50	20.16
Cotton Oil Methyl Ester (COTME)	4.24	884.01	20.23
Corn Oil Ethyl Ester (COREE)	6.67	873.69	19.98
Sunflower Oil Ethyl Ester (SUNEE)	5.85	865.71	19.78

Note: Viscosity values were obtained at 40 °C. Density and contact angle values were measured at 25 °C. Contact angle of all fuels were with glass.

3.3. Experimental Setup

Spray measurement of biodiesel fuels were performed in a constant volume combustion chamber allowing optical visualization. In this test rig, spray properties and flame lift-off length of fuels can be obtained. However, only spray measurement was performed with the fuels. The test rig is located in Internal Combustion Engines Research Laboratory in the Department of Mechanical Engineering at Izmir Institute of Technology.

A picture of the test rig is shown in Figure 3.4, and a schematic sketch of the experimental setup is shown in Figure 3.5. The experimental setup consists of eight different subsystems with different functions. These eight subsystems are constant volume combustion chamber, gas filling system, fuel injection system, optical system, control system, ignition system, heating system and exhaust system. But, two subsystems are not used for spray measurement. Ignition system is not utilized because there is no combustion in the experiments. Heating system is not employed because experiments were performed at room temperature. In the followings, each subsystem will be explained briefly.
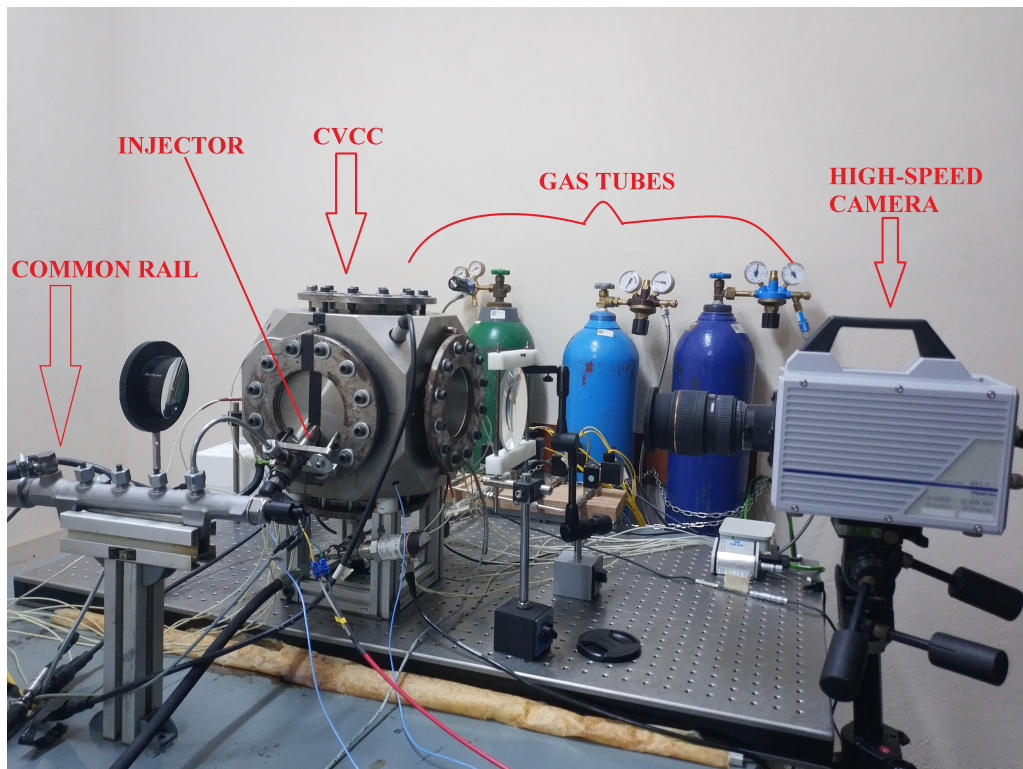

Figure 3.4. Test rig.
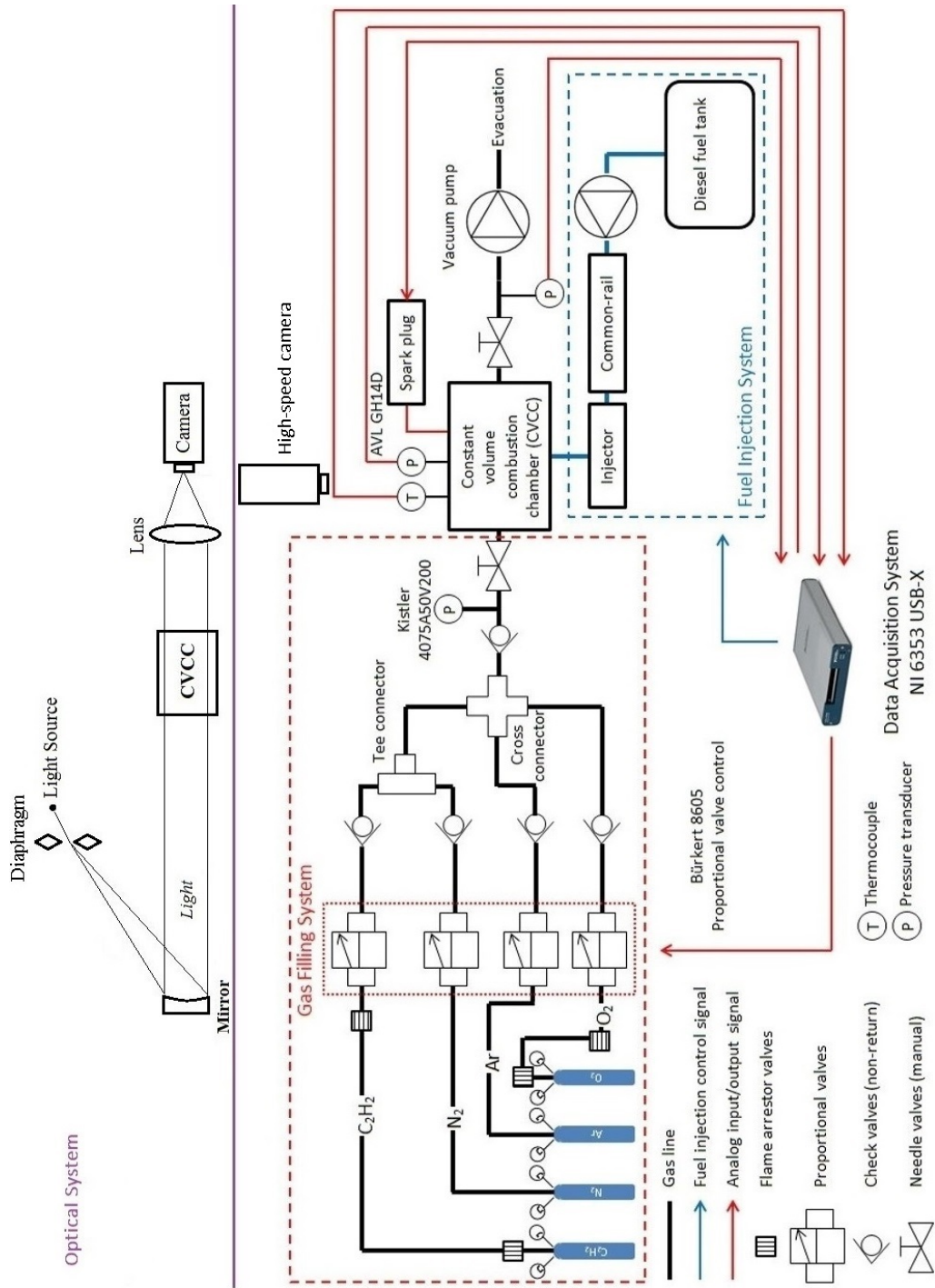
Figure 3.5. Schematic sketch of the experimental setup.

3.3.1. Constant Volume Combustion Chamber

Constant volume combustion chamber (CVCC) is a useful tool to simulate an engine-like environment in order to obtain the spray characteristics of any fuel or flame lift-off length with any injector. Chamber can be filled with different gases to simulate an engine-like condition. Besides, CVCC has optical windows allowing the spray or flame visualization via various optical techniques.
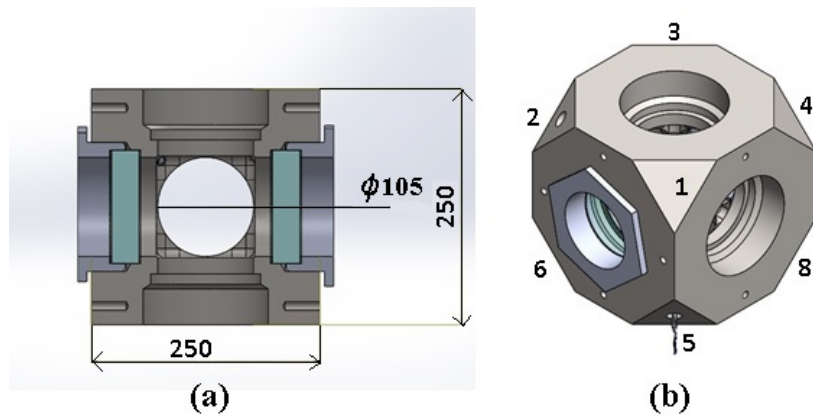
Figure 3.6. (a) Side view of CVCC and (b) its connection slots. (2, 8: spark plugs, 5: thermocouple, 6, 7: pressure sensors, 1, 4: substitute connection slots).

Figure 3.6 shows a side view of CVCC utilized in the experiments and its connection slots. 6 gaps with their lids are available on each surface of the chamber. Each one has diameter of 105 mm. 1 gap is used for gas filling and discharging. 2 of them have optical windows for spray visualization. 1 of the gaps are utilized to insert injectors to the chamber. The remaining 2 gaps are not in use, and they are reserved for future use if needed. Furthermore, main body of the chamber has 8 threaded connection slots which are located on corners, see Figure 3.6b. NPT type threads were threaded for these connection slots thus the connection of auxiliary equipment to the main body can be provided with swagelok fittings and stainless pipes. Thermocouples, spark plugs and pressure sensors can be mounted on these slots.

The chamber was designed to perform tests with up to beginning pressure of 20 bar and beginning temperature of 450 K. It was made of single piece stainless steel. The main goal of using stainless steel is its hardness, durability and tending not to react chemically

with chemicals to be used. It was produced by casting. Thus, weaknesses that may arise due to welding and improper assembling were prevented. Moreover, the chamber is cube shaped. Each edge of the chamber is length of 250 mm, and total internal volume is 2.05 liters.

2 quartz windows whose diameters and thicknesses are respectively 120 mm and 30 mm are located on two opposing surfaces of the chamber by using flanges. Windows have high light transmittance in the visible spectrum. Besides, it is not proper for a quartz window to contact with metal surfaces at high temperatures due to its physical properties. Therefore, viton gaskets are placed between quartz windows and metal surfaces, and between windows and flanges thus any possibility for cracking on windows. Additionally, flanges were made of stainless steel, and they are used to fasten the windows on the main body. Also, they compress the gaskets between windows and the main body. Figure 3.7 shows a flange which is utilized in the test rig.
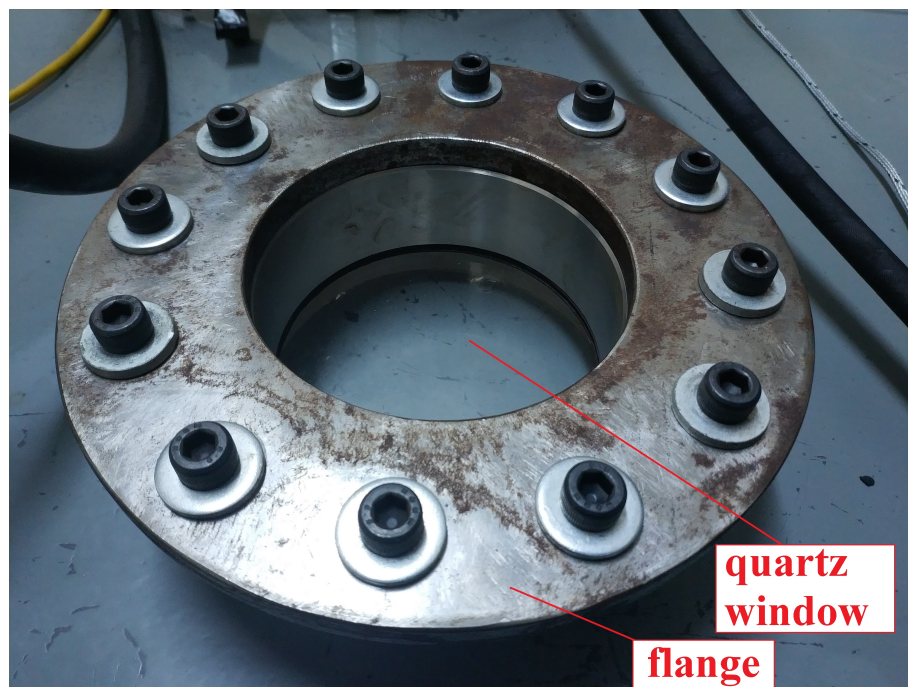
Figure 3.7. Flange and quartz window.

Furthermore, Figure 3.8 shows the schematic sketch of the constant volume combustion chamber as open shape. In this figure, all components of the CVCC are shown in assembly order.
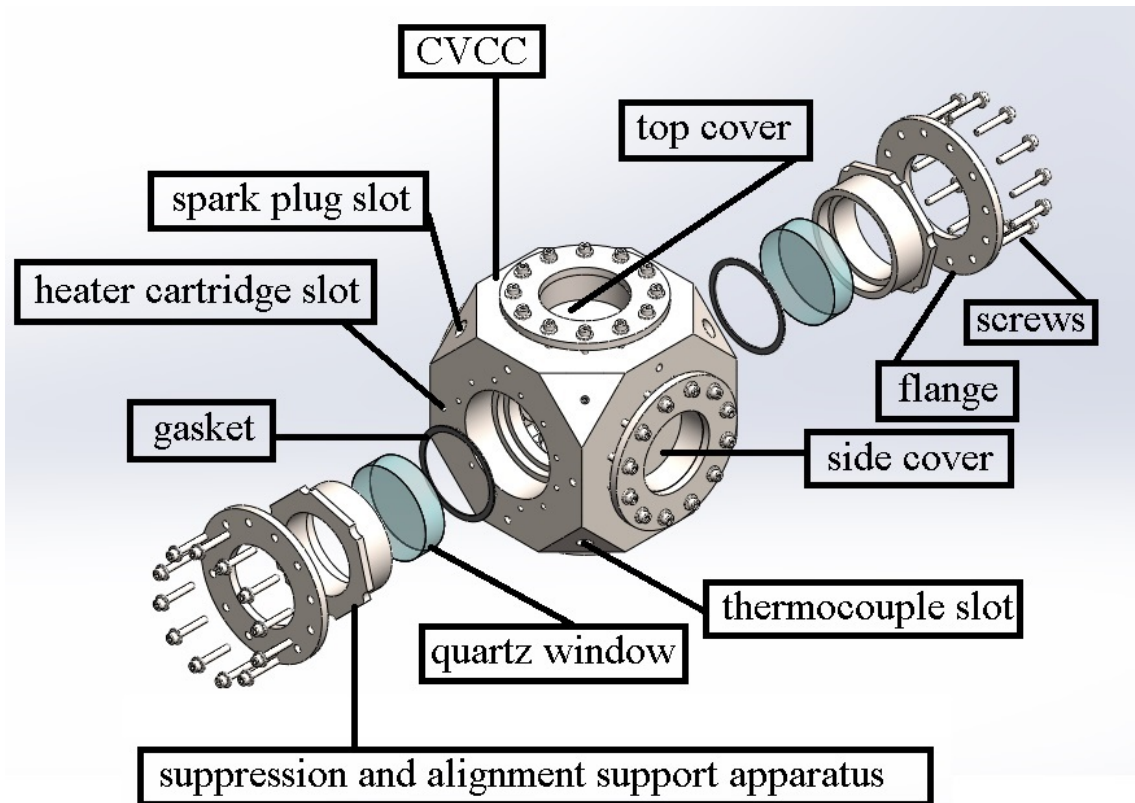
Figure 3.8. CVCC as open shape.

3.3.2. Fuel Injection System

Fuel injection system consists of fuel tank, low pressure pump, high pressure pump, common rail, injector, fuel pipes and hoses. Working principle of a common rail injection system were already explained in Section 2.5.1. In the followings, some information about the equipment used in the injection system will be given.

Fuel pump, which is shown in Figure 3.9, is run by an electric motor whose power is 2.2 kW. Fuel pump gets fuel from the fuel tank, and transfers it to the injector through a common rail whose pressure can achieve up to 2200 bar. Fuel pressure is controlled by two different valves which are volume control valve (VCV) and pressure control valve (PCV). VCV is at the inlet of the fuel pump, and PCV is located at the left side of the common rail. These valves are controlled by pulse-width modulation (PWM), signal amplifier and a data acquisition card.
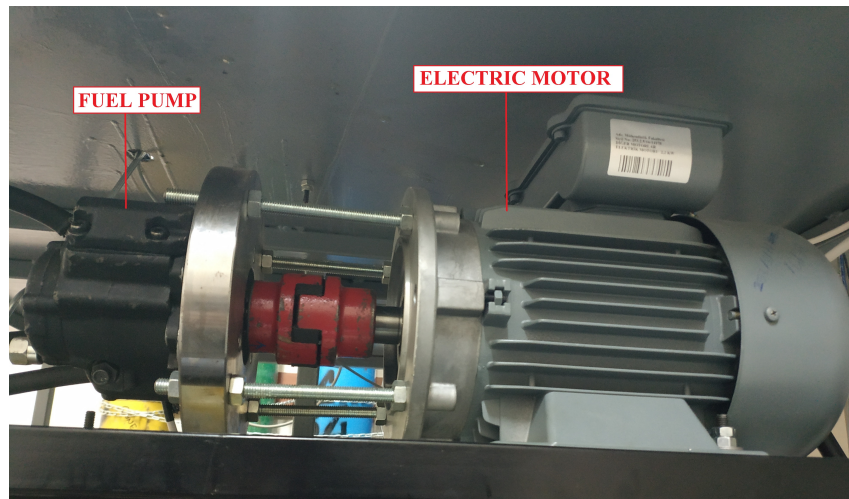
Figure 3.9. Fuel pump and electric motor.

PCV is used to keep the pressure of the fuel in required pressure range. The main reason for focusing on PCV more than VCV is that only one spray is done for each test. Namely, serial sprays are not performed. Therefore, required pressure is adjusted with the PCV while the VCV is run to supply the minimum fuel volume flow rate. The pressure of fuel in the common rail is measured with the pressure sensor which is located at the right side of the common rail. Figure 3.10 shows the common rail with pressure sensor and pressure control valve.
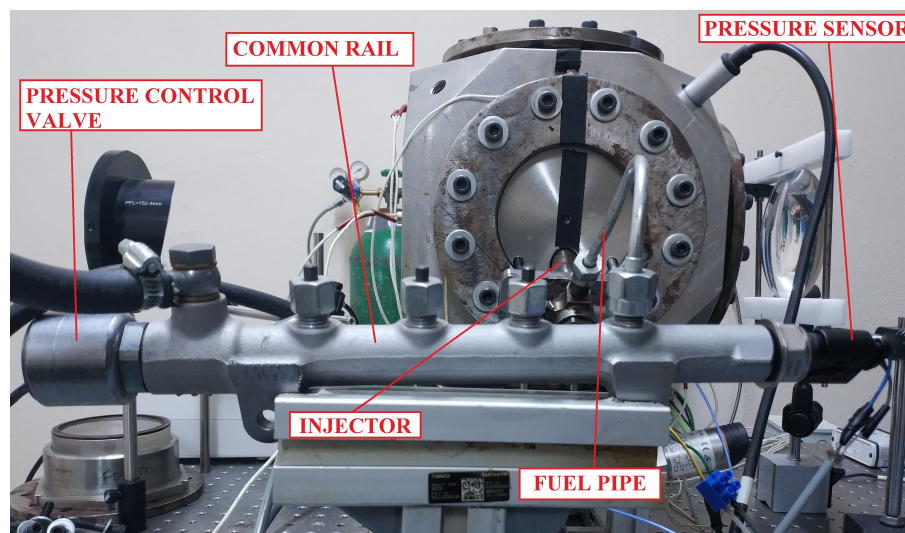
Figure 3.10. Common rail.

Figure 3.11. Motor drivers.

Pulse-width modulated signal is transmitted to valves on the fuel pump from a data acquisition (DAQ) card. Working frequencies of the valves are specified as 400 Hz. There are two valves on the fuel pump, and each one is run by a motor driver which can be able to amplify signal coming from a DAQ card. Thanks to these devices, the signal can be amplified to the required levels with minimal distortion. These motor drives are shown in Figure 3.11.

Moreover, temperatures of the fuels used in the experimental system reach high values. For this reason the fuel tank was built to have a volume of 10 liters, and it was made of stainless steel. Thus, cooling of the fuels between the tests was provided quickly during the experiments. When necessary, a heat exchanger and a cooling fan can be utilized. Besides, all pipes and hoses are selected to withstand long-term fuel transportation, high pressure and high temperature so that the fuel injection system can withstand these factors. Figure 3.12 shows the fuel tank and fuel hoses connected to the fuel tank. All hoses are connected to the fuel tank with the help of clamps which provide sealing. The clamps are tightened in such a way that fuel does not leak from the hoses, and at the same time slits do not form on the hoses.

In the experiments, a piezoelectric injector was used. Figure 3.13 demonstrates the injector that was utilized during the tests. Injector had eight holes for injection on its tip. However, seven holes were closed by laser welding. One hole was left open so

Figure 3.12. Fuel tank and fuel hoses.

that only one required spray formation could be observed. Besides, the injector is run with an injector driver which is shown in Figure 3.14a. A vibration signal is sent to the injector driver from DAQ card then injector is triggered, and fuel injection takes place. In tests, a DC 5 V signal was sent to the injector driver for 1 ms. Injection duration can be adjusted to different periods. However, the injection duration was kept constant at 1 ms in the experiments. Figure 3.14b demonstrates the signal coming from the DAQ card to the injector driver.

Figure 3.13. Piezoelectric injector used in the study.

(a)
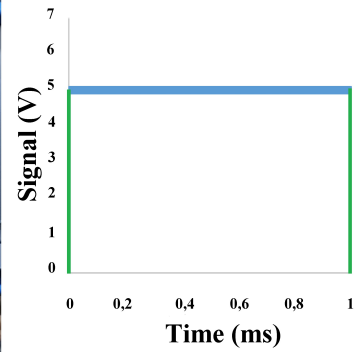
(b)

Figure 3.14. (a) Injector driver and (b) signal to the injector.

The gap on the left-hand side of the combustion chamber is reserved for inserting the injector. The tip of the injector is placed inside the combustion chamber at a 45° angle with the horizontal axis of the chamber. Thus, a longer area is provided for penetration of the spray. Figure 3.15 demonstrates how injector is connected to the combustion chamber. A metal plate through which 2 screws pass is used to fix the injector. Also, in this way, the gas inlet and outlet is prevented from the hole the injector enters.
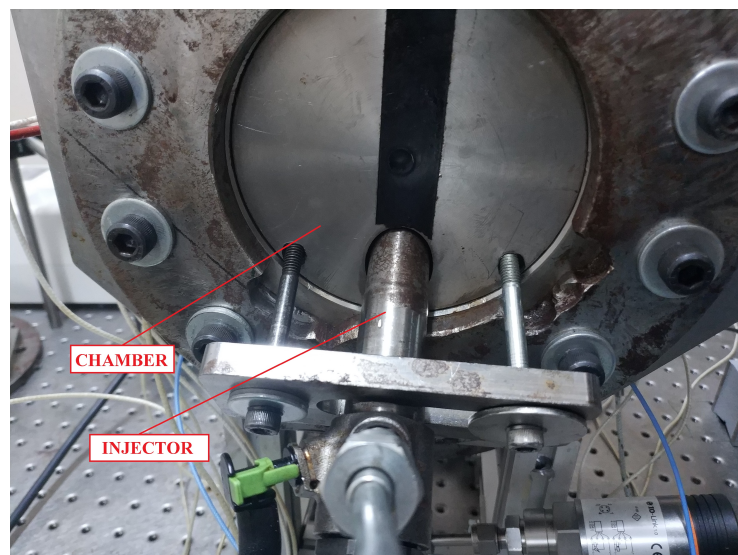
Figure 3.15. Connection of injector to the chamber

3.3.3. Gas Filling System

The purpose of the gas filling system is to supply necessary gases for experiments. For pre-combustion process, four different gases are used to be sent into the combustion chamber, which are acetylene, oxygen, argon and nitrogen. Pre-combustion technique was already explained in Section 2.6. However, there was no combustion experiment in this study. Thus, three gases which were oxygen, argon and nitrogen could be utilized. Of these gases, only nitrogen was used. Because the aim was just to adjust the room pressure, and nitrogen was unlikely to react with fuel. Also, it was easier to control the valve of nitrogen than controlling the valves of other gases, and not dealing with the adjustment of different gases saved time.
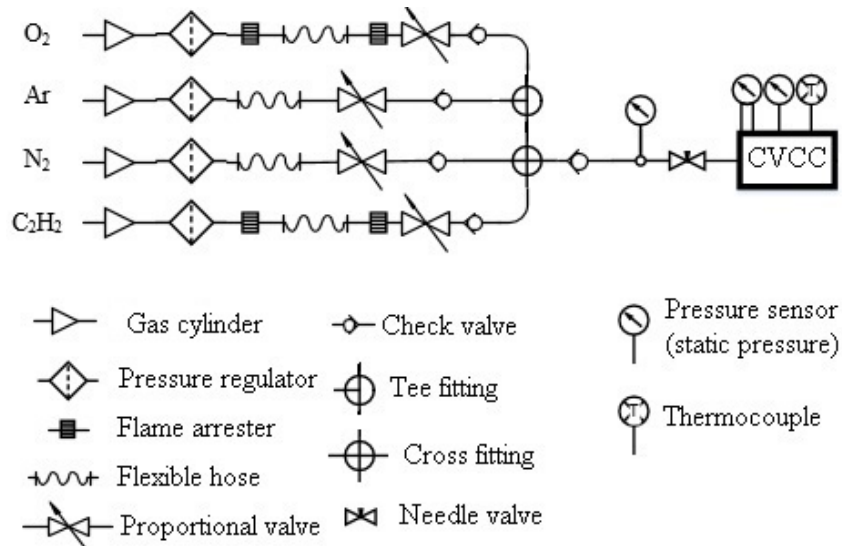
Figure 3.16. Schematic sketch of gas filling system.

Gas filling system is demonstrated schematically in Figure 3.16. In this system, each gas is supplied to the system from industrial pressurized gas cylinders which are shown in Figure 3.17. Pressure regulators were connected to each cylinder to adjust the pressure. As acetylene is flammable, and oxygen is burner, double stage flame arresters were placed after pressure regulators of acetylene and oxygen cylinders. When it comes to a situation such as flame recoil, these valves are used as an explosion preventer by preventing this flame from reaching these gas cylinders. Next, all gases are sent to pro-portional valves through flexible hoses after pressure regulators. After each proportional
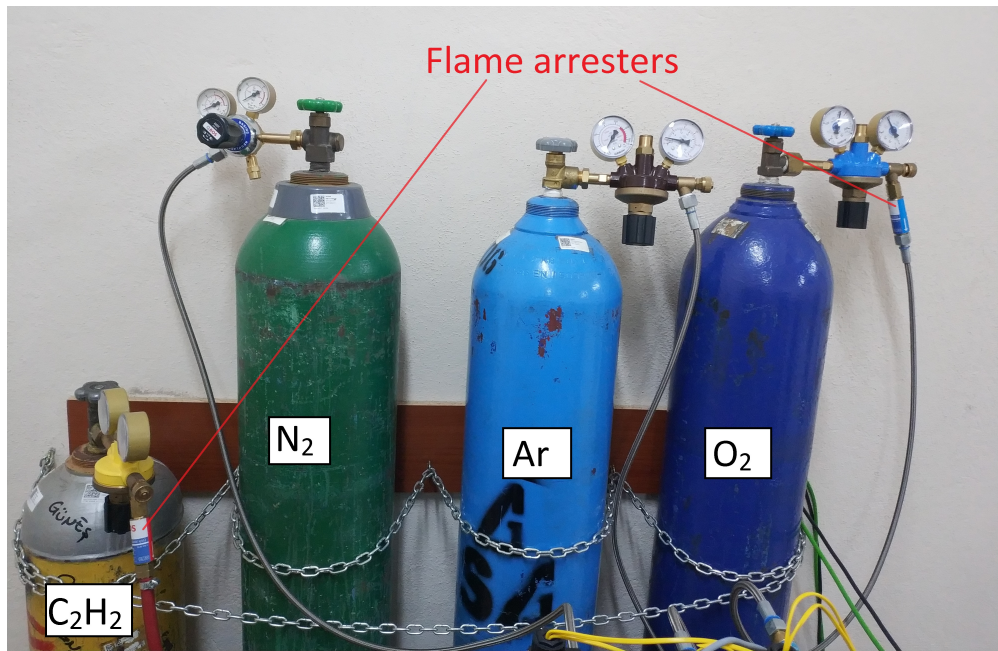
Figure 3.17. Gas cylinders.
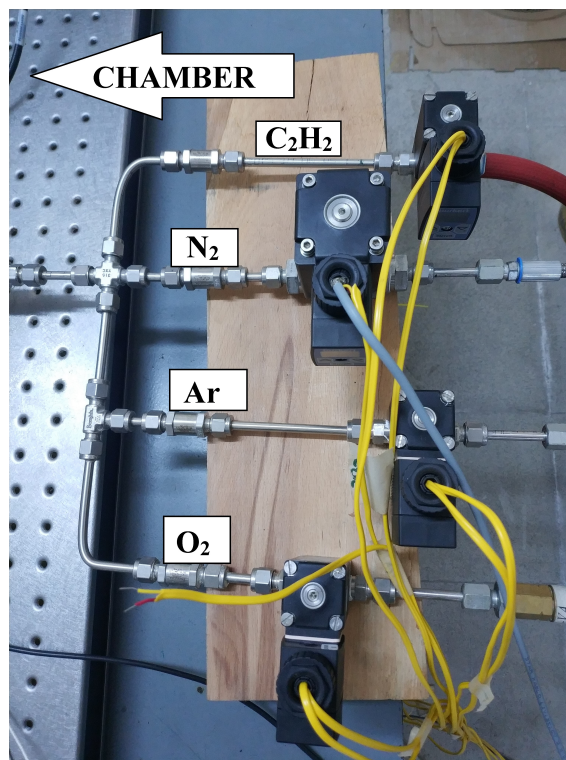
Figure 3.18. Proportional valves.

valve, check valves were mounted to the system to prevent gases from returning from the combustion chamber. Then, gas paths from the four different cylinders were connected to a single pipe, which goes to the combustion chamber, through various fittings. After this connection, a check valve which can overcome high pressures was mounted to prevent the gas from entering the feed line with high pressures that might occur during the experiments. Then, a piezoresistive pressure sensor (Kistler 4075A50V200S, up to 50 bar) was assembled to control the proportional valves during gas filling process. As a last step, after this pressure sensor, an on-off valve was connected to seal the combustion chamber before the experiments when the gas filling process was completed. In addition, all pipes assembled in the gas filling system are 316 stainless steel pipes of Swagelok Company, which have outer diameter of 6 mm and thickness of 1.5 mm.

2 different proportional valves are utilized in the gas filling system, see Figure 3.18. Bürkert Type 2873 direct acting solenoid control valve (capable of operating at pressure differences up to 16 bar) is used for acetylene, argon and oxygen gases while Bürkert Type 2875 direct acting solenoid control valve (capable of operating at pressure differences up to 20 bar) is used for nitrogen gas. These valves are controlled by Bürkert Digital Control Electronics Type 8605. These controllers help control system control the valves by creating pulse width modulation according to the incoming control signal from DAQ card in order to open the gate of proportional valves at the desired rate. The control signals generated from the proportional-integral-derivative (PID) control code prepared in the Labview software are sent to these controllers, and the desired amount of gas can be filled into the combustion chamber.

3.3.4. Heating System

Heating system keeps temperature of the body of the combustion chamber constant. The main reason is to create similar engine-like conditions inside the combustion chamber, and to reduce the heat transfer from the combustion chamber to the environment during the experiments. Besides, another reason for the installation of the heating system is to prevent the possible condensation of water that may occur after the pre-combustion process on the interior surfaces and windows.

Heating system consists of 12 cartridge heater, a type K thermocouple and a temperature control device. Each heater has a power of 125 W and a diameter of 9 mm.

Besides, the heaters were mounted in holes drilled with equal intervals on the body of the combustion chamber.

Temperature control device utilizes a PID control system which provides a more balanced and efficient control compared to on-off temperature control systems. The main reasons for choosing a PID control in the test system are to reach the target temperature without exceeding it, to keep the temperature at the desired value with minimal fluctuation, and to consume less electricity. PID coefficients are mainly related with power of heaters, beginning temperature of the combustion chamber, ambient temperature, material of the chamber and weight of the chamber. It is so hard to find correct coefficients by calculating them under specified conditions hence the ability of the temperature controller device to automatically determine the PID coefficients is used.

3.3.5. Ignition System

The purpose of the ignition system is to start the pre-combustion process by igniting air-acetylene mixture. Although ignition system is not employed during spray measurements, very little information will be given in the followings in order to explain what this system does in the test rig, and how it works.

Spark plugs are the main components of the ignition system. Figure 3.19 shows a spark plug which is used in the test rig. The system has M12 x 1.25 iridium BOSCH spark plugs, and these spark plugs are triggered by Magnet-Marelli ignition coils. The spark plugs start the combustion process of the acetylene-air mixture inside the combustion chamber. The system has two spark plugs, and these spark plugs are located at opposite corners in the combustion chamber. The reason for using two spark plugs is that combustion is tried to be provided homogeneously.

Figure 3.19. Spark plug mounted in the test rig.

Normally, injection timing is determined by engine control unit in automobiles. In this experimental setup, the delay time of the start of spray process, which follows the pre-combustion process, is determined according to the moment of ignition. Like other subsystems, the ignition system is controlled by the DAQ device.

3.3.6. Exhaust System

An exhaust system was installed to expel the excess gas and fuel vapor remaining in the combustion chamber at the end of the experiments. A schematic sketch of the exhaust system is demonstrated in Figure 3.20a.
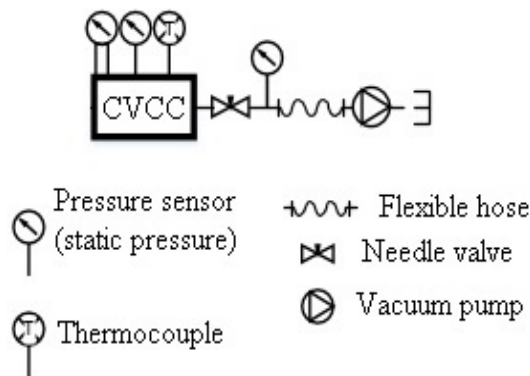
(a) Schematic sketch of exhaust system.   (b) Vacuum pump.

Figure 3.20. Exhaust system.

A high pressure resistant needle valve was installed at the outlet of the combustion chamber. This valve is opened to empty the combustion chamber, and waste gases and fuel vapour are drawn out of the combustion chamber by using a vacuum pump with a power of 0.75 kW. The vacuum pump is shown in Figure 3.20b. Besides, a piezoresistive static pressure sensor mounted before the vacuum pump is used to measure vacuum pressure.

3.3.7. Optical System

Optical system, which is used to visualize the spray process, is so important that spray data is obtained by it. The optical system was installed according to the shadow-
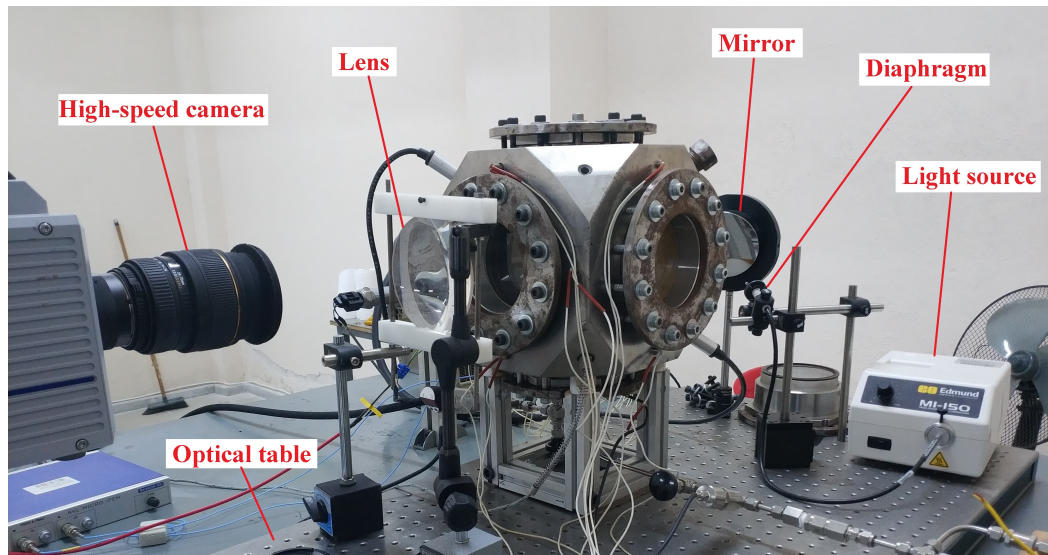
Figure 3.21. Optical system.

graph method. Because, this method can directly detect liquid phase of the spray, and it is simple. A schematic sketch of the optical system and installed system are shown in Figures 3.5 and 3.21, respectively.

Briefly speaking of the shadowgraph technique used in this experimental system, this method needs mainly a light source, an off-axis parabolic mirror, lens and a high-speed camera. The reason for using a high speed camera is to capture the events that cannot be captured by standard cameras, which have standard frame rate, with instant details. Firstly, light is produced from a point light source, and goes to the mirror through a diaphragm. Diaphragm is used to adjust the intensity of light from the light source. In other words, the diaphragm determines the conical angle of the incoming light beam. In addition, an off-axis parabolic mirror is able to send the light beam coming in one direction to another direction. Next, the light reflected from the mirror passes through the combustion chamber, and focuses on a point with the help of a convex lens. Then, camera captures the image. The successive images are recorded in the camera as a video.

In optical system of the experimental setup, there are 7 components which are light source, diaphragm, off-axis parabolic mirror, mirror mount, convex lens, high-speed camera and an optical table. Detailed information about the equipment is given in Table 3.4. In addition to these information, the high-speed camera is utilized to record an injection event at 20,000 fps, shutter speed of 1/62,000 with a resolution of 512x512 pixels during the experiments.

Table 3.4. Equipment in the optical system.

Component	Model
Light source	Edmund Optics MI-150 Fiber Light Source, 150 W quartz halogen
Diaphragm	diameter of 30.8 mm, aperture: 0.8 - 12 mm
Off-axis parabolic mirror	101.6 x 152.4 mm PFL 45° off-axis parabolic mirror
Mirror mount	parabolic mirror mount with a diameter of 101.6 mm
Convex lens	diameter: 125 mm, focal length: 250 mm
High-speed camera	Photron SA 1.1
Optical table	600 x 1200 mm metric optical table

3.3.8. Control System

Control system can:

- measure the pressure inside the CVCC,

- amplify the signal going to the motor of the fuel pump via motor drivers,

- adjust the pressure inside the common rail,

- adjust the injection time and duration,

- start the injection event,

- control the proportional valves for gas filling,

- measure the temperature of combustion chamber body, and control it,

- control the ignition time and duration,

- measure the vacuum pressure,

- adjust the properties of the successive images to be recorded,

- start, and stop the recording of spray process via high-speed camera.

In the control system, two DAQ cards and a computer are employed in addition to pressure sensors, motor drivers, injector driver, etc. The components of the control system embedded in other systems have already been explained while explaining these

systems. In the followings, some information about the DAQ cards and the computer will be given.

Control of other systems is done with the help of DAQ cards and a computer, which are part of the control system. As DAQ devices, 2 National Instruments (NI) USB 6353 DAQ cards are used. These cards are shown in Figure 3.22, and their properties are given in Appendix B according to the reference [151].

Figure 3.22. NI USB 6353 DAQ cards used in the study.

Processing of the data coming to the control system and giving the necessary commands are done by the programs prepared in Labview software. The computer inside the control system ensures that the data read through the prepared programs are seen, and gives the necessary commands to the required systems through the DAQ cards. These programs will be explained in Section 3.5.

3.4. Test Conditions

During the experiments, two different injection pressures were utilized, which were 600 and 800 bar. Ambient pressure was adjusted from 0 bar to 10 bar by increasing the pressure 5 bar. Operating conditions are presented in Table 3.5. Besides, experiments were repeated three times to ensure the accuracy of the experiments.

Table 3.5. Test conditions in the study.

Injector Type	Piezo CRDI injector
Number of the nozzle holes	1
Injection angle	45°
Injection duration (ms)	1
Injection pressure (bar)	600, 800
Ambient pressure (bar)	0, 5, 10
Repetition	3

3.5. Procedure of Spray Analysis

In this section, the way followed to conduct the experiments will be explained, including the programs prepared in Labview to transfer and process the data and to control the hardware in the experimental setup. Firstly, gas filling process will be explained with the control of the valves and the program prepared in Labview for this purpose. Then, spray process and Labview program prepared for this process will be explained. After that, the process of recording spray images will be explained briefly.

The first step is gas filling to the combustion chamber. Gas filling to combustion chamber is performed by electronic proportional valves as explained in Section 3.3.3. Correct control of these valves is so important for all experiments. Because, improper control of these valves can cause wrong results. In literature, it is stated that the gas filling process to a combustion chamber can be carried out in two different ways [92, 152, 153]. In the first method, the desired amount of gas is determined outside the combustion chamber with a mass flow meter, and gases are drawn from the supply to the combustion chamber with this device. In the second method, gases are filled in an order to the combustion chamber with electronic proportional valves by considering the feedback data coming from a static pressure sensor. The first method is more accurate compared to the second method however it is more expensive. Therefore, the second method was installed to the experimental setup, and it has been used in the experiments.

To control the electronic valves, a PID controller is utilized. PID controllers are widely used in industrial process control, and can also be used in processes using feedback mechanisms [154]. The PID controller of this system has two variables which are the input and output variables, and PID controller controls the system according to the

difference between the input and output variables. The input variable specifies the value of required quantity to be reached while the output variable specifies the value of measurable quantity during the process. The difference between these two values is named as error (e), Equation 3.1.

$$e = input\ value - output\ value \tag{3.1}$$

And, the controller has a transfer function [154]:

$$G_C(s) = K_P + \frac{K_I}{s} + K_D s \tag{3.2}$$

where $G_c(s)$ indicates the transfer function, K_P, K_I and K_D, all non-negative, indicate the coefficients for proportional, integral and derivative terms, respectively. The equation for the output in the time domain, y (t) is [154]

$$y(t) = K_P e(t) + K_I \int e(t)\, dt + K_D \frac{de(t)}{dt} \tag{3.3}$$

where e (t) indicates the error function. According to Equation 3.3, Equations 3.4, 3.5 and 3.6 show proportional, integral and derivative control processes, respectively.

$$K_P e(t) \tag{3.4}$$

$$K_I \int e(t)\, dt \tag{3.5}$$

$$K_D \frac{de(t)}{dt} \tag{3.6}$$

It is important to determine the coefficients of proportional, integral and derivative terms in a PID controller. Several methods to determine these coefficients are available in literature. In this study, PID Tuner app of MATLAB, which benefits from system identification method, is used to determine these PID coefficients. The response values of the system to the step function sent to each gas valve are entered to this app. Then, system is identified according to these values, and K_P, K_I and K_D are found.

```
                        ┌─────────────┐
                        │    START    │
                        └──────┬──────┘
                               ▼
                ╱──────────────────────────────╲
                ╲    INPUT OF GAS DENSITY DATA   ╱
                 ╲──────────────┬───────────────╱
                               ▼
          ┌────────────────────────────────────────┐
          │    MEASUREMENT OF PRESSURE SET VALUE    │
          └──────────────────┬─────────────────────┘
                             ▼
          ┌────────────────────────────────────────┐
          │      STARTING OF GAS FILLING PROCESS    │
          └──────────────────┬─────────────────────┘
                             ▼
          ┌────────────────────────────────────────┐◄──┐
          │       GAS FILLING WITH PID CONTROL      │   │
          └──────────────────┬─────────────────────┘   │
                             ▼                      NO  │
              ╱────────────────────────────╲           │
             ╱      HAS THE SET VALUE        ╲──────────┘
             ╲        BEEN REACHED?          ╱
              ╲────────────────┬────────────╱
                          YES  ▼
                    ┌─────────────────┐
                    │     FINISH      │
                    └─────────────────┘
```
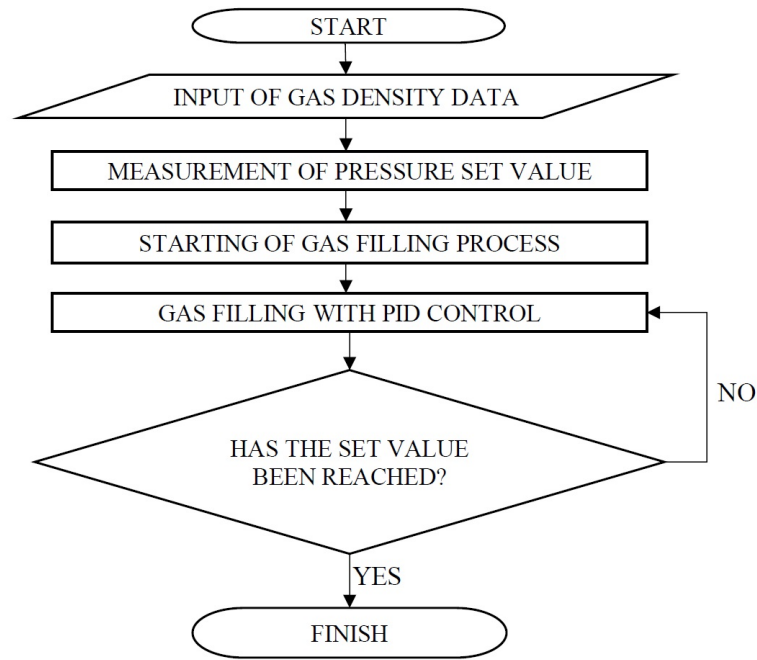
Figure 3.23. Flow chart of gas filling program.

PID coefficients found are written in a Labview program, which is called as gas filling program. This program is responsible to fill the combustion chamber with gases by adjusting the amounts of them. Gas filling program reads and produces analog data with NI USB 6353 DAQ card. Acetylene, argon, nitrogen and oxygen gases can be sent to the chamber by this program. However, only nitrogen gas is sent to the chamber for spray experiments because of the reasons explained before. Before starting the program, gases available in the chamber is vacuumed until pressure inside the chamber reaches to 0. Then, program is started, and control of the proportional valve of nitrogen begins to operate. In the meantime, other three valves do not operate. After the program starts, pressure inside the combustion chamber starts to be read by pressure sensor in the gas filling line of the chamber. Then, feedback is sent to the PID controller prepared in the program, and required analog voltage signal for the control of this valve is produced and sent to the valve. When required amount of nitrogen is filled to the chamber, valve of nitrogen is closed, and the program ends. Figure 3.23 shows the flow chart of the program. Besides, at the end of the program, deviation of the amount of gas filled from a set value is calculated as a percentage. This error is guaranteed to be below 1%.

Second step is the spray process. Before starting the spray process, existing fuel is drained from fuel tank. In order to completely drain existing fuel from the injection

system, the fuel pump is operated while the drain line of the fuel tank is open so that fuel is drained from the fuel lines. Besides, injector is also operated to expel the remaining fuel droplets. After the old fuel is completely drained from the fuel injection system, new fuel to be researched is added to the fuel tank.

Then, pre-combustion and spray program starts. This program can perform both pre-combustion and spray processes by controlling spark plugs, VCV valve, injector and motor drivers. In addition, this program controls these equipment via NI USB 6353 DAQ card. When the program starts, necessary adjustments are done manually in the program to drive the valves. Then, PWM signals start to be sent to PCV and VCV valves, and fuel is brought to the required pressure level. After that, injector is triggered by the injector driver with the incoming signal from the program through DAQ card. Thus, spray of the fuel begins then ends.

After spray process is completed, the gas and fuel vapor inside the combustion chamber must be discharged. Therefore, the discharge valve opens, and vacuum pump is started. The vacuum pump runs until the chamber pressure drops to 0. When there is no gas inside the chamber, the discharge valve and then the vacuum pump turns off. In this manner, the combustion chamber is ready for another test. Meanwhile, if necessary, windows of the chamber must be cleaned before the tests.

The last step is the recording of the spray images. Before starting the spray process, high-speed camera is set up to record the spray event. Then, properties of images to be captured are adjusted. Injection event are shot at 20,000 fps with a shutter speed of 1/62,000 and a resolution of 512x512 pixels. Camera must start recording at the same time with start of injection. For this purpose, a cable is connected between the injector driver and the camera to provide communication between them. When the injector driver sends a signal to the injector in order to trigger it, a signal goes to the camera at the same time, and the camera starts recording. In this way, the entire spray process can be recorded without any loss of spray frame. The time required to stop recording is predefined to the camera. After this time elapses while recording, the camera stops recording.

3.6. Image Processing

Spray images obtained from experiments are processed in computer environment then required data are revealed. Necessary parameters are spray penetration length and

spray cone angle. These parameters were already explained in Section 2.5.4. In this section, processing the spray images obtained and revealing the data will be explained.

Two different algorithms were created to measure the required parameters. The reason for the creation of two different algorithms was to examine the two parameters independently. These algorithms are shown in Appendix C. In the light of these algorithms, two different Matlab programs were written. These programs are given in Appendix D.

Firstly, measurement of the spray penetration length will be explained. During the experiments, video is obtained by taking four images of the respective sequence before fuel injection. These images are used for correction of the raw images taken from each complete injection. When the program starts, video is opened, and the number of frames of the video are obtained. Then, a for loop starts. In this loop, each frame is read, and these frames are converted into grayscale from colored scale. After that, each frame is substracted from the first frame. Hence, only the spray images remains without background. Next, a threshold value is calculated, and each frame is converted to binary scale from grayscale. Thus, the image becomes completely black and white. In these images, white indicates the spray. Then, the last pixels of spray images are defined, and the point where the nozzle is located is also defined. Eventually, spray penetration lengths are calculated between these points.

Secondly, measurement of spray angles will be mentioned. The program for spray angles consists of three parts that are frame extracting, creating angle measurement tool and the angle measurement. The first part is the frame extraction. Some of the steps followed for the measurement of spray penetration length also followed for the measurement of spray angle. These steps are: getting the number of frames, converting frames from colored scale into grayscale and background substraction. Then, each frame is separately saved to the computer in order to measure the spray angles manually. Hence, frame extraction ends, and the step of creating angle measurement tool starts. This tool is received from the website of MathWorks [155]. In this step, necessary equipment to measure the angle is created. 3 arbitrary points and two arbitrary lines formed by connecting the points are placed on the picture. These lines and points can be moved manually in order to determine the spray angle. Besides, the code to display the angle on the image is compiled in the angle measurement tool. In the next step, user can manually place the points (one of them indicating the nozzle while the other two points indicating the outermost parts of the spray boundary) and lines on the spray image. Once the vectors are placed onto the spray outline, the angle is shown on that figure.

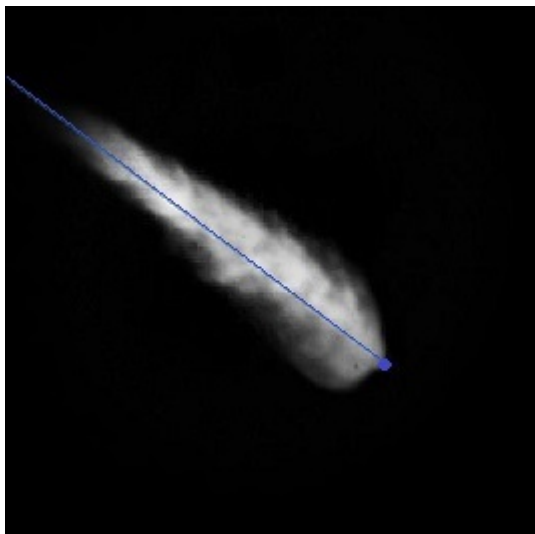Figure 3.24 shows an example for image processing steps. In this figure, the transition from original image to binary image, the points between which the spray penetration length is measured and the lines created for the angle measurement are shown.

(a) Original image.

(b) Binary image.

(c) Penetration length measurement.

(d) Angle measurement.

Figure 3.24. An example for image processing.

CHAPTER 4

RESULTS AND DISCUSSIONS

In this chapter, results of the experiments are given in two sections. The first section investigates the spray characteristics of methyl esters, and the second section investigates the spray characteristics of ethyl esters.

The aim of the study was to investigate the spray characteristics of various biodiesel fuels in terms of spray penetration length and spray cone angle. For this purpose, experiments were performed at chamber pressures of 0, 5 and 10 bar, and injection pressures of 600 and 800 bar, and each experiment were repeated at least three times. Images of each experiments were processed with image processing programs, and results were obtained by averaging three experiments for each test condition. Variations of the characteristics corresponding to different ambient and fuel injection pressures are given in several graphs. The data obtained at each time during the injection are not given in the charts. In order to make the graphs simpler and more understandable, the data are marked at intervals of approximately 0.1 ms. Besides, the first data was able to be obtained at 0.05 ms of the injection because tip of the injector was not visible due to mechanical constraints of the combustion chamber. In addition, the uncertainty and repeatability values were calculated for the experiments. Uncertainty values were found to be ± 4 mm for spray tip penetration length values and ± 0.7° for spray cone angle values. These uncertainty values are shown on the charts. As explained before, three experiments were done for each specific test condition. Repeatability value was obtained by averaging the results from each test, and it was found to be at most 3% for both spray penetration lengths and cone angles.

4.1. Investigation of Methyl Esters

Firstly, spray penetration lengths of the methyl esters were investigated. Figure 4.1 shows the variation of spray tip penetration lengths for corn oil, canola oil, sunflower oil and cotton oil methyl esters at ambient pressures of 0, 5 and 10 bar in comparison with fossil diesel fuel. Figure 4.2 demonstrates the variation of spray penetration lengths for the methyl esters at injection pressures of 600 and 800 bar compared with diesel fuel.
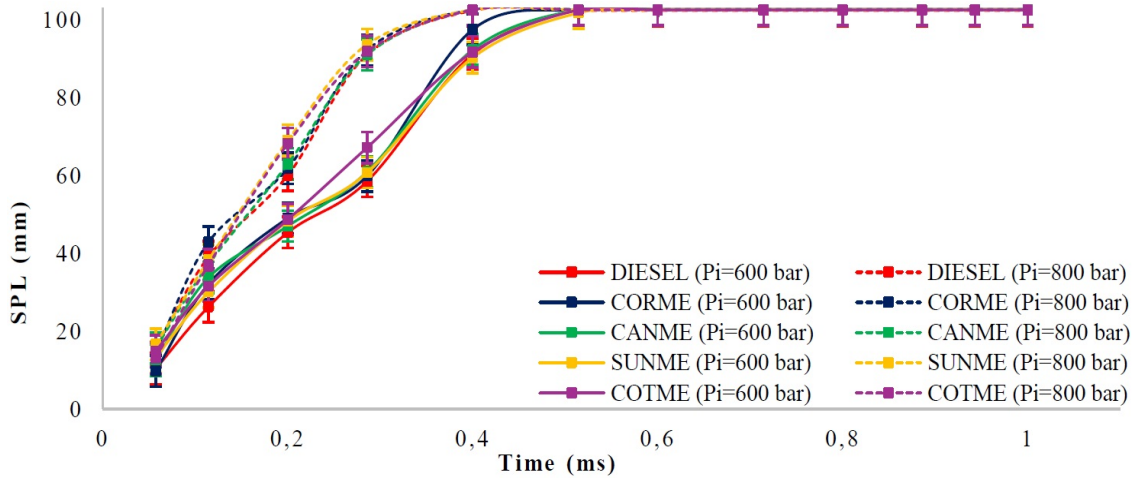
(a) Chamber pressure of 0 bar.
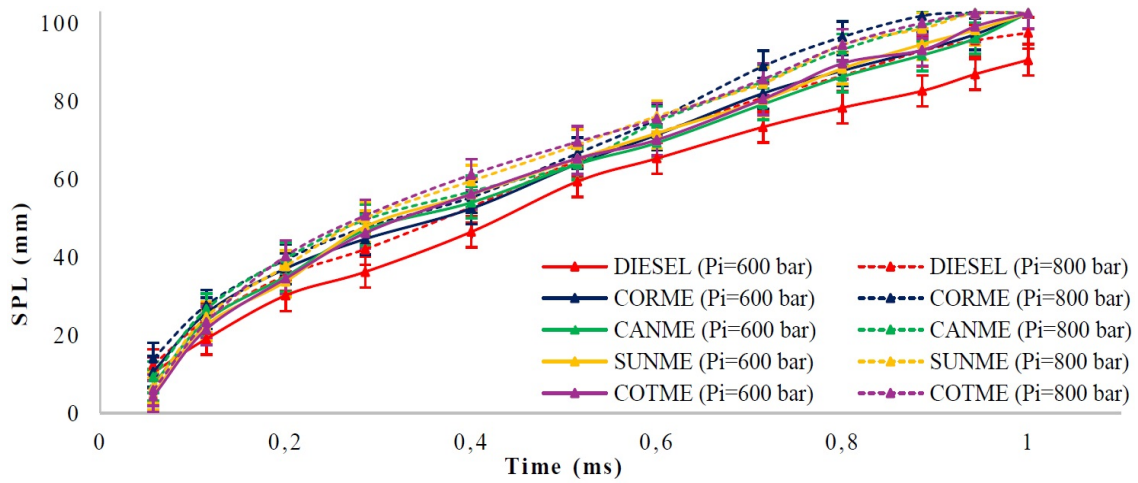
(b) Chamber pressure of 5 bar.
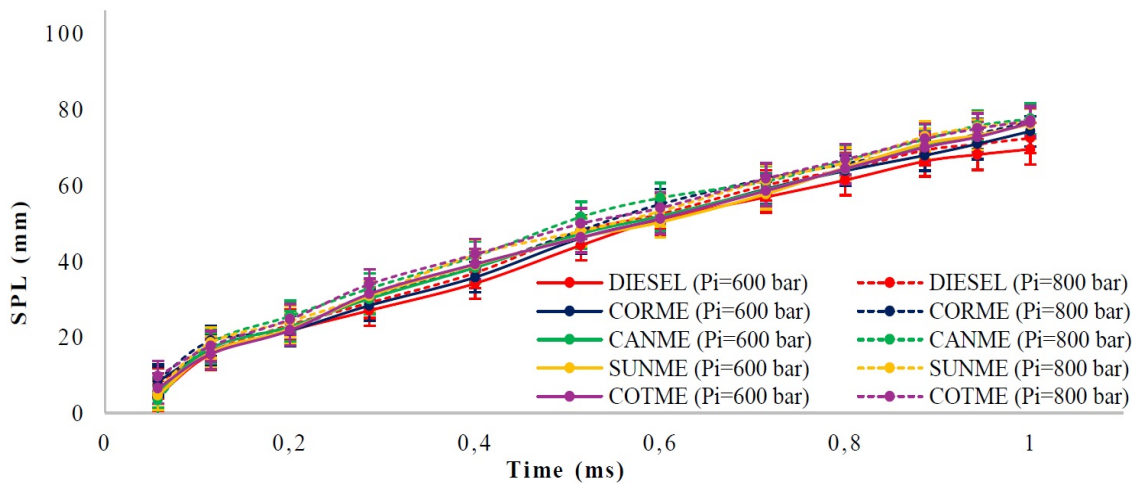
(c) Chamber pressure of 10 bar.

Figure 4.1. Variations in spray tip penetration lengths for methyl esters at different chamber pressures in comparison with conventional diesel fuel, (uncertainty: $\pm$ 4 mm, repeatability: $\pm$ 3%).
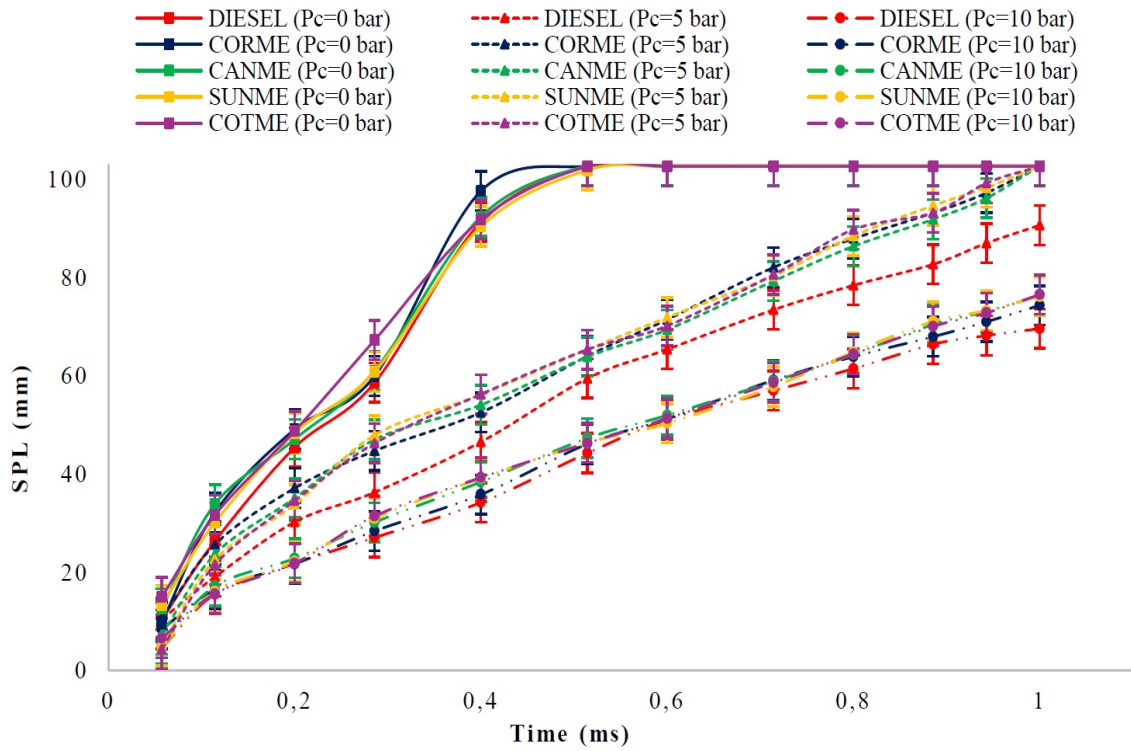
(a) Injection pressure of 600 bar.
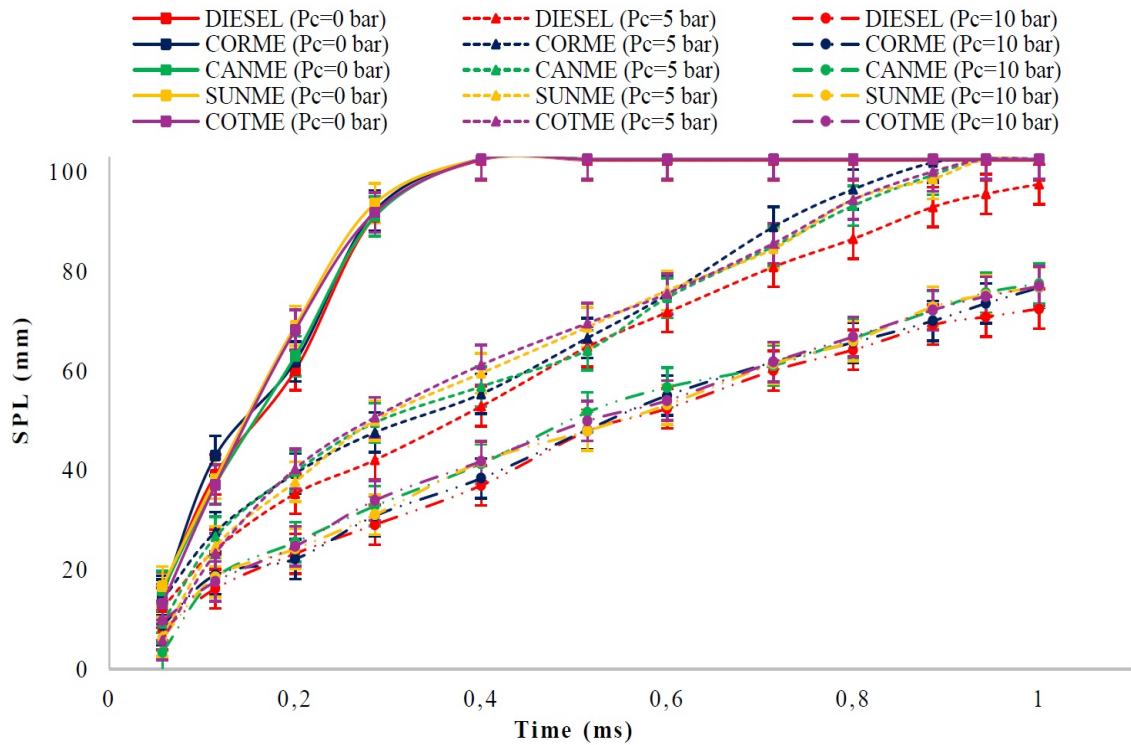
(b) Injection pressure of 800 bar.

Figure 4.2. Variations in spray penetration lengths for methyl esters at different fuel injection pressures in comparison with conventional diesel fuel, (uncertainty: $\pm$ 4 mm, repeatability: $\pm$ 3%)

All methyl esters and reference diesel fuel showed similar spray patterns with small distinctions under variable injection conditions and variable chamber conditions. As a general inference, increasing the injection pressure raised the spray penetration lengths of all fuels while raising the chamber pressure decreased the spray penetration lengths. Besides, ambient pressure was more effective on spray penetration than injection pressure under these experimental conditions. For example, spray penetration lengths of diesel at zero chamber pressure at 0.4 ms of the injection were approximately 91.2 mm and 102.4 mm for injection pressures of 600 and 800 bar, respectively. The difference was approximately 11.2 mm. From another point of view, penetration lengths of diesel fuel at injection pressure of 600 bar at the same instant of the injection were approximately 91.2 mm and 46.5 mm for ambient pressures of 0 and 5 bar. To be specific, the difference was 44.7 mm. Eventually, these values showed that chamber pressure was more effective on penetration than injection pressure in these experimental conditions. In addition, the difference between spray penetration lengths at injection pressures of 600 bar and 800 bar decreased as the pressure inside the combustion chamber increased. For instance, this difference was found as 32.6 mm for diesel fuel at 0.3 ms of the injection when chamber pressure was 0. However, this difference decreased to 4.1 mm when the ambient pressure was increased to 10 bar. Namely, increasing the chamber pressure reduced the effects of increasing the injection pressure.

Spray penetration curves can be divided into two parts. In the first part, it can be seen that spray penetration length increases rapidly. In the second part, penetration length rises steadily except spray at chamber pressure of 0 bar (spray impingement to the wall was observed early for all fuels at zero ambient pressure). The first and second parts can be named as transient and steady regions, respectively. Because the penetration length suddenly rises with a decreasing slope in the first part. Then, it stabilizes, and continues to increase with an almost constant slope. An example of determining these regions is illustrated in Figure 4.3. Also, trend lines are drawn on these curves according to the point where transition from transient region to steady region occurs. Because, this transition can be better shown visually with trend lines. Besides, transitions from transient regions to steady regions of penetration curves were affected by chamber and injection pressures. However, chamber pressure was more effective on these transition times than injection pressure. The transition times dramatically reduced when the chamber pressure increased while they slightly decreased as the injection pressure raised. On average, these transition times for methyl esters at injection pressure of 600 bar were found as 0.18 ms and 0.12

ms for ambient pressures of 5 bar and 10 bar, respectively. At injection pressure of 800 bar, they were calculated as 0.16 ms and 0.11 ms for chamber pressures of 5 bar and 10 bar, respectively. The reason why transition times of methyl esters were averaged was that there were negligible small differences between them. In addition, the sprays of all fuels at both injection pressures penetrated rapidly until they impinge to the chamber wall at zero chamber pressure, and could not pass to the steady region. Average time sfor sprays of methyl esters to impinge to the wall ware found as 0.39 ms and 0.33 ms for injection pressures of 600 bar and 800 bar, respectively. Moreover, to compare these times with those of diesel fuel, transition times for diesel fuel at injection pressure of 600 bar were respectively found as 0.22 ms and 0.14 ms for ambient pressures of 5 bar and 10 bar, and these times were respectively calculated as 0.19 ms and 0.13 ms for chamber pressures of 5 bar and 10 bar at injection pressure of 800 bar. Besides, average times for diesel spray to impinge to the chamber wall were computed as 0.42 ms and 0.37 ms for injection pressures of 600 bar and 800 bar, respectively.

It was aimed at comparing the spray penetration lengths of methyl esters with those of diesel fuel. At zero chamber pressure, considering the uncertainty and repeatability values, no significant distinctions between methyl esters and diesel fuel were observed. This was the case for both injection pressures. This can be explained by the fact that sprays of all fuels penetrated very fast, and impinged to the chamber wall. There might have been no time for the difference to occur. At chamber pressure of 5 bar, big differences were found between the penetration lengths of methyl esters and diesel fuel for both injection pressures. For example, spray penetration length of diesel at injection pressure of 600 bar was 73.3 mm at 0.7 ms of injection while penetration length of COTME was measured 80.9 mm under the same conditions. As another example, SUNME and diesel fuel can be compared under injection pressure of 800 bar at 0.9 ms of the injection. Penetration lengths were found as 92.9 mm and 99.0 mm for diesel and SUNME, respectively. Additionally, all methyl ester fuels impinged to the chamber wall at the end of injection under ambient pressure of 5 bar for both injection pressures. On the other hand, diesel fuel impingement to the wall was not observed for both injection pressures although sprays of diesel fuel approached the wall at the end of the injection period. At chamber pressure of 10 bar, no wall impingement was observed for all fuels. Besides, difference between penetration lengths of diesel and methyl esters reduced although methyl esters had still slightly bigger values. For example, penetration lengths of diesel and COTME for injection pressure of 600 bar at 5 bar ambient pressure were compared at 0.7 ms of
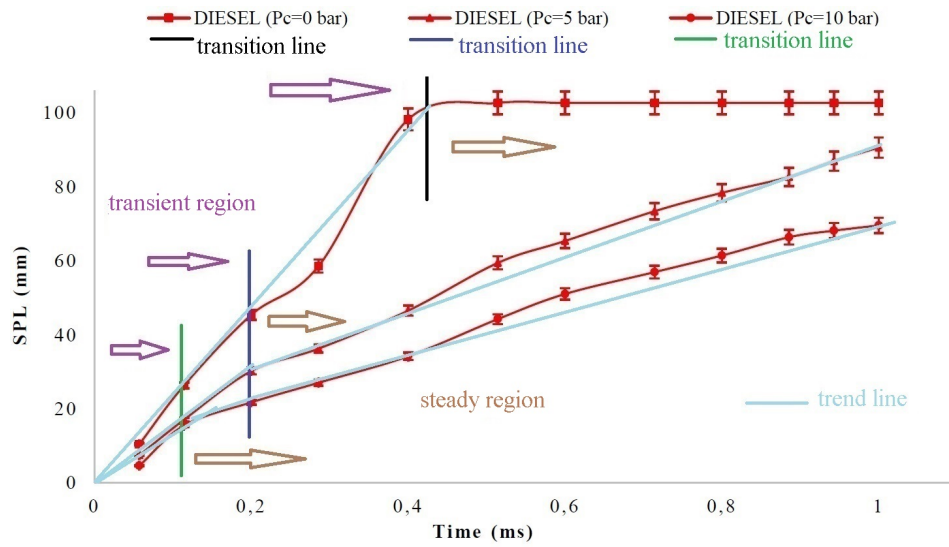
(a) According to chamber pressure.
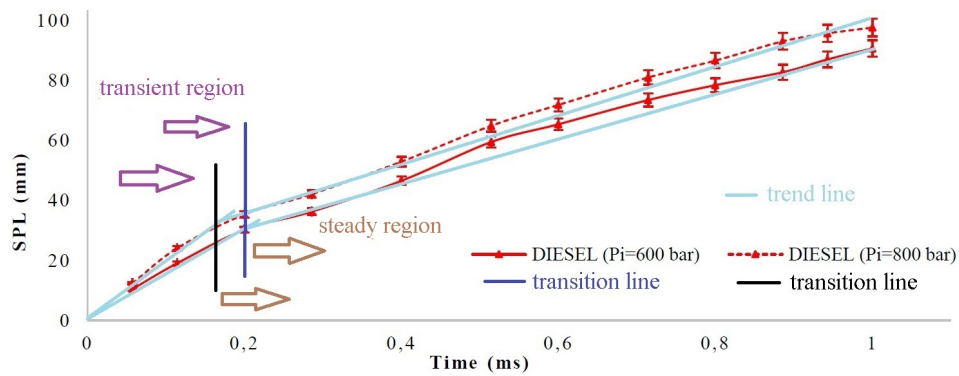
(b) According to injection pressure.

Figure 4.3. An example for transition of spray penetration curves from transient region to steady region.

injection, and the difference was found as 7.6 mm. This difference decreased to 1.7 mm when the ambient pressure was increased from 5 bar to 10 bar. Another example was to compare diesel and SUNME at 5 bar chamber pressure. When the ambient pressure was raised from 5 bar to 10 bar under the previously described conditions, the distinction between penetration lengths of these fuels reduced to 2.9 mm from 6.1 mm. Consequently, it can be stated that methyl esters showed slightly or much longer penetrations than fossil diesel fuel depending on the experimental conditions. This can be explained by having higher density, viscosity and contact angle values than diesel fuel. Having higher density can lead larger momentum thus spray velocity resulting in deeper penetrations. Higher viscosity can adversely affect atomization of fuel spray resulting in increased liquid pen-

etrations. Also, higher contact angle means that surface tension effects are larger for biodiesel fuels resulting in poor atomization and increased liquid lengths.

Methyl esters should also be compared among themselves. Small differences in penetration lengths were observed. However, these small distinctions have no point when the uncertainty and repeatability rates are taken into account. Namely, it could be stated that all methyl esters showed similar spray penetration lengths with negligible differences.

Secondly, spray cone angles of methyl esters were examined. Figure 4.5 demonstrates the variation of spray cone angle for methyl esters and diesel fuel at ambient pressures of 0, 5 and 10 bar. Figure 4.6 shows the variation of cone angle for methyl esters at injection pressures of 600 bar and 800 bar in comparison with those of fossil diesel fuel.

As a general inference, spray cone angles increased when ambient pressure raised while they reduced as injection pressure increased. Moreover, chamber pressure affected spray cone angle more than injection pressure under these experimental conditions. For example, spray cone angles of CANME at zero chamber pressure at 0.8 ms of the injection were approximately found as 8.6° and 6.1° for injection pressures of 600 bar and 800 bar, respectively. Namely, the difference was 1.5°. Contrarily, cone angles of CANME at injection pressure of 600 bar at the same instant of injection were around 8.6° and 13.2° for chamber pressures of 0 and 5 bar. The difference were 4.6°. Consequently, these values showed that spray angles were more affected by chamber pressure than injection pressure in these experiments. Additionally, effects of increasing injection pressure on spray cone angle was reduced by a raise in ambient pressure. For example, the difference between the spray angles of diesel fuel at injection pressures of 600 bar and 800 bar for zero chamber pressure was found as 2.7° at 0.6 ms of the injection. However, this difference was measured as 1.3° when the chamber pressure increased to 10 bar.

Like penetration curves, spray angle curves can also be divided into two regions which are transient and steady regions as shown in Figure 4.4. In transient region spray angle rapidly decreases to a degree then enters steady region. In steady region angle keeps almost constant at this degree. Transition times from transient region to steady region were affected by both ambient and injection pressures. However, chamber pressure was more effective on transition times than injection pressure. These times were sharply decreased when the ambient pressure rose (see Figure 4.4a) while they slightly reduced as the injection pressure increased (see Figure 4.4b). Besides, these transition times were very similar to transition times that were observed in spray penetration curves. This may be logical because both spray penetration length and spray cone angle are used to describe
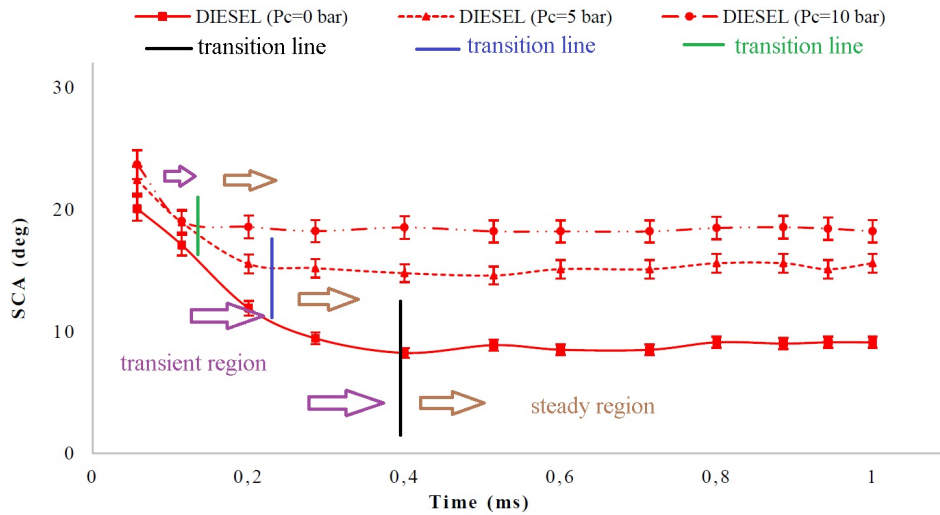
(a) According to chamber pressure.
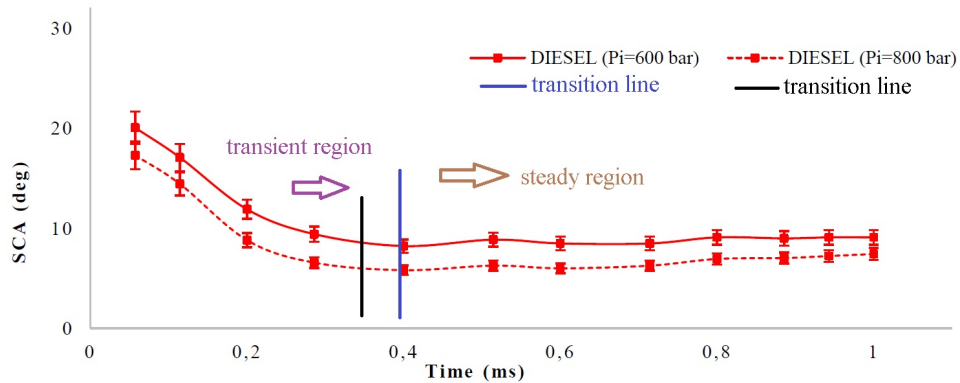
(b) According to injection pressure.

Figure 4.4. An example for transition of spray cone angle curves from transient region to steady region.

the spray shape. Spray passes from transient region to steady region as a whole. Therefore, when one parameter passes, the other can be expected to pass. These transition times were explained before while explaining the spray penetration curves. Therefore they will not be mentioned here again.

When comparing the methyl esters with diesel fuel, different results were obtained depending on the experimental conditions. At zero ambient pressure, no important differences between the spray angles of methyl esters and diesel fuel were observed for both injection pressures when considering the uncertainty and repeatability ratios. Sprays of all fuels impinged to the chamber wall at early stages of injection thus there might not have been any time for any differences to occur. However, significant distinctions were
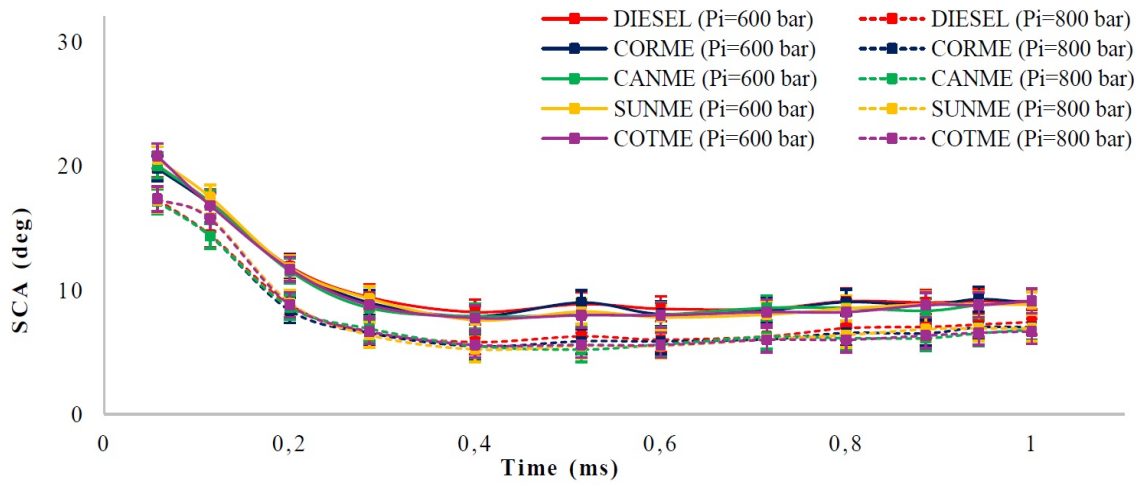
(a) Chamber pressure of 0 bar.
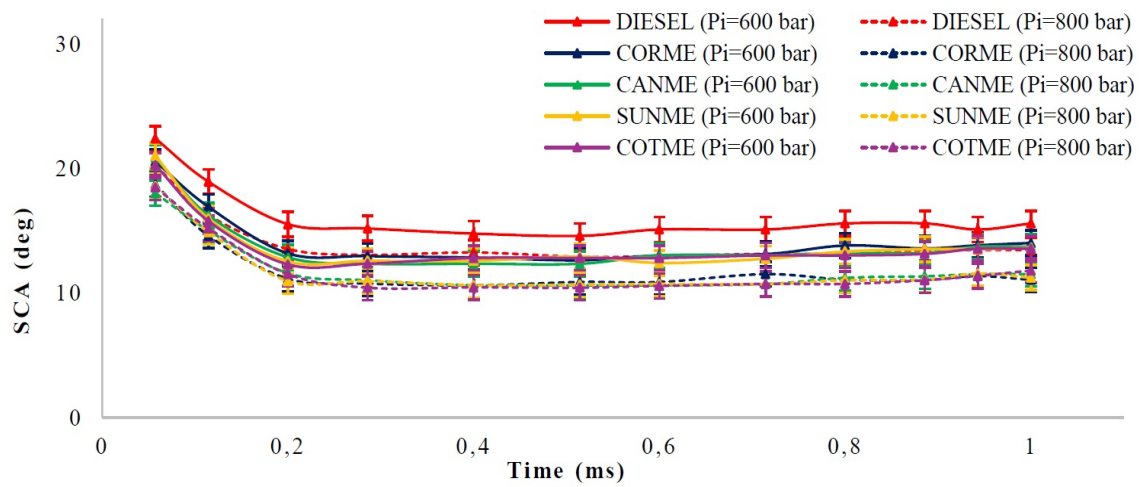
(b) Chamber pressure of 5 bar.
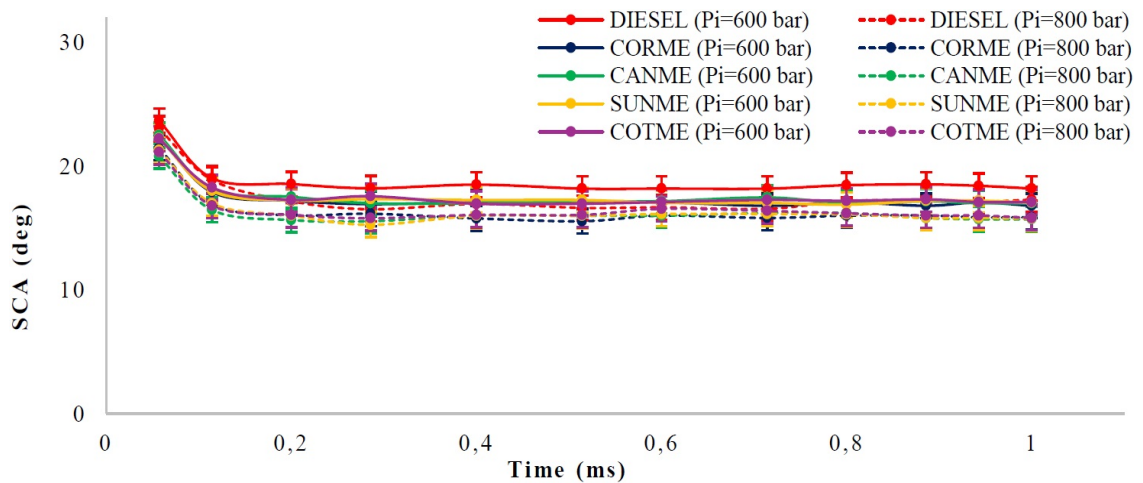
(c) Chamber pressure of 10 bar.

Figure 4.5. Variations in spray cone angles for methyl esters at different chamber pressures in comparison with conventional diesel fuel, (uncertainty: $\pm$ 0.7°, repeatability: $\pm$ 3%).

(a) Injection pressure of 600 bar.

(b) Injection pressure of 800 bar.

Figure 4.6. Variations in spray cone angles for methyl esters at different fuel injection pressures in comparison with conventional diesel fuel, (uncertainty: ± 0.7°, repeatability: ± 3%)

obtained when the chamber pressure was increased to 5 bar. For example, spray cone angle of diesel at injection pressure of 800 bar was 13.4° at the end of the injection while spray angle of SUNME was found as 11.2° under the same conditions. As another example, CANME and diesel can be compared under injection pressure of 600 bar at 0.2 ms of the injection. Spray cone angles were measured as 15.5° and 12.9° for diesel and CANME, respectively. At the chamber pressure of 10 bar, difference between the spray angles of diesel fuel and methyl esters slightly reduced compared to the values at chamber pressure of 5 bar, and methyl esters still had smaller values than reference diesel. For instance, spray cone angles of diesel and SUNME at injection pressure of 800 bar were respectively found as 17.3° and 15.8° at the end of the injection. Besides, diesel and SUNME were compared at the chamber pressure of 5 bar. When the ambient pressure was increased from 5 bar to 10 bar under pre-described conditions, the difference decreased to 1.2° from 2.6°. As a result, it can be stated that methyl esters had slightly or much smaller spray cone angles than conventional diesel fuel depending on the experimental conditions. This may be due to having higher viscosity, and contact angle values (higher surface tension effects) resulting in poor atomization. Moreover, big distinctions were not found among the methyl esters in terms of spray cone angle. Although there were some differences, these were insignificant when considering the uncertainty and repeatability.

4.2. Investigation of Ethyl Esters

In this section, ethyl esters will be compared with methyl esters in terms of spray penetration length and spray cone angle. There is an important point to be explained before this comparison is made. The curves obtained for both fuels are similar in shape. Transient and steady regions are valid and similar for both types of fuels. Besides, the most important point is that effects of chamber pressure and injection pressure are similar for the two kinds of fuels. This may be because methyl esters and ethyl esters are the same in terms of the feed stock and production method thus they are not physically completely different. Indeed, there are no huge distinctions in viscosity and density values despite differences. For these reasons, effects of injection and chamber pressures on the parameters to be investigated will not be mentioned in this section because they were already explained in the previous section. However, transition times from transient region to steady region will be mentioned to show the similarity.

(a) Chamber pressure of 0 bar.
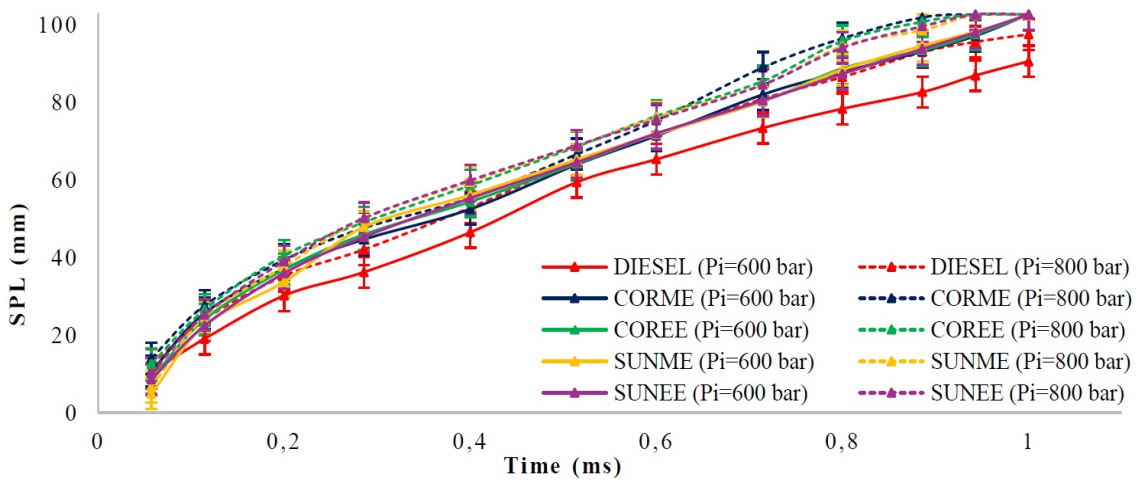
(b) Chamber pressure of 5 bar.
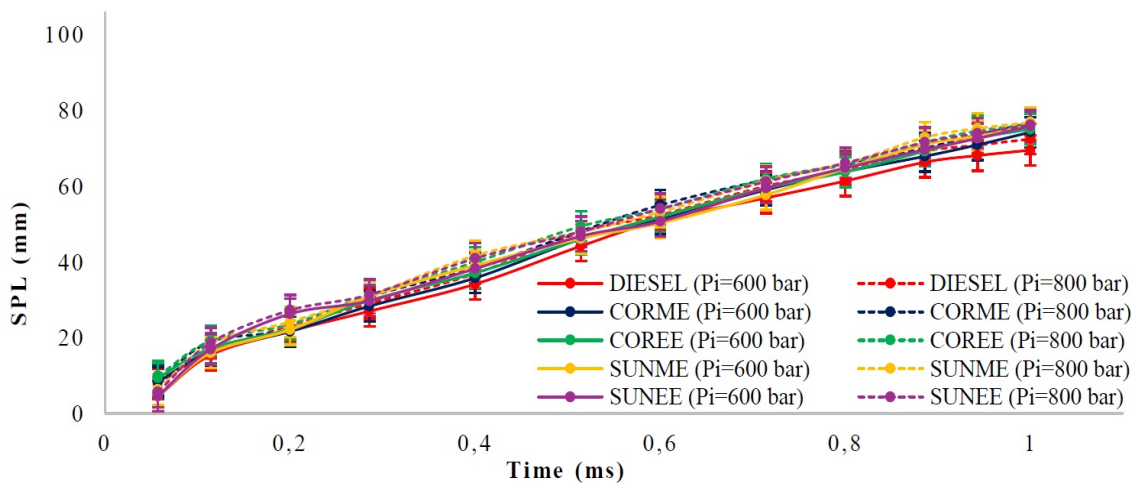
(c) Chamber pressure of 10 bar.

Figure 4.7. Variations in spray penetration lengths for ethyl esters at different chamber pressures in comparison with methyl esters, and traditional diesel fuel, (uncertainty: $\pm$ 4 mm, repeatability: $\pm$ 3%).
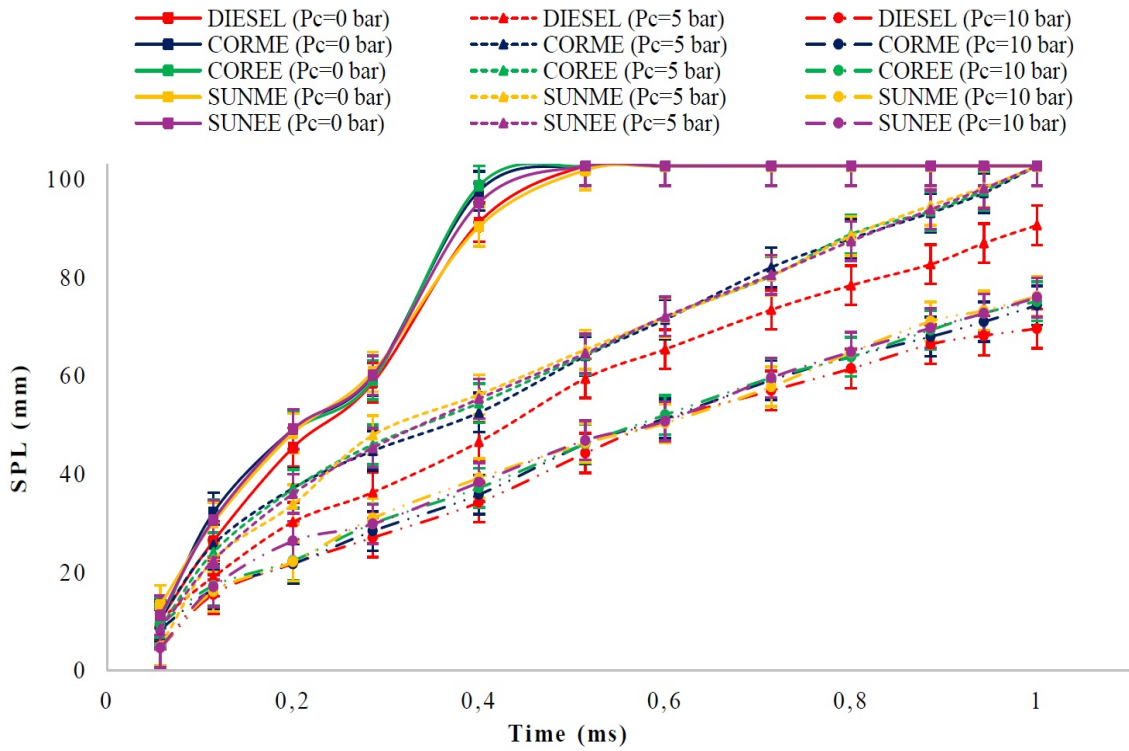
(a) Injection pressure of 600 bar.
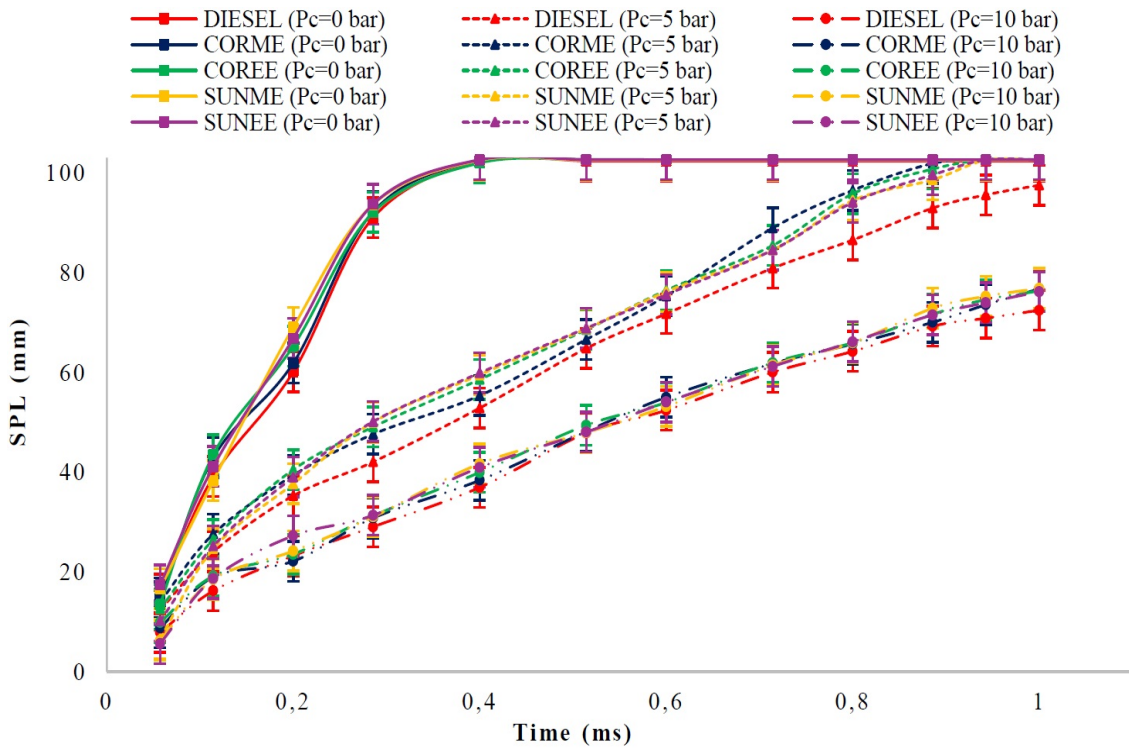
(b) Injection pressure of 800 bar.

Figure 4.8. Variations in spray penetration lengths for ethyl esters at different injection pressures in comparison with methyl esters, and traditional diesel fuel, (uncertainty: ± 4 mm, repeatability: ± 3%).

Figure 4.7 shows the variation of the spray tip penetration lengths for ethyl esters at ambient pressures of 0, 5 and 10 bar in comparison with methyl esters. Figure 4.8 demonstrates the variation of spray tip penetration lengths for ethyl esters at injection pressures of 600 bar and 800 bar compared to methyl esters. Moreover, Figures 4.9 and 4.10 show respectively variation of spray cone angles of ethyl esters at different chamber and injection pressures. Also the curves of diesel fuel are drawn to provide a better understanding.

Like methyl esters, transition times from transient region to steady region for ethyl esters were very similar for both spray penetration and spray cone angle curves under all experimental conditions. On average, transition times for ethyl esters at the injection pressure of 600 bar were measured as 0.17 ms and 0.12 ms for the ambient pressures of 5 bar and 10 bar, respectively. When the pressure was 800 bar, the transition times were found as 0.16 ms and 0.10 ms for the chamber pressures of 5 bar and 10 bar, respectively. In addition, average times for sprays of ethyl esters to impinge to the chamber wall were obtained as 0.39 ms and 0.34 ms for injection pressures of 600 and 800 bar, respectively. These values are very similar to those of methyl esters which were previously explained in Section 4.1.

When comparing the spray parameters of ethyl esters with methyl esters, a similarity was observed. For example, spray penetration lengths at 0.6 ms of the injection for CORME and COREE were respectively measured as 71.4 mm and 71.9 mm at injection pressure of 600 bar under chamber pressure of 5 bar. As another example, penetration lengths of SUNME and SUNEE were respectively found as 71.7 mm and 71.8 mm under the same conditions. Besides, this likeness was observed for spray cone angle curves of both types of fuels. For instance, spray angles of CORME and COREE were respectively measured as 16.8° and 17.2° at injection pressure of 600 bar under chamber pressure of 10 bar. As another example, SUNME and SUNEE had respectively spray angles of 10.9° and 11.2° at 0.2 ms of injection under injection pressure of 800 bar and chamber pressure of 5 bar. These similarities can be explained with the differences in density, viscosity and contact angle values. The ethyl esters have larger viscosity values than the methyl esters nevertheless the methyl esters have bigger density and contact angle (and surface tension) values than the ethyl esters. These properties may have compensated each other, and may have prevented differences in spray properties to occur. When the ethyl esters are compared in themselves, the similarity in spray parameters is again remarkable, as it is seen in Figures 4.7 through 4.10.
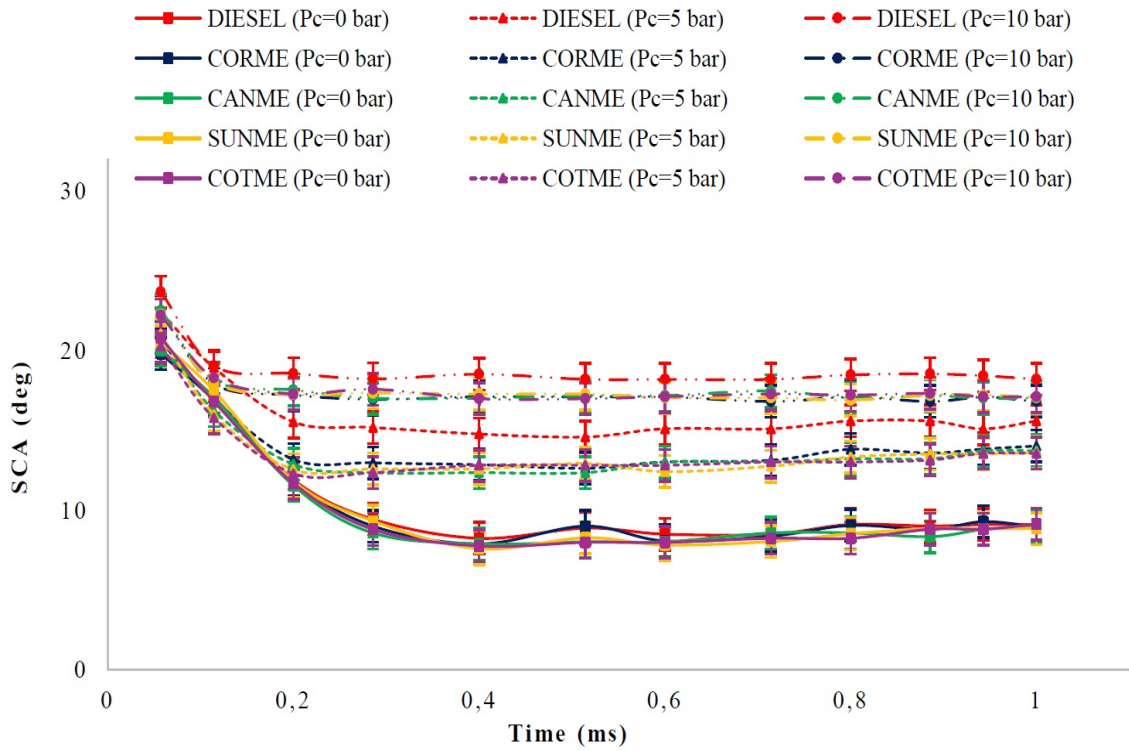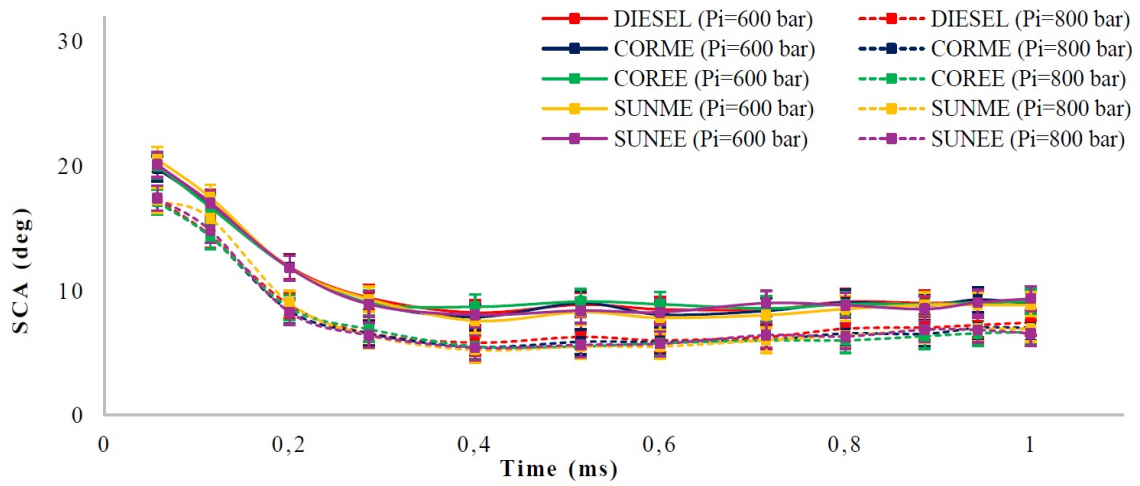
(a) Chamber pressure of 0 bar.
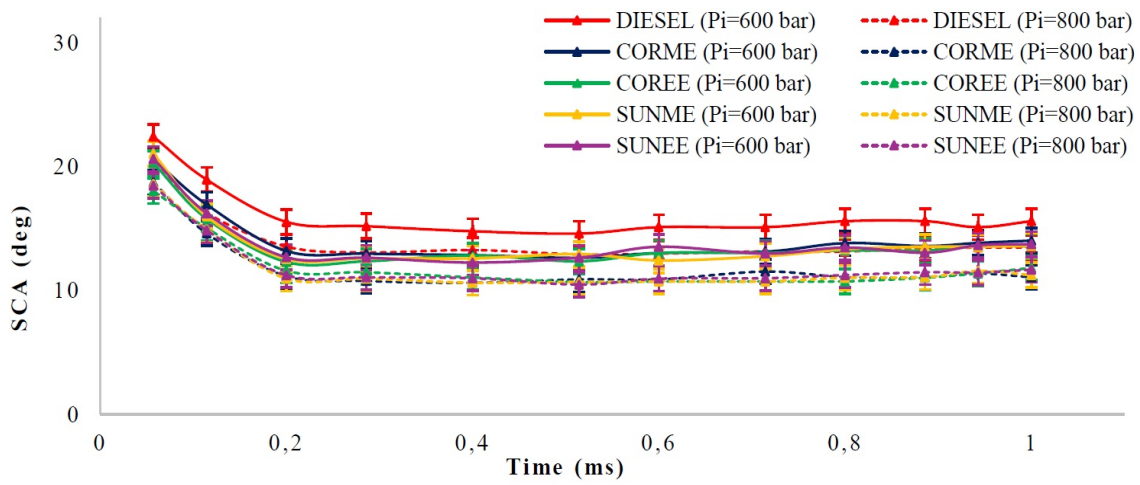
(b) Chamber pressure of 5 bar.
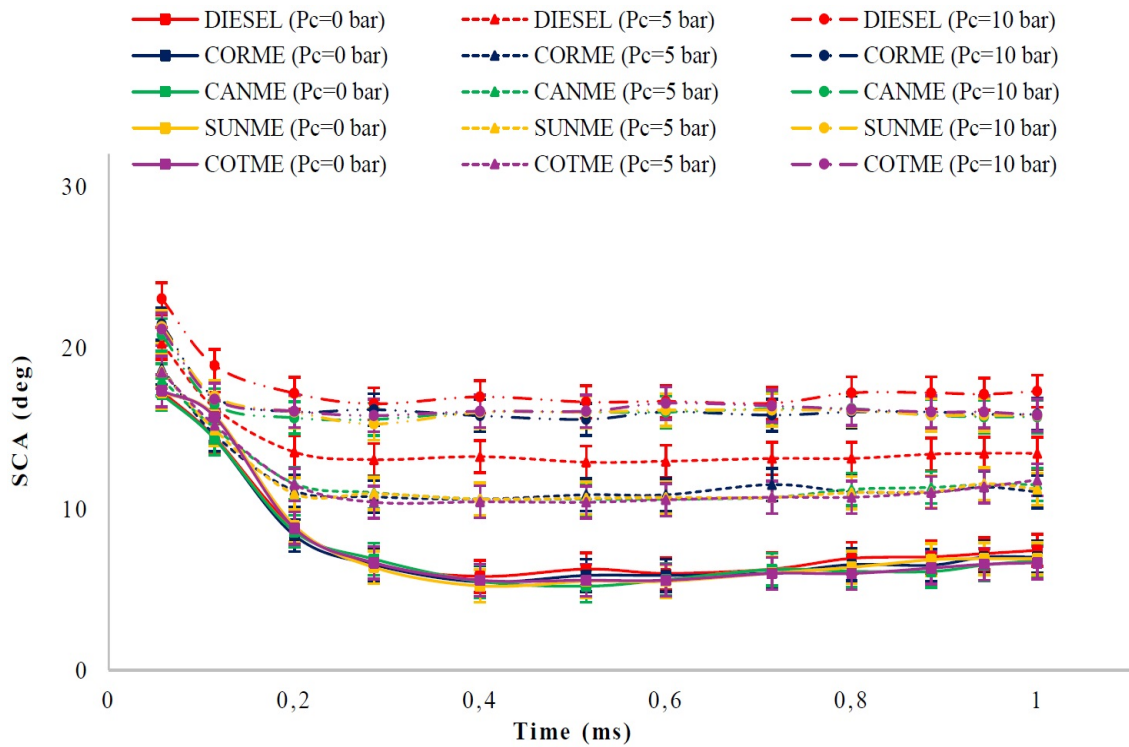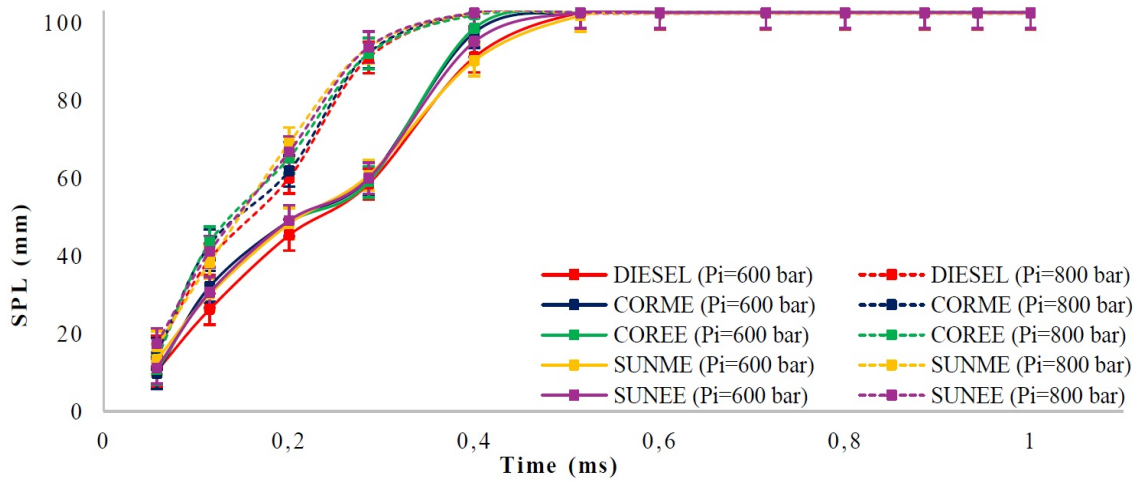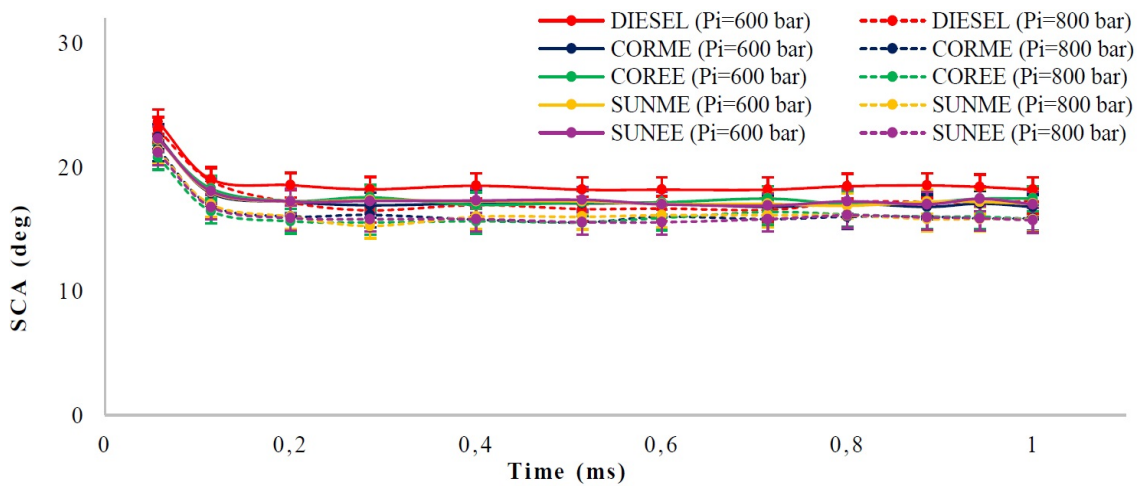

(c) Chamber pressure of 10 bar.

Figure 4.9. Variations in spray cone angles for ethyl esters at different chamber pressures in comparison with methyl esters, and traditional diesel fuel, (uncertainty: $\pm 0.7°$, repeatability: $\pm 3\%$).
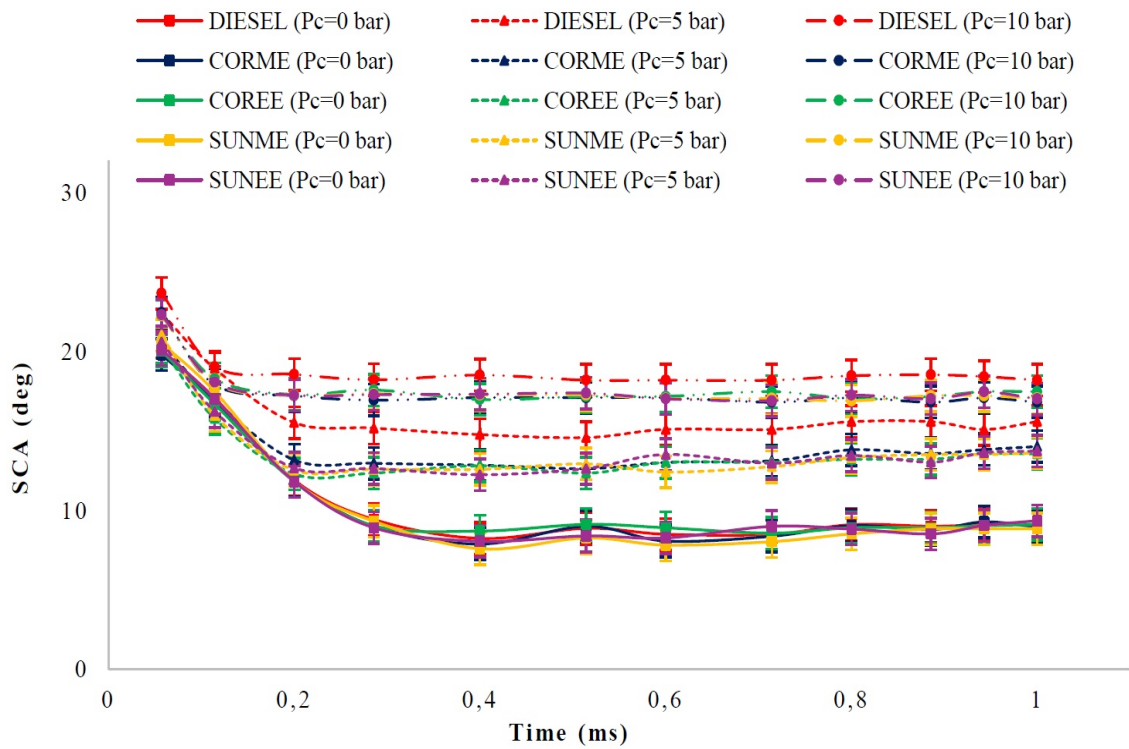
(a) Injection pressure of 600 bar.
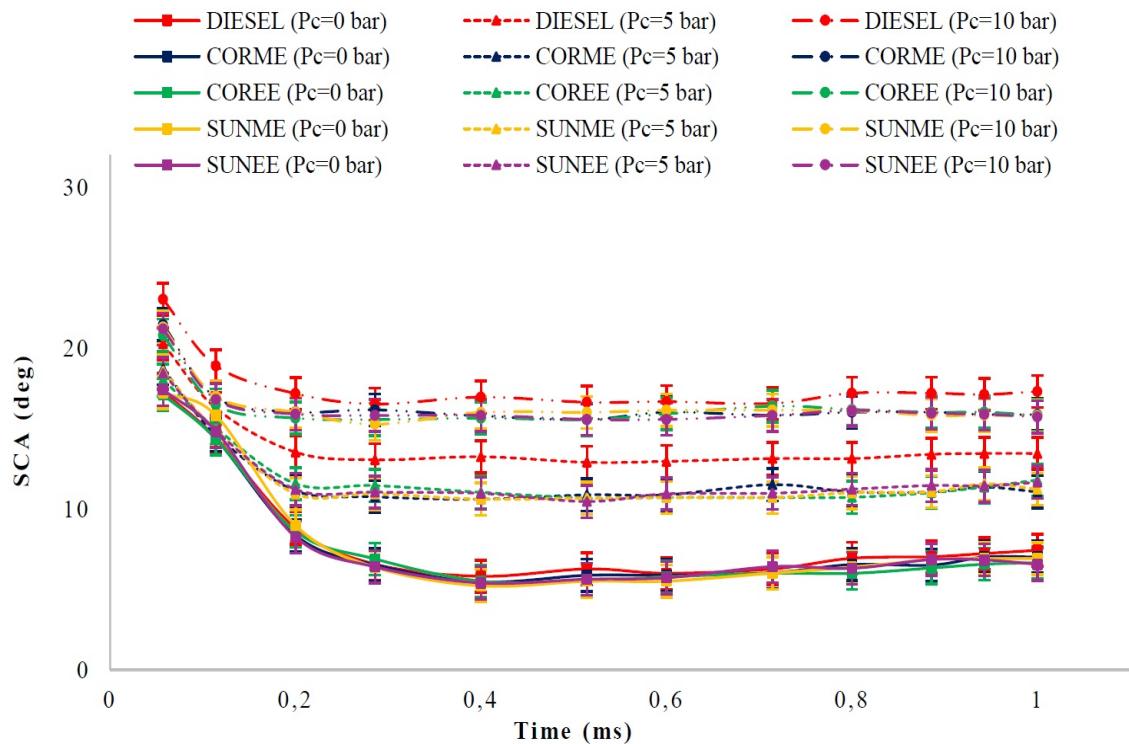
(b) Injection pressure of 800 bar.

Figure 4.10. Variations in spray cone angles for ethyl esters at different fuel injection pressures in comparison with methyl esters, and traditional diesel fuel, (uncertainty: ± 0.7°, repeatability: ± 3%).

Figure 4.11 shows a comparison of spray parameters of a fuel under different experimental conditions. This figure can help to understand the effects of injection and chamber pressures on spray parameters in this study. Figure 4.12 shows a comparison of spray parameters of different fuels under an experimental condition to demonstrate differences or similarities in spray parameters for different fuels under the same conditions.
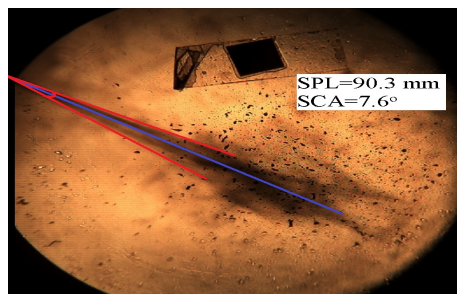
(a) P_c=0 bar, P_i=600 bar, t=0.4 ms.
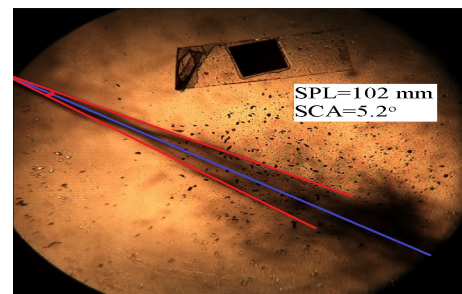
(b) P_c=0 bar, P_i=800 bar, t=0.4 ms.
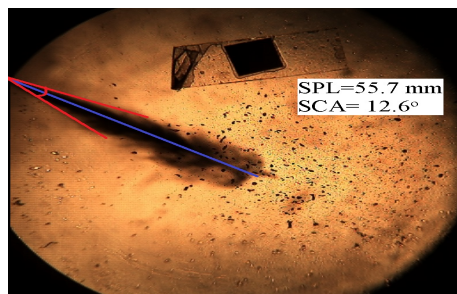
(c) P_c=5 bar, P_i=600 bar, t=0.4 ms.
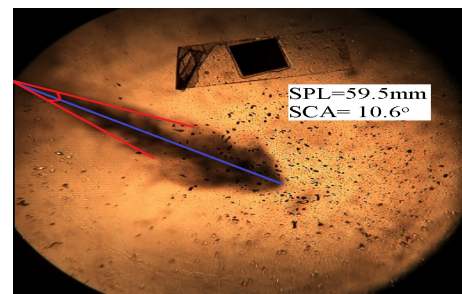
(d) P_c=5 bar, P_i=800 bar, t=0.4 ms.
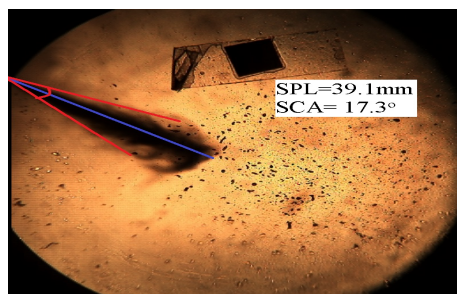
(e) P_c=10 bar, P_i=600 bar, t=0.4 ms.
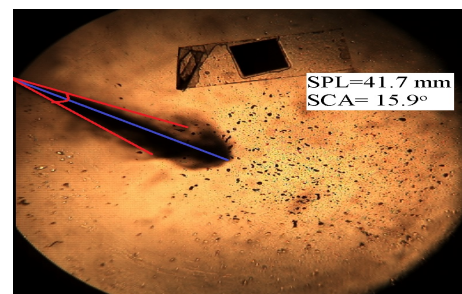
(f) P_c=10 bar, P_i=800 bar, t=0.4 ms.

Figure 4.11. An example for comparison of spray parameters of a fuel under different experimental conditions. (Fuel: SUNME, P_c=chamber pressure, P_i=injection pressure, t=time).
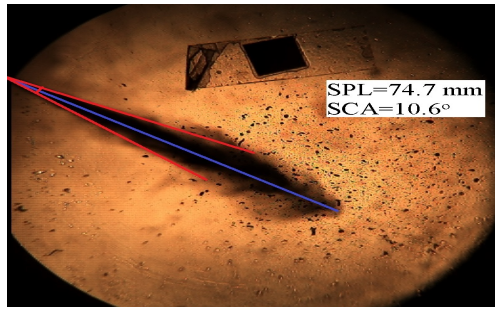
(a) CANME.
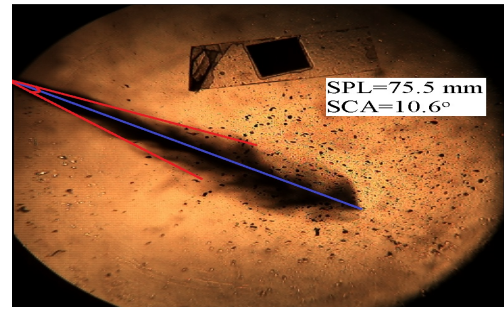
(b) COTME.
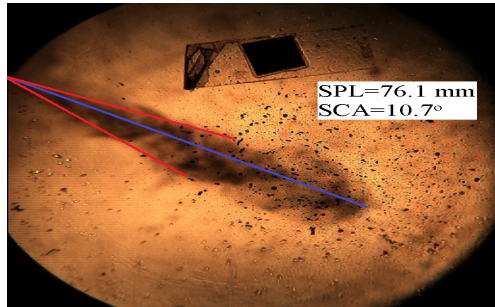
(c) SUNME.
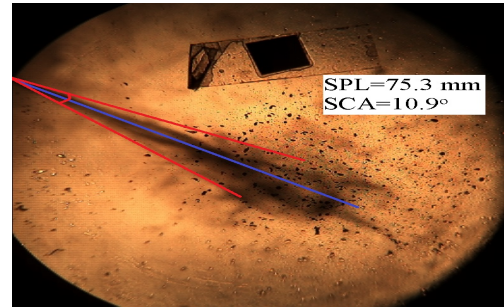
(d) CORME.
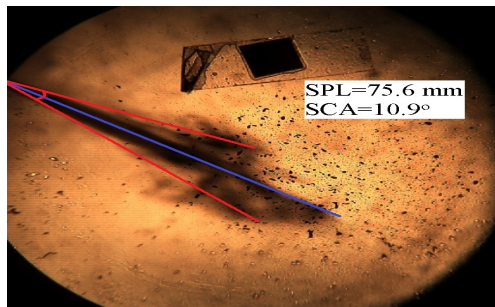
(e) SUNEE.
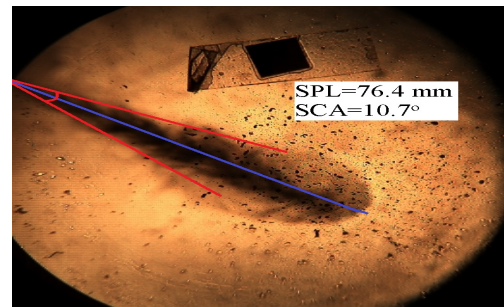
(f) COREE.
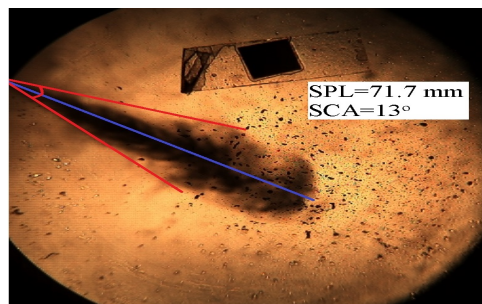
(g) DIESEL.

Figure 4.12. An example for comparison of spray parameters of different fuels under a specified experimental condition. (Chamber pressure=5 bar, injection pressure=800 bar, time=0.6 ms).

CHAPTER 5

CONCLUSION

5.1. Conclusions

Various studies in the literature showed that biodiesel fuels could decrease emissions from diesel engines, and research studies on biodiesel are still ongoing. New fuels from new resources are being produced by many researchers with the use of different production methods, and different parameters of these fuels are being examined. Considering this, it is seen that biodiesel research in every aspect is still important. Based on this importance, this study aimed at investigating the spray characteristics of several biodiesel fuels including methyl esters and ethyl esters. Besides, studies on ethyl esters in the literature are very limited compared to methyl esters, despite their advantages over methyl esters. Also, these studies have mostly focused on performance and emission characteristics, and studies examining the spray characteristics are very rare. Given the significance of spray research, this study intended to fill this gap in the literature.

For this purpose, 4 different methyl esters were produced from corn, canola, sunflower and cotton oils, and 2 ethyl esters were produced from corn and sunflower oils by using transesterification method. In addition, fossil diesel fuel was used as the reference. In order to better compare spray characteristics of these fuels, physical properties were needed to be determined before. Therefore, viscosity and density values of all fuels were measured. It was found that all biodiesel fuels had larger viscosity and density values than diesel fuel. Besides, ethyl esters had slightly lower density and relatively higher viscosity values than methyl esters.

Experiments were carried out by means of a constant volume combustion chamber and an optical system having a high-speed camera based on shadowgraph technique. Spray investigation was performed under injection pressures of 600 and 800 bar and chamber pressures of 0, 5 and 10 bar. To get the required data, a high-speed camera was employed to record the spray events. After experiments, spray images were processed by image processing programs then spray cone angles and spray penetration lengths of all fuels were obtained.

The main results of this study can be summarized as follows:

- Chamber and injection pressures are both effective parameters on spray characteristics. However, effects of chamber pressure were more significant than those of injection pressure. Besides, increasing the injection pressure increased the spray penetration length, and reduced the spray cone angle. Increasing the ambient pressure decreased the penetration lengths, and widened the cone angles.

- Spray penetration length and cone angle curves could be divided into two parts which were transient and steady regions. In transient part, the change of parameters was affected by time. In steady region, the spray penetration length changed almost steadily, and spray cone angle kept almost constant at a value. Additionally, transition times from transient region to steady region were also affected by chamber and injection pressures. Increasing chamber pressure dramatically reduced these times while increasing injection pressure slightly decreased these transition times.

- The physical properties of a fuel have a direct effect on spray characteristics. In this study, biodiesel fuels showed slightly or significantly increased penetrations and decreased spray angles in comparison to reference fuel depending on the experimental conditions. For example, the penetration length of COTME under injection pressure of 600 bar and chamber pressure of 5 bar was 10% higher than that of reference diesel fuel at 0.7 ms of injection. When these fuels were compared in terms of spray cone angle under the same conditions, it was found that COTME had 9% smaller spray angle than diesel. This may be due to having higher density, viscosity and contact angle values resulting in poorer atomization and increased spray momentums. Furthermore, it was found that the transitions of biodiesel fuels from transient region to steady region were a bit later than diesel fuel.

- Ethyl esters performed similar spray penetrations and angles with methyl esters. The difference between the fuels in terms of spray parameters were in the range of 1-3%. When taking the uncertainty values and repeatability ratio into account, this difference is not significant. This may be explained by considering density, viscosity and contact angle values. Ethyl esters had higher viscosity values on the contrary they had smaller density and contact angle values. These properties may have compensated each other thus similar spray characteristics may have been observed.

As a result, it can be stated that biodiesel fuels had worse fuel-air mixing than fossil diesel fuel in this study, however without huge differences. Therefore, it can be concluded that biodiesel fuels can replace traditional diesel fuel without compromising too much from fuel-air mixture quality. When environmental considerations are taken into account, the use of biodiesel is becoming even more important in terms of decreasing pollutant emissions and reducing dependence on fossil fuels. Moreover, the use of ethanol instead of methanol in biodiesel production is not a big problem for diesel engines. Because it was found in the present study that the mixture of ethyl ester with air was very similar to methyl ester-air mixture, and that ethyl esters could have a potential to be used instead of methyl esters in diesel engines with no or small modifications. Thus, biodiesel can be provided to be completely renewable, and vehicles can have better performances in cold weathers with these fuels.

5.2. Recommendations for Potential Future Works

Based on this study, the following recommendations can be made for potential future studies:

- Because of the time consuming nature of experiments, the present study was limited to certain fuel injection duration, chamber and injection pressures. It would be useful to extend this work by including more variations in injection quantities, ambient and injection pressures.

- Although it was found that biodiesel fuels performed longer penetrations and narrower spray angles, the results can be different when applying to an engine, where the temperature is taken into account. Hence, it would be beneficial to conduct these experiments with a real diesel engine. Besides, ethyl esters should be investigated in real compression-ignition engines to see the effects of temperature on spray characteristics of them. Also, experiments with ethyl ester should also be carried out at low temperatures.

- This work showed that ethyl esters can have a possibility to replace methyl esters. Considering that limited studies have been done on ethyl esters so far, works on this subject should be increased. Various ethyl esters should be produced from

different feed stocks, and they should be investigated in terms of spray, combustion, performance and emission characteristics.

- In this study, pure biodiesel fuels were studied. However, blends of ethyl esters with diesel would give different results. Thus, it would be useful to investigate the spray characteristics of diesel-ethyl ester blends with different blend ratios.

- Some studies in the literature showed that split injection technique can help reduce emissions. Thus, application of the split injection technique on ethyl esters would be a good study in terms of both combustion and spray study.

- It is too early to completely replace fossil diesel with biodiesel due to stability and quality problems. This is also the case for ethyl esters. Therefore, studies should be done to increase the stability of ethyl esters.

- Some studies in the literature showed that different alcohols could be used in biodiesel production. However, these studies are limited. Thus, more studies should be done on the use of different alcohols in biodiesel production. And, the usability of these fuels in diesel engines should be investigated.

- Available technologies for biodiesel production are limited, and they are less efficient and expensive. Thence, further researches need to be performed to develop cost effective and more efficient biodiesel production methods.

REFERENCES

[1] Ulu, Anılcan; Çellek, Seven Burçin; Rodriguez, Alvaro Diez; Özkol, Ünver. Experimental Spray Investigation of Biodiesel Fuels Derived from Corn Oil and Canola Oil. *The Eurasia Proceedings of Science, Technology, Engineering & Mathematics* (2019), *7*, 346–356.

[2] Rodríguez, Alvaro Diez. Investigation of Split Injection in a Single Cylinder Optical Diesel Engine. PhD Thesis, Brunel University, London, (2009).

[3] Science in the News (Harvard University). http://sitn.hms.harvard.edu/flash/2012/why-sustainable/ (accessed Jan 9, 2020).

[4] Maximo, Guilherme José.; Magalhāes, Ana Maria dos Santos; Gonçalves, Mariana M.; Esperança, Eduardo de Souza; Costa, Mariana; Meirelles, Antonio; Coutinho, Joāo. A. P. Improving the cold flow behavior of methyl biodiesel by blending it with ethyl esters. *Fuel* (2018), *226*, 87–92.

[5] Verma, Puneet; Sharma, Mahendra Pal. Comparative analysis of effect of methanol and ethanol on Karanja biodiesel production and its optimisation. *Fuel* (2016), *180*, 164–174.

[6] Heywood, John B. *Internal combustion engine fundamentals*; McGraw-Hill: New York, (1988).

[7] Razzak, Shaikh Abdur; Hossain, Mohammad Mozahar; Lucky, Rahima A.; Bassi, Amarjeet; de Lasa, Hugo. Integrated CO_2 capture, wastewater treatment and biofuel production by microalgae culturing—A review. *Renewable and Sustainable Energy Reviews* (2013), *27*, 622–653.

[8] Oumer, Ahmed N.; Hasan, Mohammad Mehedi; Baheta, Aklilu Tesfamichael; Mamat, Rizalman; Adam, Abdullah. Bio-based liquid fuels as a source of renewable energy: A review. *Renewable and Sustainable Energy Reviews* (2018), *88*, 82–98.

[9] Baskar, Gurunathan; Selvakumari, I. Aberna Ebenezer; Aiswarya, Ravi. Biodiesel production from castor oil using heterogeneous Ni doped ZnO nanocatalyst. *Bioresource Technology* (2018), *250*, 793–798.

[10] Ndiaye, Mbalo; Arhaliass, Abdellah; Legrand, Jack; Roelens, Guillaume; Kerihuel, Anthony. Reuse of waste animal fat in biodiesel: Biorefining heavily-degraded contaminant-rich waste animal fat and formulation as diesel fuel additive. *Renewable Energy* (2020), *145*, 1073–1079.

[11] Fonseca, Jhessica Marchini; Teleken, Joel Gustavo; Almeida, Vitor de Cinque; da Silva, Camila. Biodiesel from waste frying oils: Methods of production and purification. *Energy Conversion and Management* (2019), *184*, 205–218.

[12] Verma, Puneet; Sharma, Mahendra Pal; Dwivedi, Gaurav. Impact of alcohol on biodiesel production and properties. *Renewable and Sustainable Energy Reviews* (2016), *56*, 319–333.

[13] Zhao, Shuang; Niu, Shengli; Yu, Hewei; Ning, Yilin; Zhang, Xiangyu; Li, Ximing; Zhang, Yujiao; Lu, Chunmei; Han, Kuihua. Experimental investigation on biodiesel production through transesterification promoted by the La-dolomite catalyst. *Fuel* (2019), *257*, 1–9.

[14] Mofijur, Md; Rasul, Mohammad Golam; Hyde, Justin; Azad, Abul Kalam; Mamat, Rizalman; Bhuiya, Muhammad Mostafa Kamal. Role of biofuel and their binary (diesel-biodiesel) and ternary (ethanol-biodiesel-diesel) blends on internal combustion engines emission reduction. *Renewable and Sustainable Energy Reviews* (2016), *53*, 265–278.

[15] Reyero, Inés; Arzamendi, Gurutze; Zabala, Silvia; Gandía, Luis Maria. Kinetics of the NaOH-catalyzed transesterification of sunflower oil with ethanol to produce biodiesel. *Fuel Processing Technology* (2015), *129*, 147–155.

[16] Likozar, Blaž; Levec, Janez. Transesterification of canola, palm, peanut, soybean and sunflower oil with methanol, ethanol, isopropanol, butanol and tert-butanol to biodiesel: Modelling of chemical equilibrium, reaction kinetics and mass transfer based on fatty acid composition. *Applied Energy* (2014), *123*, 108–120.

[17] Verma, Puneet; Sharma, Mahendra Pal; Dwivedi, Gaurav. Effect of Short Chain Alcohols on Yield of Biodiesel Produced from Pongamia Oil. *Materials Today: Proceedings* (2018), *5* (11), 22916–22921.

[18] Munsin, Ronnachart; Shing, Bodin Chung Lim; Phunpheeranurak, Khansorn; Phongphankasem, Thanisorn; Laoonual, Yossapong; Jugjai, Sumrerng; Chanchaona, Somchai. Design of Constant Volume Combustion Chamber (CVCC) with Pre-Combustion Technique for Simulation of CI Engine Conditions. In *Proceedings of the 4th TSME International Conference on Mechanical Engineering (TSME-ICOME)*: The 4th TSME International Conference on Mechanical Engineering, Pattaya, Tailand, Oct 16-18, 2013; TSME-Thai Society of Mechanical Engineers, (2014). http://www.tsme.org/home/ (accessed May 13, 2020).

[19] European Automobile Manufacturers' Association. https://www.acea.be/statistics/tag/category/passenger-cars-production (accessed May 12, 2020).

[20] European Automobile Manufacturers' Association. https://www.acea.be/statistics/article/trends-in-fuel-type-of-new-cars-between-2016-and-2017-by-country (accessed May 12, 2020).

[21] European Commission. https://ec.europa.eu (accessed Nov 29, 2019).

[22] Khan, Mohammed Yahaya; Karim, Zainal Ambri Abdul; Hagos, Ftwi Yohaness; Aziz, Abd Rashid Abd; Tan, Isa Mohd. Current Trends in Water-in-Diesel Emulsion as a Fuel. *The Scientific World Journal* **2014**, (2014), 1–15.

[23] Wamankar, Arun Kumar; Satapathy, Ashok Kumar; Murugan, S. Experimental investigation of the effect of compression ratio, injection timing & pressure in a DI (direct injection) diesel engine running on carbon black-water-diesel emulsion. *Energy* (2015), *93*, 511–520.

[24] Ghojel, Jamil; Honnery, Damon; Al-Khaleefi, Khaled. Performance, emissions and heat release characteristics of direct injection diesel engine operating on diesel oil emulsion. *Applied Thermal Engineering* (2006), *26* (17-18), 2132–2141.

[25] Abu-Zaid, Mahmoud. Performance of single cylinder, direct injection Diesel engine using water fuel emulsions. *Energy Conversion and Management* (2004), *45* (5), 697–705.

[26] Vellaiyan, Suresh; Amirthagadeswaran, Sankaranarayanan. The role of water-in-diesel emulsion and its additives on diesel engine performance and emission levels: A retrospective review. *Alexandria Engineering Journal* (2016), *55* (3), 2463–2472.

[27] Park, Jun Wuk; Huh, Kang Yul; Lee, Jeong Hyuk. Reduction of NO_x, smoke and brake specific fuel consumption with optimal injection timing and emulsion ratio of water-emulsified diesel. *Proceedings of the Institution of Mechanical Engineers, Part D: Journal of Automobile Engineering* (2001), *215* (1), 83–93.

[28] Mata, Teresa M.; Martins, António A.; Caetano, Nidia. S. Microalgae for biodiesel production and other applications: A review. *Renewable and Sustainable Energy Reviews* (2010), *14* (1), 217–232.

[29] Yah, Nor Fadilah; Oumer, Ahmed N.; Idris, Mat Sahat. Small scale hydro-power as a source of renewable energy in Malaysia: A review. *Renewable and Sustainable Energy Reviews* (2017), *72*, 228–239.

[30] Dragone, Giuliano; Fernandes, Bruno Daniel; Vicente, António; Teixeira, José A. Third generation biofuels from microalgae. In *Current Research, Technology and Education Topics in Applied Microbiology and Microbial Biotechnology*; Méndez-Vilas, A., Eds.; Microbiology book series, no. 2; Formatex Research Center: Badajoz, (2010), pp 1355–1366.

[31] Surriya, O.; Saleem, S. S.; Waqar, K.; Kazi, A. G.; Öztürk, M. Bio-fuels: A Blessing in Disguise. In *Phytoremediation for Green Energy*; Öztürk, M., Ashraf, M., Aksoy, A., Ahmad, M. S. A., Eds.; Springer: Dordrecht, (2015), pp 11–54.

[32] *International Energy Outlook 2019 with projections to 2050*; U.S. Energy Information Administration: Washington, DC, (2019); pp 31–32.

[33] European Commission. https://ec.europa.eu/clima/policies/strategies/2030_en (accessed May 31, 2020).

[34] European Commission. https://ec.europa.eu/jrc/en/jec/renewable-energy-recast-2030-red-ii (accessed May 31, 2020).

[35] Nigam, Poonam Singh; Singh, Anoop. Production of liquid biofuels from renewable resources. *Progress in Energy and Combustion Science* (2011), *37* (1), 52–68.

[36] Wei, Hongjian; Liu, Wenzhi; Chen, Xinyu; Yang, Qing; Li, Jiashuo; Chen, Hanping. Renewable bio-jet fuel production for aviation: A review. *Fuel* (2019), *254*, 1–16.

[37] Akhlaghi, Shahin; Gedde, Ulf W.; Hedenqvist, Mikael S.; Braña, Maria Teresa Conde; Bellander, Martin. Deterioration of automotive rubbers in liquid biofuels: A review. *Renewable and Sustainable Energy Reviews* (2015), *43*, 1238–1248.

[38] Shi, Aimin; Du, Zhenyi; Ma, Xiaochen; Cheng, Yanling; Min, Min; Deng, Shaobo; Chen, Paul; Li, Dong; Ruan, Roger. Production and evaluation of biodiesel and bioethanol from high oil corn using three processing routes. *Bioresource Technology* (2013), *128*, 100–106.

[39] Martinelli, Luiz Antonio; Filoso, Solange. Expansion of sugarcane ethanol production in Brazil: Environmental and social challenges. *Ecological Applications* (2008), *18* (4), 885–898.

[40] Fargione, Joseph; Hill, Jason; Tilman, David; Polasky, Stephen; Hawthorne, Peter. Land Clearing and the Biofuel Carbon Debt. *Science* (2008), *319* (5867), 1235–1238.

[41] Crutzen, Paul Jozef; Mosier, Arvin R.; Smith, Keith A.; Winiwarter, Wilfried. N_2O release from agro-biofuel production negates global warming reduction by replacing fossil fuels. *Atmospheric Chemistry and Physics* (2008), *8*, 389–395.

[42] Mihaela, Patrascoiu; Josef, Rathbauer; Monica, Negrea; Rudolf, Zeller. Perspectives of safflower oil as biodiesel source for South Eastern Europe (comparative study: Safflower, soybean and rapeseed). *Fuel* (2013), *111*, 114–119.

[43] Cavalett, Otávio; Ortega, Enrique. Integrated environmental assessment of biodiesel production from soybean in Brazil. *Journal of Cleaner Production* (2010), *18* (1), 55–70.

[44] Sajjadi, Baharak; Raman, Abdul Aziz Abdul; Arandiyan, Hamidreza. A comprehensive review on properties of edible and non-edible vegetable oil-based biodiesel: Composition, specifications and prediction models. *Renewable and Sustainable Energy Reviews* (2016), *63*, 62–92.

[45] Ramkumar, Shanmugam; Kirubakaran, Victor. Biodiesel from vegetable oil as alternate fuel for C.I engine and feasibility study of thermal cracking: A critical review. *Energy Conversion and Management* (2016), *118*, 155–169.

[46] Nikkhah, Amin; Khojastehpour, Mehdi; Emadi, Bagher; Taheri-Rad, Alireza; Khorramdel, Surur. Environmental impacts of peanut production system using life cycle assessment methodology. *Journal of Cleaner Production* (2015), *92*, 84–90.

[47] Jiang, Jian-Jhong; Tan, Chung-Sung. Biodiesel production from coconut oil in supercritical methanol in the presence of cosolvent. *Journal of the Taiwan Institute of Chemical Engineers* (2012), *43* (1), 102–107.

[48] İçöz, Erkan; Tuğrul, K. Mehmet; Saral, Ahmet; İçöz, Ebru. Research on ethanol production and use from sugar beet in Turkey. *Biomass and Bioenergy* (2009), *33* (1), 1–7.

[49] Sims, Ralph E. H.; Mabee, Warren; Saddler, Jack N.; Taylor, Michael. An overview of second generation biofuel technologies. *Bioresource Technology* (2010), *101* (6), 1570–1580.

[50] Gomez, Leonardo D.; Steele-King, Clare G.; McQueen-Mason, Simon J. Sustainable liquid biofuels from biomass: the writing's on the walls. *New Phytologist* (2008), *178* (3), 473–485.

[51] Koh, May Ying; Ghazi, Tinia Idaty Mohd. A review of biodiesel production from Jatropha curcas L. oil. *Renewable and Sustainable Energy Reviews* (2011), *15* (5), 2240–2251.

[52] Tapanes, Neyda C. Om; Aranda, Donato A. Gomes; Carneiro, José W. de Mesquita; Antunes, Octavio A.Ceva. Transesterification of Jatropha curcas oil glycerides: Theoretical and experimental studies of biodiesel reaction. *Fuel* (2008), *87* (10-11), 2286–2295.

[53] Shonnard, David R.; Williams, Larry; Kalnes, Tom N. Camelina-derived jet fuel and diesel: Sustainable advanced biofuels. *Environmental Progress & Sustainable Energy* (2010), *29* (3), 382–392.

[54] Ramadhas, Arumugam Sakunthalai; Jayaraj, Simon; Muraleedharan, Chandrasekharan. Use of vegetable oils as I.C. engine fuels–A review. *Renewable Energy* (2004), *29* (5), 727–742.

[55] Kulkarni, Mangesh G.; Dalai, Ajay K. Waste Cooking Oil An Economical Source for Biodiesel: A Review. *Industrial & Engineering Chemistry Research* (2006), *45*, 2901–2913.

[56] Murphy, Cynthia Folsom; Allen, David T. Energy-Water Nexus for Mass Cultivation of Algae. *Environmental Science and Technology* (2011), *45* (13), 5861–5868.

[57] Jorquera, Orlando; Kiperstok, Asher; Sales, Emerson A.; Embiruçu, Marcelo; Ghirardi, Maria Lucia. Comparative energy life-cycle analyses of microalgal biomass production in open ponds and photobioreactors. *Bioresource Technology* (2010), *101* (4), 1406–1413.

[58] Cohen, Ephraim; Arad, Shoshana (Malis). A closed system for outdoor cultivation of Porphyridium. *Biomass* (1989), *18* (1), 59–67.

[59] Chisti, Yusuf. Biodiesel from microalgae. *Biotechnology Advances* (2007), *25* (3), 294–306.

[60] Ugwu, Charles U.; Aoyagi, Hideki; Uchiyama, Hiroo. Photobioreactors for mass cultivation of algae. *Bioresource Technology* (2008), *99* (10), 4021–4028.

[61] Adey, Walter; Bannon, Jeffrey. Algal Turf Scrubbers: Cleaning Water While Capturing Solar Energy. In *Proceedings of the Third Environmental Physics Conference*: The Third Environmental Physics Conference, Aswan, Egypt, Feb 19-23, 2008; International Nuclear Information System, (2008). https://inis.iaea.org/collection/NCLCollectionStore/_Public/41/057/41057395.pdf (accessed May 31, 2020).

[62] Adey, Walter H.; Kangas, Patrick C.; Mulbry, Walter. Algal Turf Scrubbing: Cleaning Surface Waters with Solar Energy while Producing a Biofuel. *BioScience* (2011), *61* (6), 434–441.

[63] Dahmani, Siham; Zerrouki, Djamal; Ramanna, Luveshan; Rawat, Ismail; Bux, Faizal. Cultivation of Chlorella pyrenoidosa in outdoor open raceway pond using domestic wastewater as medium in arid desert region. *Bioresource Technology* (2016), *219*, 749–752.

[64] Ma, Xiaochen; Zhou, Wenguang; Fu, Zongqiang; Cheng, Yanling; Min, Min; Liu, Yuhuan; Zhang, Yunkai; Chen, Paul; Ruan, Roger. Effect of wastewater-borne bacteria on algal growth and nutrients removal in wastewater-based algae cultivation system. *Bioresource Technology* (2014), *167*, 8–13.

[65] Brennan, Liam; Owende, Philip. Biofuels from microalgae–A review of technologies for production, processing, and extractions of biofuels and co-products. *Renewable and Sustainable Energy Reviews* (2010), *14* (2), 557–577.

[66] Adams, Paul; Bridgwater, Tony; Lea-Langton, Amanda; Ross, Andrew; Watson, Ian. Biomass Conversion Technologies. In *Greenhouse Gas Balances of Bioenergy Systems*; Thornley, P., Adams, P., Eds.; Academic Press, (2018), pp 107–139.

[67] Patel, Madhumita; Zhang, Xiaolei; Kumar, Amit. Techno-economic and life cycle assessment on lignocellulosic biomass thermochemical conversion technologies: A review. *Renewable and Sustainable Energy Reviews* (2016), *53*, 1486–1499.

[68] Elliott, Douglas C.; Hart, Todd R.; Schmidt, Andrew J.; Neuenschwander, Gary G.; Rotness, Leslie J.; Olarte, Mariefel V.; Zacher, Alan H.; Albrecht, Karl O.; Hallen, Richard T.; Holladay, Johnathan E. Process development for hydrothermal liquefaction of algae feedstocks in a continuous-flow reactor. *Algal Research* (2013), *2* (4), 445–454.

[69] Pourkarimi, Sara; Hallajisani, Ahmad; Alizadehdakhel, Asghar; Nouralishahi, Amideddin. Biofuel production through micro- and macroalgae pyrolysis – A review of pyrolysis methods and process parameters. *Journal of Analytical and Applied Pyrolysis* (2019), *142*, 1–19.

[70] Kebelmann, Katharina; Hornung, Andreas; Karsten, Ulf; Griffiths, Gareth. Intermediate pyrolysis and product identification by TGA and Py-GC/MS of green microalgae and their extracted protein and lipid components. *Biomass and Bioenergy* (2013), *49*, 38–48.

[71] Luo, Guanqun; Chandler, Devin S.; Anjos, Luiz C. A.; Eng, Ryan J.; Jia, Pei; Resende, Fernando L. P. Pyrolysis of whole wood chips and rods in a novel ablative reactor. *Fuel* (2017), *194*, 229–238.

[72] Garcìa-Pèrez, Manuel; Chaala, Abdelkader; Roy, Christian. Vacuum pyrolysis of sugarcane bagasse. *Journal of Analytical and Applied Pyrolysis* (2002), *65* (2), 111–136.

[73] Varatharajan, K.; Cheralathan, M. Influence of fuel properties and composition on NO_x emissions from biodiesel powered diesel engines: A review. *Renewable and Sustainable Energy Reviews* (2010), *16* (6), 3702–3710.

[74] *Nitrogen Oxides (NO_x), Why and How They Are Controlled*; U.S. Environmental Protection Agency: North Carolina, (1999); pp 2–4.

[75] Çengel, Yunus A.; Boles, Michael A. *Thermodynamics: An Engineering Approach*; McGraw-Hill, (2004), pp 752–756.

[76] Fenimore, Charles P. Formation of nitric oxide in premixed hydrocarbon flames. *Symposium (International) on Combustion* (1971), *13* (1), 373–380.

[77] Amann, Charles A.; Siegla, Donald C. Diesel Particulates–What They Are and Why. *Aerosol Science and Technology* (1981), *1* (1), 73–101.

[78] Baumgarten, Carsten. *Mixture formation in internal combustion engines*; Heat and mass transfer; Springer-Verlag Berlin Heidelberg: Berlin, (2006).

[79] d'Ambrosio, Stefano; Ferrari, Alessandro. Diesel engines equipped with piezoelectric and solenoid injectors: hydraulic performance of the injectors and comparison of the emissions, noise and fuel consumption. *Applied Energy* (2018), *211*, 1324–1342.

[80] Chung, Myungchul; Kim, Jinsu; Kim, Sangmyeong; Sung, Gisu; Lee, Jinwook. Effects of hydraulic flow and spray characteristics on diesel combustion in CR direct-injection engine with indirect acting Piezo injector. *Journal of Mechanical Science and Technology* (2015), *29*, 2517–2528.

[81] Payri, Raul; Salvador, F. Javier; Gimeno, Jaime; De la Morena, Joaquín. Influence of injector technology on injection and combustion development - Part 1: Hydraulic characterization. *Applied Energy* (2011), *88* (4), 1068–1074.

[82] Reitz, Rolf Deneys; Bracco, Frediano V. Mechanisms of Breakup of Round Liquid Jets. *Encyclopedia of Fluid Mechanics* (1986), *3*, 233–249.

[83] Payri, Raul; Salvador, F. Javier; Gimeno, Jaime; De la Morena, Joaquín. Analysis of diesel spray atomization by means of a near-nozzle field visualization technique. *Atomization and Sprays* (2011), *21* (9), 753–774.

[84] Hwang, Sang Soon; Liu, Zhien; Reitz, Rolf D. Breakup Mechanisms and Drag Coefficients of High-Speed Vaporizing Liquid Drops. *Atomization and Sprays* (1996), *6* (3), 353–376.

[85] Krzeczkowski, Stefan A. Measurement of Liquid Droplet Disintegration Mechanisms. *International Journal of Multiphase Flow* (1980), *6* (3), 227–239.

[86] Hiroyasu, Hiro; Arai, Masataka. Structures of Fuel Sprays in Diesel Engines. *SAE Technical Paper 900475* (1990).

[87] Arai, M.; Shimizu, M.; Hiroyasu, H. Similarity Between the Break-up Lengths of a High Speed Liquid Jet in Atmospheric and Pressurized Conditions. In *Proceedings of the Fifth International Conference on Liquid Atomization and Spray Systems*: The Fifth International Conference on Liquid Atomization and Spray Systems, Gaithersburg, MD, U.S.A., Jul 15-18, 1991; National Institute of Standards and Technology, (1991). https://nvlpubs.nist.gov/nistpubs/Legacy/SP/nistspecialpublication813.pdf (accessed May 15, 2020).

[88] Hiroyasu, H.; Shimizu, M.; Arai, M. Break-up Length of a Liquid Jet and Internal Flow in a Nozzle. In *Proceedings of the Fifth International Conference on Liquid Atomization and Spray Systems*: The Fifth International Conference on Liquid Atomization and Spray Systems, Gaithersburg, MD, U.S.A., Jul 15-18, 1991; National Institute of Standards and Technology, (1991). https://nvlpubs.nist.gov/nistpubs/Legacy/SP/nistspecialpublication813.pdf (accessed May 15, 2020).

[89] Soteriou, Celia; Andrews, Richard; Smith, Mark. Direct Injection Diesel Sprays and the Effect of Cavitation and Hydraulic Flip on Atomization. *SAE Technical Paper 950080* (1995).

[90] Urlaub, A. G.; Chmela, F. G. High-Speed, Multifuel Engine: L9204 FMV. *SAE Technical Paper 740122* (1974).

[91] Oren, Daniel C.; Wahiduzzaman, Syed; Ferguson, Colin R. A Diesel Combustion Bomb: Proof of Concept. *SAE Technical Paper 841358* (1984).

[92] Baert, Rik S. G.; Frijters, Peter J. M.; Somers, Bart; Luijten, Carlo C. M.; de Boer, Wout. Design and Operation of a High Pressure, High Temperature Cell for HD Diesel Spray Diagnostics: Guidelines and Results. *SAE Technical Paper 2009-01-0649* (2009).

[93] Settles, Gary S. *Schlieren and Shadowgraph Techniques*; Experimental Fluid Mechanics; Springer-Verlag Berlin Heidelberg: Berlin, (2001).

[94] *The California Diesel Fuel Regulations*; California Air Resources Board: California, (2014); pp 1–57.

[95] *International Fuel Quality Standards and Their Implications for Australian Standards*; Technical Report for Australian Government, Department of the Environment; Hart Energy, (2014); pp 7–98.

[96] U.S. Department of Energy. https://afdc.energy.gov/fuels/biodiesel_specifications.html (accessed Jan 22, 2020).

[97] Rutz, Dominik; Janssen, Rainer. *Overview and Recommendations on Biofuel Standards for Transport in the EU*; WIP Renewable Energies: München, (2006); pp 1–26.

[98] Costenoble, Ortwin. *Worldwide Fuels Standards: Overview of specifications and regulations on (bio)fuels*; Technical Report for Netherlands Agency for Innovation, Energy and Environment; the Netherlands Standardization Institute: Delft, (2006); pp 6–17.

[99] Qi, Donghui; Chen, Hao; Geng, Limin; Bian, Y. Zh. Experimental studies on the combustion characteristics and performance of a direct injection engine fueled with biodiesel/diesel blends. *Energy Conversion and Management* (2010), *51* (12), 2985–2992.

[100] Chauhan, Bhupendra Singh; Kumar, Naveen; Cho, Haeng Muk. A study on the performance and emission of a diesel engine fueled with Jatropha biodiesel oil and its blends. *Energy* (2012), *37* (1), 616–622.

[101] Shrivastava, Pankaj; Verma, Tikendra Nath; Pugazhendhi, Arivalagan. An experimental evaluation of engine performance and emisssion characteristics of CI engine operated with Roselle and Karanja biodiesel. *Fuel* (2019), *254*, 1–12.

[102] Nirmala, N.; Dawn, S. S.; Harindra, C. Analysis of performance and emission characteristics of Waste cooking oil and Chlorella variabilis MK039712.1 biodiesel blends in a single cylinder, four strokes diesel engine. *Renewable Energy* (2020), *147*, 284–292.

[103] Patel, Chetankumar; Chandra, Krishn; Hwang, Joonsik; Agarwal, Rashmi A.; Gupta, Neeraj; Bae, Choongsik; Gupta, Tarun; Agarwal, Avinash Kumar. Comparative compression ignition engine performance, combustion, and emission characteristics, and trace metals in particulates from Waste cooking oil, Jatropha and Karanja oil derived biodiesels. *Fuel* (2019), *236*, 1366–1376.

[104] Nabi, M. N.; Rasul, Mohammad Golam. Influence of second generation biodiesel on engine performance, emissions, energy and exergy parameters. *Energy Conversion and Management* (2018), *169*, 326–333.

[105] Soto, Felipe; Marques, Gian; Torres-Jiménez, Eloisa; Vieira, Bráulio; Lacerda, André; Armas, Octavio; Guerrero-Villar, Francisca. A comparative study of performance and regulated emissions in a medium-duty diesel engine fueled with sugarcane diesel-farnesane and sugarcane biodiesel-LS9. *Energy* (2019), *176*, 392–409.

[106] Das, Mithun; Sarkar, Mouktik; Datta, Amitava; Santra, Apurba Kumar. An experimental study on the combustion, performance and emission characteristics of a diesel engine fuelled with diesel-castor oil biodiesel blends. *Renewable Energy* (2018), *119*, 174–184.

[107] Raman, Lakshmipathi Anantha; Deepanraj, B.; Rajakumar, S.; Sivasubramanian, Velmurugan. Experimental investigation on performance, combustion and emission analysis of a direct injection diesel engine fuelled with rapeseed oil biodiesel. *Fuel* (2019), *246*, 69–74.

[108] Özçelik, Abdullah Engin; Aydoğan, Hasan; Acaroğlu, Mustafa. Determining the performance, emission and combustion properties of camelina biodiesel blends. *Energy Conversion and Management* (2015), *96*, 47–57.

[109] Mistri, Gayatri K.; Aggarwal, Suresh K.; Longman, Douglas; Agarwal, Avinash K. Performance and Emission Investigations of Jatropha and Karanja Biodiesels in a Single-Cylinder Compression-Ignition Engine Using Endoscopic Imaging. *Journal of Energy Resources Technology* (2016), *138* (1), 1–13.

[110] Chokri, Boubahri; Ridha, Ennetta; Rachid, Said; Jamel, Bessrour. Experimental Study of a Diesel Engine Performance Running on Waste Vegetable Oil Biodiesel Blend. *Journal of Energy Resources Technology* (2012), *134* (3), 1–6.

[111] Agarwal, Avinash Kumar; Dhar, Atul. Comparative Performance, Emission, and Combustion Characteristics of Rice-Bran Oil and Its Biodiesel in a Transportation Diesel Engine. *Journal of Engineering for Gas Turbines and Power* (2010), *132* (6), 1–4.

[112] Patel, Chetankumar; Lee, Sanghoon; Tiwari, Nachiketa; Agarwal, Avinash Kumar; Lee, Chang Sik; Park, Sungwook. Spray characterization, combustion, noise and vibrations investigations of Jatropha biodiesel fuelled genset engine. *Fuel* (2016), *185*, 410–420.

[113] Yu, Shenghao; Yin, Bifeng; Deng, Weixin; Jia, Hekun; Ye, Ze; Xu, Bin; Xu, Huaping. Experimental study on the diesel and biodiesel spray characteristics emerging from equilateral triangular orifice under real diesel engine operation conditions. *Fuel* (2018), *224*, 357–365.

[114] Kuti, Olawole Abiola; Zhu, Jingyu; Nishida, Keiya; Wang, Xiangang; Huang, Zuohua. Characterization of spray and combustion processes of biodiesel fuel injected by diesel engine common rail system. *Fuel* (2013), *104*, 838–846.

[115] Seraç, Mehmet Reşit; Aydın, Selman; Yılmaz, Adem; Şevik, Seyfi. Evaluation of comparative combustion, performance, and emission of soybean-based alternative biodiesel fuel blends in a CI engine. *Renewable Energy* (2020), *148*, 1065–1073.

[116] Asokan, M. A.; Prabu, S. S.; Bade, P. K. K.; Nekkanti, V. M.; Gutta, S. S. G. Performance, combustion and emission characteristics of juliflora biodiesel fuelled DI diesel engine. *Energy* (2019), *173*, 883–892.

[117] Gümüş, Metin; Kaşifoğlu, Sadık. Performance and emission evaluation of a compression ignition engine using a biodiesel (apricot seed kernel oil methyl ester) and its blends with diesel fuel. *Biomass and Bioenergy* (2010), *34* (1), 134–139.

[118] Panwar, N. L.; Shrirame, Hemant Y.; Rathore, Narendra S.; Jindal, Sudhakar; Kurchania, Anilkumar K. Performance evaluation of a diesel engine fueled with methyl ester of castor seed oil. *Applied Thermal Engineering* (2010), *30* (2-3), 245–249.

[119] Ong, Hwai Chyuan; Masjuki, Haji Hassan; Mahlia, Teuku Meurah Indra; Silitonga, Arridina Susan; Chong, Wen Tong; Yusaf, Talal. Engine performance and emissions using Jatropha curcas, Ceiba pentandra and Calophyllum inophyllum biodiesel in a CI diesel engine. *Energy* (2014), *69*, 427–445.

[120] El-Kasaby, Mohammed; Nemit-Allah, Medhat Ahmed. Experimental investigations of ignition delay period and performance of a diesel engine operated with Jatropha oil biodiesel. *Alexandria Engineering Journal* (2013), *52* (2), 141–149.

[121] Mancaruso, Ezio; Perozziello, Carmela; Sequino, Luigi; Vaglieco, Bianca Maria. Characterization of pure and blended biodiesel spray in a compression ignition engine by means of advanced diagnostics and 1D model. *Fuel* (2019), *239*, 1102–1114.

[122] Lee, Sanghoon; Lee, Chang Sik; Park, Sungwook; Gupta, Jai Gopal; Maurya, Rakesh Kumar; Agarwal, Avinash Kumar. Spray characteristics, engine performance and emissions analysis for Karanja biodiesel and its blends. *Energy* (2017), *119*, 138–151.

[123] Mohan, Balaji; Yang, Wenming; Tay, Kun Lin; Yu, Wenbin. Experimental study of spray characteristics of biodiesel derived from waste cooking oil. *Energy Conversion and Management* (2014), *88*, 622–632.

[124] Subramanian, Kizhaeral A.; Lahane, Subhash. Comparative evaluations of injection and spray characteristics of a diesel engine using karanja biodiesel-diesel blends. *International Journal of Energy Research* (2013), *37* (6), 582–597.

[125] Patel, Chetankumar; Hwang, Joonsik; Chandra, Krishn; Agarwal, Rashmi A.; Bae, Choongsik; Gupta, Tarun; Agarwal, Avinash Kumar. In-Cylinder Spray and Combustion Investigations in a Heavy-Duty Optical Engine Fueled With Waste Cooking Oil, Jatropha, and Karanja Biodiesels. *Journal of Energy Resources Technology* (2019), *141* (1), 1–12.

[126] Agarwal, Avinash Kumar; Som, Sibendu; Shukla, Pravesh Chandra; Goyal, Harsh; Longman, Douglas. In-nozzle flow and spray characteristics for mineral diesel, Karanja, and Jatropha biodiesels. *Applied Energy* (2015), *156*, 138–148.

[127] Gupta, Jai Gopal; Agarwal, Avinash Kumar. Macroscopic and Microscopic Spray Characteristics of Diesel and Karanja Biodiesel Blends. *SAE Technical Paper 2016-01-0869* (2016).

[128] Deng, Jun; Li, Chunwang; Hu, Zongjie; Wu, Zhijun; Li, Liguang. Spray Characteristics of Biodiesel and Diesel Fuels under High Injection Pressure with a Common Rail System. *SAE Technical Paper 2010-01-2268* (2010).

[129] Tinprabath, Padipan; Hespel, Camille; Chanchaona, Somchai; Foucher, Fabrice. Influence of Biodiesel and Diesel Fuel Blends on the Injection Rate and Spray Injection in Non-Vaporizing Conditions. *SAE Technical Paper 2013-24-0032* (2013).

[130] Lin, Yung-Sung; Lin, Hai-Ping. Study on the spray characteristics of methyl esters from waste cooking oil at elevated temperature. *Renewable Energy* (2010), *35* (9), 1900–1907.

[131] Mancaruso, Ezio; Sequino, Luigi; Vaglieco, Bianca Maria; Ciaravino, Claudio; Vassallo, Alberto. Spray Formation and Combustion Analysis in an Optical Single Cylinder Engine Operating with Fresh and Aged Biodiesel. *SAE International Journal of Engines* (2011), *4* (1), 1963–1977.

[132] Hwang, Joonsik; Bae, Choongsik; Patel, Chetan; Agarwal, Avinash Kumar; Gupta, Tarun. An Experimental Investigation on Spray Characteristics of Waste Cooking Oil, Jatropha, and Karanja Biodiesels in a Constant Volume Combustion Chamber. *SAE Technical Paper 2016-01-2263* (2016).

[133] Xie, Hongzhan; Song, Lanbo; Xie, Yizhi; Pi, Dong; Shao, Chunyu; Lin, Qizhao. An Experimental Study on the Macroscopic Spray Characteristics of Biodiesel and Diesel in a Constant Volume Chamber. *Energies* (2015), *8* (6), 5952–5972.

[134] Nerva, Jean-Guillaume; Genzale, Caroline L.; Kook, Sanghoon; García-Oliver, Jose M.; Pickett, Lyle M. Fundamental spray and combustion measurements of soy methyl-ester biodiesel. *International Journal of Engine Research* (2013), *14* (4), 373–390.

[135] Wang, Xiangang; Huang, Zuohua; Kuti, Olawole Abiola; Zhang, Wu; Nishida, Keiya. Experimental and analytical study on biodiesel and diesel spray characteristics under ultra-high injection pressure. *International Journal of Heat and Fluid Flow* (2010), *31* (4), 659–666.

[136] Lahane, Subhash; Subramanian, Kizhaeral A. Effect of different percentages of biodiesel-diesel blends on injection, spray, combustion, performance, and emission characteristics of a diesel engine. *Fuel* (2015), *139*, 537–545.

[137] Sanli, Huseyin; Canakci, Mustafa; Alptekin, Ertan; Turkcan, Ali; Ozsezen, Ahmet Necati. Effects of waste frying oil based methyl and ethyl ester biodiesel fuels on the performance, combustion and emission characteristics of a DI diesel engine. *Fuel* (2015), *159*, 179–187.

[138] Alptekin, Ertan; Sanli, Huseyin; Canakci, Mustafa. Combustion and performance evaluation of a common rail DI diesel engine fueled with ethyl and methyl esters. *Applied Thermal Engineering* (2019), *149*, 180–191.

[139] Gautam, Raghvendra; Kumar, Naveen; Sharma, Pritam. Comparative Assessment of Performance, Emission and Combustion Characteristics of Blends of Methyl and Ethyl Ester of Jatropha Oil and Diesel in Compression Ignition Engine. *SAE Technical Paper 2013-01-2664* (2013).

[140] Murugesan, A.; Subramaniam, D.; Vijayakumar, C.; Avinash, A.; Nedunchezhian, N. Analysis on performance, emission and combustion characteristics of diesel engine fueled with methyl-ethyl esters. *Journal of Renewable and Sustainable Energy* (2012), *4*, 1–12.

[141] Gautam, Raghvendra; Kumar, Naveen; Pali, Harveer Singh; Kumar, Parvesh. Experimental studies on the use of methyl and ethyl esters as an extender in a small capacity diesel engine. *Biofuels* (2016), *7* (6), 637–646.

[142] da Silva, Marcelino Aurélio Vieira; Ferreira, Beatriz Lagnier Gil; Marques, Luiz Guilhermeda Costa; Murta, Aurélio Lamare Soares; de Freitas, Marcos Aurelio Vasconcelos. Comparative study of NOx emissions of biodiesel-diesel blends from soybean, palm and waste frying oils using methyl and ethyl transesterification routes. *Fuel* (2017), *194*, 144–156.

[143] Singh, Neetu; Kumar, Himansh; Jha, M. K.; Sarma, Anil Kumar. Complete heat balance, performance, and emission evaluation of a CI engine fueled with Mesua ferrea methyl and ethyl ester's blends with petrodiesel. *Journal of Thermal Analysis and Calorimetry* (2015), *122*, 907–916.

[144] Eliçin, Ahmet Konuralp; Öztürk, Ferhat; Baran, Mehmet Fırat; Esgici, Reşat. The use of rapeseed oil methyl and ethyl esters and of rapeseed oil-diesel mixtures as fuels for diesel engine. *Fresenius Environmental Bulletin* (2019), *28*, 7915–7923.

[145] Quader, M. Abdul; Ahmed, Syed Shaheer Uddin. Bioenergy With Carbon Capture and Storage (BECCS): Future Prospects of Carbon-Negative Technologies. In *Clean Energy for Sustainable Development: Comparisons and Contrasts of New Approaches*; Rasul, M. G.; Azad, A. K.; Sharma, S. C., Eds.; Academic Press, (2017), pp 91–140.

[146] Schuchardt, Ulf; Sercheli, Ricardo Silva; Vargas, Rogério Matheus. Transesterification of vegetable oils: a review. *Journal of the Brazilian Chemical Society* (1998), *9*, 199–210.

[147] Daud, Nurull Muna; Abdullah, Siti Rozaimah Sheikh; Hasan, Hassimi Abu; Yaakob, Zahira. Production of biodiesel and its wastewater treatment technologies: A review. *Process Safety and Environmental Protection* (2015), *94*, 487–508.

[148] Demir, Veli Gökhan.; Soyhan, H. S. Biodiesel Production Using Wet and Dry Purification Methods. *European Journal of Engineering and Natural Sciences* (2017), *2* (1), 137–143.

[149] *Rheometers*; TA Instruments: New Castle, DE.
http://www.tainstruments.com/pdf/brochure/2006_AR_Brochure.pdf (accessed Mar 9, 2020).

[150] Biolin Scientific. https://www.biolinscientific.com/attension/optical-tensiometers /theta-technical-specifications (accessed Jul 9, 2020).

[151] *Device Specifications, NI 6353*; National Instruments: Austin, TX, (2016). http://www.ni.com/pdf/manuals/374592d.pdf (accessed Apr 13, 2020).

[152] Elegeert, Wesley. The visualization of vaporizing fuel sprays on the GUCCI setup. MSc Thesis, Ghent University, Ghent, (2014).

[153] Galle, Jonas; Van De Maele, Christophe; Defruyt, Sander; Verhelst, Sebastian; Verschaeren, Roel. Evaluation of Some Important Boundary Conditions for Spray Measurements in a Constant Volume Combustion Chamber. *SAE Technical Paper 2013-01-1610* (2013).

[154] Dorf, Richard C.; Bishop, Robert H. *Modern Control Systems*, 12th ed.; Prentice Hall: New Jersey, (2011).

[155] Create Angle Measurement Tool Using ROI Objects. https://www.mathworks.com/help/images/create-angle-measurement-tool-using-roi-objects.html (accessed Feb 18, 2019).

APPENDIX A

CALCULATIONS FOR BIODIESEL PRODUCTION

In this appendix, methodology of calculation for biodiesel production will be explained step by step. Calculation of the amount of alcohol and catalyst to be used to produce biodiesel from 1 liter of vegetable oil will be explained. Before calculations, some properties such as chemical formula, density and molecular weight of the alcohols used in this study are given in Table A.1.

Table A.1. Properties of the alcohols used in this study.

Type of alcohol	Chemical Formula	Molecular Weight (g/mol)	Density (g/l) @ 25 °C
Methanol	CH_3OH	32.04	792
Ethanol	C_2H_5OH	46.07	790

Four different types of vegetable oils were used in this study, which are sunflower oil, corn oil, canola oil and cotton oil. They had different density values and molecular weights. However, these values did not differ so much. Therefore, the density and molecular weights of all oils were averaged, and one value is revealed for each property in order to make the calculations simpler, and to save time by avoiding calculating again and again. Averaged values are presented in Table A.2.

Table A.2. Average properties of the vegetable oils used in this study.

Molecular Weight (g/mol)	Density (g/l) @ 25 °C
890	910

In the followings, calculations for production of methyl ester and ethyl ester will be explained separately. Because, methanol and ethanol have different values of density and molecular weight. In addition, different alcohol to lipid ratio and different amounts of catalyst are used for each type of biodiesel.

A.1. Calculations for Methyl Ester Production

- Methanol to lipid ratio is used as 6 for the production of methyl ester.

- Density of vegetable oil and methanol are 910 and 792 g/l, respectively.

- Molecular weights of vegetable oil and methanol are 890 and 32.04 g/mol, respectively.

- Equation A.1 will be used to calculate the required amount of methanol.

$$\frac{\text{grams of oil to be used}}{\text{molecular weight of oil}} = \frac{\text{grams of methanol to be calculated}}{\text{6 x molecular weight of methanol}} \tag{A.1}$$

By writing the mass of vegetable oil, and molecular weights of vegetable oil and methanol in Equation A.1, the following relationship is obtained.

$$\frac{910 \text{ grams of oil}}{890 \text{ g/mol}} = \frac{?}{6 \text{ x } 32.04 \text{ g/mol}} \tag{A.2}$$

Solving Equation A.2 gives the required amount of methanol in mass as 196.56 grams. Because the density of methanol is 792 g/l, required amount of methanol is 248.8 ml by volume.

Moreover, catalyst to oil ratio is used as 1wt%. Namely, 9.1 grams of catalyst is used to produce methyl ester from 910 grams of vegetable oil.

A.2. Calculations for Ethyl Ester Production

- Ethanol to lipid ratio is used as 24 for the production of ethyl ester.

- Density of vegetable oil and ethanol are 910 and 790 g/l.

- Molecular weights of vegetable oil and ethanol are 890 and 46.07 g/mol, respectively.

- Equation A.3 will be used to calculate the required amount of methanol.

$$\frac{\text{grams of oil to be used}}{\text{molecular weight of oil}} = \frac{\text{grams of ethanol to be calculated}}{24 \text{ x molecular weight of ethanol}} \qquad \text{(A.3)}$$

By writing the mass of vegetable oil, and molecular weights of vegetable oil and ethanol in Equation A.3, the following relationship is obtained.

$$\frac{910 \text{ grams of oil}}{890 \text{ g/mol}} = \frac{?}{24 \text{ x } 46.07 \text{ g/mol}} \qquad \text{(A.4)}$$

Solving Equation A.4 gives the required amount of ethanol in mass as 1130.5 grams. Because the density of ethanol is 790 g/l, required amount of ethanol is 1431.1 ml by volume.

Moreover, catalyst to oil ratio is used as 0.1wt%. Namely, 0.91 grams of catalyst is used to produce ethyl ester from 910 grams of vegetable oil.

APPENDIX B

PROPERTIES OF THE DAQ CARD

NI USB 6353 DAQ card is used as the DAQ card in the present study. Properties of this DAQ card is given in Table B.1. Further information can be found in reference [151].

Table B.1.: Properties of NI USB 6353 DAQ card. (Data source: [151]).

Analog Input	
Number of channels	16 differential or 32 single ended
ADC resolution	16 bits
Single channel maximum sample rate	1.25 MS/s
Multichannel maximum (aggregate) sample rate	1.00 MS/s
Timing resolution	10 ns
Timing accuracy	50 ppm of sample rate
Input coupling	DC
Input range	± 0.1 V, ± 0.2 V, ± 0.5 V, ± 1 V, ± 2 V, ± 5 V, ± 10 V
Maximum working voltage (signal+common mode)	± 11 V of AI GND
Analog Output	
Number of channels	4
DAC resolution	16 bits
Maximum update rate (1 channel)	2.86 MS/s
Maximum update rate (2 channels)	2.00 MS/s
Maximum update rate (3 channels)	1.54 MS/s
Maximum update rate (4 channels)	1.25 MS/s
Timing resolution	10 ns

Timing accuracy	50 ppm of sample rate
Output coupling	DC
Output range	$\pm$10 V, $\pm$5 V, $\pm$external reference on APFI $<$0..1$>$
Output current drive	$\pm$5 mA
Digital Input/Output	
Static Characteristics	
Number of channels	48 total, 32 (P0.$<$0..31$>$), 16 (PFI $<$0..7$>$/P1, PFI $<$8..15$>$/P2)
Ground reference	D GND
Direction control	Each terminal individually programmable as input or output
Waveform Characteristics (Port 0 only)	
Terminals used	Port 0 (P0.$<$0..31$>$)
Port/sample size	Up to 32 bits
Waveform generation (DO) FIFO	2,047 samples
Waveform acquisition (DI) FIFO	255 samples
Recommended Operating Conditions	
Input High Voltage	2.2 V (minimum), 5.25 V (maximum)
Input Low Voltage	0 V (minimum), 0.8 V (maximum)

ADC: Analog to digital converter, DAC: Digital to analog converter.

APPENDIX C

FLOW CHARTS FOR IMAGE PROCESSING
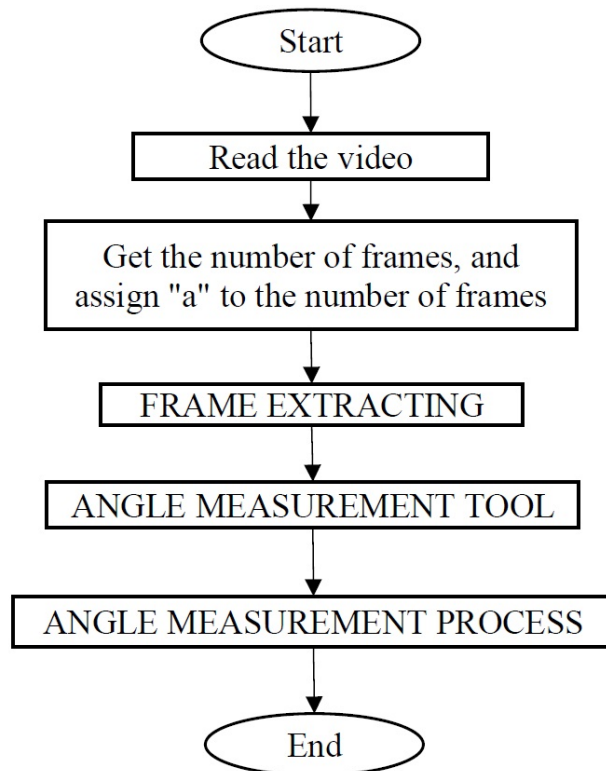
Figure C.1. Flow chart for the measurement of spray cone angle.

Figure C.1. (cont.)

```
                    ┌─────────────────────┐
                    │        ANGLE        │
                    │     MEASUREMENT     │
                    └─────────────────────┘
                              │
                              ▼
        ┌─────────────────────────────────────────────────┐
        │   Define function "my_angle_measurement_tool     │
        └─────────────────────────────────────────────────┘
                              │
                              ▼
          ┌─────────────────────────────────────────┐
          │     Create figure, and set up properties │
          └─────────────────────────────────────────┘
                              │
                              ▼
          ┌─────────────────────────────────────────┐
          │         Display image on x-y plane       │
          └─────────────────────────────────────────┘
                              │
                              ▼
            ┌───────────────────────────────────┐
            │        Get the size of image      │
            └───────────────────────────────────┘
                              │
                              ▼
      ┌─────────────────────────────────────────────────┐
      │  Get the centre point of image for initial positioning │
      └─────────────────────────────────────────────────┘
                              │
                              ▼
       ┌───────────────────────────────────────────────┐
       │    Position first point vertically above the centre │
       └───────────────────────────────────────────────┘
                              │
                              ▼
    ┌────────────────────────────────────────────────────────┐
    │  Create a two-segment right-angle polyline centered in the image │
    └────────────────────────────────────────────────────────┘
                              │
                              ▼
            ┌───────────────────────────────────┐
            │        Display initial position   │
            └───────────────────────────────────┘
                              │
                              ▼
     ┌──────────────────────────────────────────────────────┐
     │  Set up callback function to update angle in title of the image │
     └──────────────────────────────────────────────────────┘
                              │
                              ▼
   ┌───────────────────────────────────────────────────────────┐
   │  Receive an array containing the current x,y position the three vertices │
   └───────────────────────────────────────────────────────────┘
                              │
                              ▼
          ┌─────────────────────────────────────────┐
          │     Create two vectors from the vertices │
          └─────────────────────────────────────────┘
                              │
                              ▼
              ┌─────────────────────────────┐
              │         Find the angle       │
              └─────────────────────────────┘
                              │
                              ▼
            ┌───────────────────────────────────┐
            │        Convert it to degrees      │
            └───────────────────────────────────┘
                              │
                              ▼
       ┌───────────────────────────────────────────────┐
       │    Display the angle in the title of the figure │
       └───────────────────────────────────────────────┘
                              │
                              ▼
       ┌───────────────────────────────────────────────┐
       │    Display the angle in the title of the figure │
       └───────────────────────────────────────────────┘
                              │
                              ▼
                        ┌───────────┐
                        │    End    │
                        └───────────┘
```

Figure C.1. (cont.)

Figure C.1. (cont.)

```
                    ┌─────────────┐
                    │   START     │
                    └──────┬──────┘
                           ▼
              ┌────────────────────────┐
              │    Read the video      │
              └───────────┬────────────┘
                          ▼
    ┌──────────────────────────────────────────────────────┐
    │ Get the number of frames, and assign "a" to the       │
    │                number of frames                        │
    └───────────────────────────┬──────────────────────────┘
                                ▼
        ┌────────────────────────────────────────┐
        │      i=1 ("i" specifies the frames)     │
        └───────────────────┬────────────────────┘
                            ▼
                       ◇ i<=a ◇ ──── NO ────┐
                          │                 │
                         YES                │
                          ▼                 │
        ┌────────────────────────────────┐  │
        │      Read "i" from the video   │  │
        └───────────────┬────────────────┘  │
                        ▼                    │
  ┌──────────────────────────────────────┐  │
  │ Convert "i" to grayscale from colored │  │
  │              scale                    │  │
  └──────────────┬───────────────────────┘  │
                 ▼                           │
  ┌──────────────────────────────────────┐  │
  │ Read the first frame of the video,    │  │
  │     and convert it into grayscale     │  │
  └──────────────┬───────────────────────┘  │
                 ▼                           │
  ┌──────────────────────────────────────┐  │
  │   Subtract the first frame from "i"   │  │
  └──────────────────────────────────────┘  │
                 ▼                           │
        ┌────────────────────────┐ ◄────────┘
        │     End "for loop"     │
        └───────────┬────────────┘
                    ▼
  ┌──────────────────────────────────────────────────────┐
  │ Record the video which is with grayscale and          │
  │ background removed, and name it as "Grayscale_video"   │
  └───────────────────────────┬──────────────────────────┘
                              ▼
        ┌────────────────────────────────────────┐
        │       Read "Grayscale_video"            │
        └───────────────────┬────────────────────┘
                            ▼
        ┌────────────────────────────────────────┐
        │      j=1 ("j" specifies the frames)     │
        └───────────────────┬────────────────────┘
                            ▼
                       ◇ j<=a ◇ ──── NO ────┐
                          │                 │
                         YES                │
                          ▼                 │
        ┌────────────────────────────────┐  │
        │      Read "i" from the video   │  │
        └───────────────┬────────────────┘  │
                        ▼                    │
  ┌──────────────────────────────────────┐  │
  │ Convert "i" to grayscale from colored │  │
  │              scale                    │  │
  └──────────────┬───────────────────────┘  │
                 ▼                           │
  ┌──────────────────────────────────────┐  │
  │ Read the first frame of the video,    │  │
  │     and convert it into grayscale     │  │
  └──────────────┬───────────────────────┘  │
                 ▼                           │
  ┌──────────────────────────────────────┐  │
  │   Subtract the first frame from "i"   │  │
  └──────────────────────────────────────┘  │
                 ▼                           │
        ┌────────────────────────┐ ◄────────┘
        │     End "for loop"     │
        └───────────┬────────────┘
                    ▼
  ┌──────────────────────────────────────────────────────┐
  │ Write the spray penetration lengths in an Excel file  │
  └───────────────────────────┬──────────────────────────┘
                              ▼
                    ┌─────────────┐
                    │    END      │
                    └─────────────┘
```
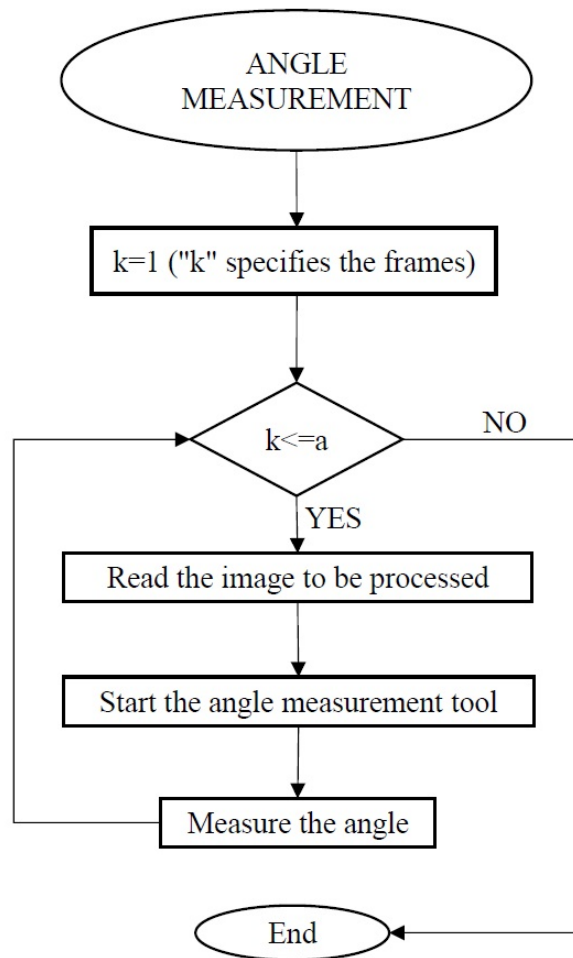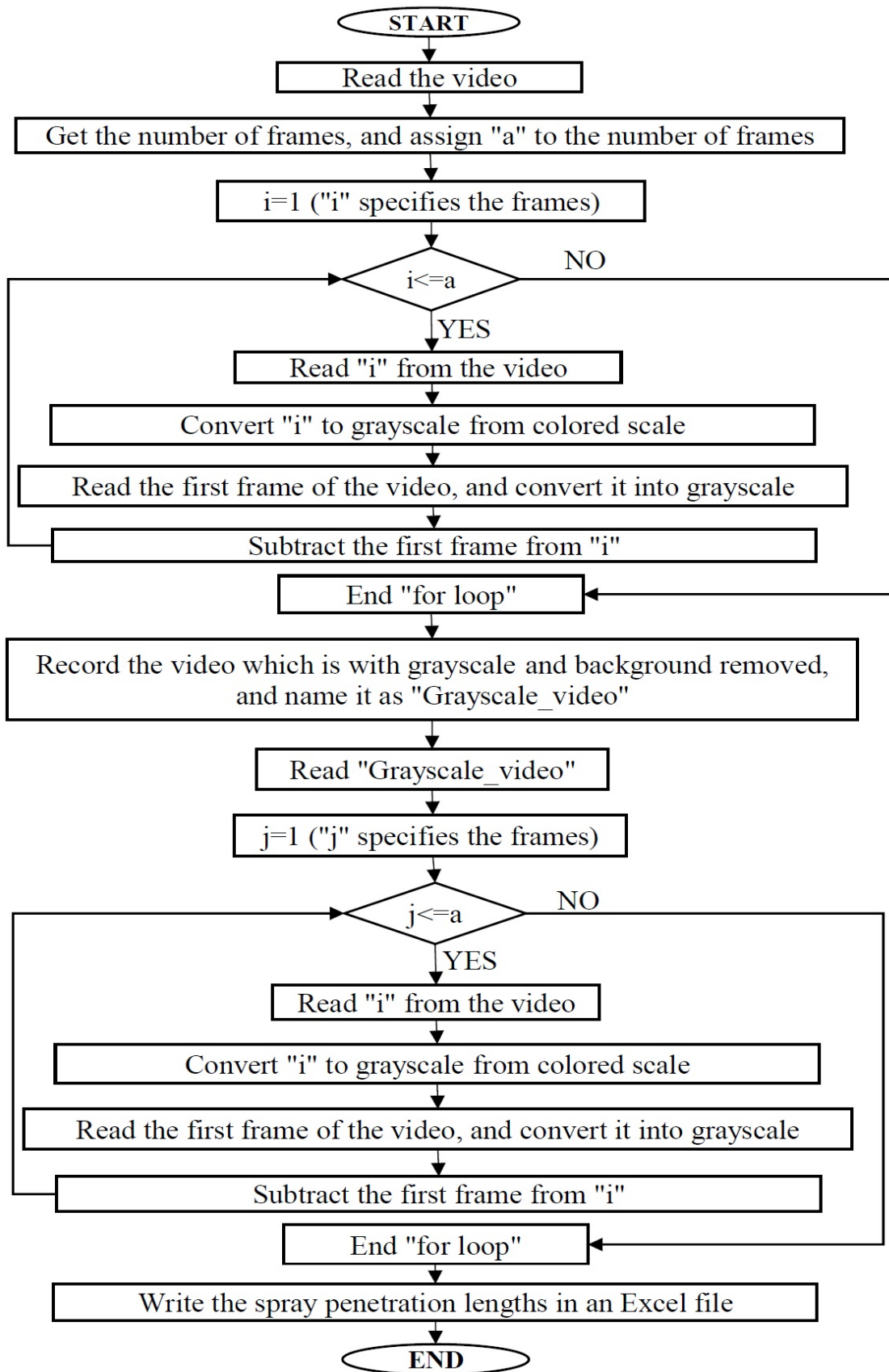
Figure C.2. Flow chart for the measurement of spray penetration length.

APPENDIX D

MATLAB PROGRAMS FOR SPRAY ANALYSIS

In this study, two different Matlab programs were generated for the measurement of spray penetration and spray cone angle, separately. The purpose of creating two different programs instead of one program was to make the examinations independent from each other.

D.1. Program for Measurement of Spray Penetration Length

The Matlab program for the measurement of spray penetration length is given below. It directly measures the required values from the video by analyzing each frame. With the help of this program, it is not required the extract each frame before the measurement.

clc, clear all;

video=VideoReader('Video_Name.avi'); *%Reads the video to be processed. %Write the name of the video to be processed.*

Grayscale_Video=VideoWriter('GrayScale_Video'); *%The video will be recorded with this name after converting it to grayscale.*

a=video.NumberOfFrames; *%Gets the number of frames.*

for i=1:a; *%Specifies the interval between 1 and number of frames.*

    b=read(video,i); *%Reads each frame in the video.*

    c=rgb2gray(b); *%Converts each frame to grayscale from colored scale.*

    c1=rgb2gray(read(video,1)); *%Reads specifically the first frame, and convert it into grayscale from colored scale. First frame is the frame before the spray process, and it is the background of the video.*

    d=imsubtract(c1,c); *%Subtracts the first frame from other frames in order to obtain clear spray images.*

    open(Grayscale_Video);

```
        writeVideo(Grayscale_Video,d); %Records the video which is returned into
grayscale.
    end
    close(Grayscale_Video);
    video_2=VideoReader('Grayscale_Video.avi'); %Opens the grayscale video.
    f=[];
    for j=1:a; %Specifies the interval between 1 and number of frames.
        k=rgb2gray(read(video_2,j)); %Reads each frame in the grayscale video.
        level=graythresh(k);
        l=im2bw(k,0.1); %Converts each frame into binary scale from grayscale.
        [x y]=find(l, 1, 'last'); %Finds the farthest point on the spray axis.
        m=insertMarker(k, [y x]); %Inserts marker on the farthest point on the
spray axis.
        f=[f,(sqrt((8-x).^2+(72-y).^2))];
    end
    f=transpose(f);
    xlswrite('pcalc',f); %Writes the spray penetration lengths of this experiment.
    figure, imshow(l) %Shows the last binary image.
    figure, imshow(k) %Shows the last grayscale image.
```

D.2. Program for Measurement of Spray Cone Angle

The Matlab program for the measurement of spray cone angle is given below. The program consists of three main parts. First one is a program to extract the frames from the video clips in a binary scale. Second one is a tool which creates the necessary equipment for angle measurement, and it is obtained from the website of MathWorks [155]. Third one is the application of this tool into frames extracted to measure the spray angles.

Frame extracting:

```
    clc; clear all;
    video=VideoReader('Video_Name.avi'); %Reads the video to be processed. %Write
the name of the video to be processed.
```

Grayscale_Video=VideoWriter('Grayscale_Video'); *%The video will be recorded with this name after converting it to grayscale.*

a=video.NumberOfFrames; *%Gets the number of frames.*

for i=1:a; *%Specifies the interval between 1 and number of frames.*

b=read(video,i); *%Reads each frame in the video.*

c=rgb2gray(b); *%Converts each frame to grayscale from colored scale.*

c1=rgb2gray(read(video,1)); *%Reads specifically the first frame, and convert it into grayscale from colored scale. First frame is the frame before the spray process, and it is the background of the video.*

d=imsubtract(c1,c); *%Substracts the first frame to other frames in order to obtain clear spray images.*

open(Grayscale_Video);

writeVideo(Grayscale_Video,d); *%Records the video which is returned into grayscale.*

end

close(Grayscale_Video);

video2=VideoReader('Grayscale_Video.avi'); *%Opens the grayscale video.*

b=video2.NumberOfFrames; *%Gets the number of frames.*

for j=1:b; *%Specifies the interval between 1 and number of frames.*

filename=strcat('frame',num2str(i),'.jpg'); *%Creates the file names.*

c=read(video2,i); *%Reads the frames from grayscale video.*

imshow(c); *%Shows all frames.*

imwrite(c,filename); *%Writes all frames separately in a folder.*

end

Angle Measurement Tool:

This tool can be found in the reference [155].

Angle Measurement Process:

a=imread('Image_Name.jpg'); *%Read the image to be processed. %Please write the name of the image to this line.*

my_angle_measurement_tool(a); *%Start the angle measurement tool.*